H E R ● N

Contents

CONTROL OF CRACK WIDTH IN DEEP REINFORCED CONCRETE BEAMS

C. R. Braam

Publication in HERON since 1970

Summary and conclusions

In the research, the cracking behaviour of deep reinforced concrete beams is analysed. Attention is focused on the amount of horizontal web reinforcement required to control the cracking in the web. On the basis of experimental results, a model is presented to calculate steel stresses and crack spacings. The model is also applicable to tensile members provided with reinforcement located at the side-faces. For these type of elements a relation between the minimum reinforcement and the cracking behaviour is derived.

In Chapter 2 an overview is given of the most commonly used formulae to predict the cracking behaviour of reinforced concrete beams and tensile members.

Thick tensile members with reinforcement concentrated at two opposite side-faces are discussed in Chapter 3. Much attention is paid to the experiments performed by Helmus at Darmstadt University of Technology. On the basis of Helmus' results, a model to calculate the steel stress and the crack spacing at the side-faces is introduced. Next, attention is focused on deep beams. Experimental results found in the literature are shown. Subsequently, several formulae describing the cracking behaviour of these elements are given. It is observed, however, that these formulae have a rather limited validity. Therefore, an experimental research programme was set up. This research should provide the information for the derivation of practical design rules for the web reinforcement.

In the first instance surveying calculations were performed with the finite element program DIANA. The results of these calculations are presented in Chapter 4 are shown to give close agreement with the experimental observations as presented in Chapter 3.

In Chapter 5 a "beam model" is introduced. This model is specially suited for the analysis of the overall structural behaviour of deep beams. Chapter 6 contains the set up of the experimental programme and a number of representative results. In Chapter 7 a comparison is made between the experimental results on the one hand and the newly developed cracking model (see Chapter 3) and the "beam model" (see Chapter 5) on the other. It is demonstrated that there is good agreement between the experiments and the theory.

In order to make the newly developed theories suitable for use in engineering practice it is decided to present the results by design curves. These curves are shown in Chapter 8. Their use is explained by two working examples. The first example concerns a reinforced T-beam that was analysed previously by Leonhardt. Furthermore, attention is focused on a thick tensile member with reinforcement placed at two opposite side-faces. In the latter example, both the required minimum reinforcement and the cracking behaviour are discussed in detail. It is stated that both phenomena are defined by the behaviour of the reinforced zones.

Samenvatting en conclusies

In het onderzoek is het scheurgedrag van "hoge" gewapend-betonliggers geanalyseerd. De aandacht ging met name uit naar de hoeveelheid langswapening die is vereist voor het beheersen van de scheurvorming in het lijf. Aan de hand van experimentele resultaten is een model opgesteld waarmee staalspanningen en scheurafstanden kunnen worden berekend. Dit model is tevens toepasbaar voor op trek belaste elementen met aan de randen geconcentreerde wapening. Aldus kon voor dit type elementen een verband worden gelegd tussen de wapening en het scheurgedrag.

In Hoofdstuk 2 wordt een kort overzicht gegeven van gangbare formules die het scheurgedrag van gewapende liggers en trekstaven beschrijven.

Trekstaven met aan de randen geconcentreerde wapening komen aan bod in Hoofdstuk 3. Er wordt uitvoerig ingegaan op recent aan de TU Darmstadt door Helmus uitgevoerde experimenten. Op basis van Helmus' resultaten is een model opgesteld waarmee staalspanningen en scheurafstanden worden berekend. Vervolgens is de overstap naar "hoge" liggers gemaakt. In de literatuur beschreven resultaten van experimenten worden getoond. Hierna volgt de behandeling van enkele formules waarmee het scheurgedrag van deze elementen is te bepalen. Deze formules blijken echter slechts beperkt geldig te zijn. Daarom is een experimenteel onderzoek opgezet dat moest leiden tot praktijkgerichte dimensioneringsregels voor de lijfwapening.

In eerste instantie zijn verkennende berekeningen met het eindige elementenprogramma DIANA uitgevoerd. Deze berekeningen, die worden besproken in Hoofdstuk 4, geven resultaten die goed aansluiten bij de experimentele waarnemingen die in Hoofdstuk 3 zijn getoond.

In Hoofdstuk 5 wordt een "ligger model" besproken dat speciaal is ontwikkeld voor het bestuderen van het "over-all" gedrag van "hoge" liggers. De opzet van het proevenprogramma en de proefresultaten worden beschreven in Hoofdstuk 6. Vervolgens worden in Hoofdstuk 7 de experimentele uitkomsten enerzijds vergeleken met de resultaten verkregen met het scheurmodel voor de randzone (zie Hoofdstuk 3) en het "ligger model" (zie Hoofdstuk 5) anderzijds. Aangetoond wordt dat er goede overeenstemming met de experimenten is.

Om de ontwikkelde theorieën geschikt te maken voor toepassing in de praktijk is gekozen voor een presentatie aan de hand van nomogrammen. Deze nomogrammen worden besproken in het laatste hoofdstuk. De werking ervan wordt toegelicht aan de hand van twee rekenvoorbeelden. Het eerste voorbeeld betreft een gewapende T-ligger die reeds door Leonhardt is geanalyseerd. Vervolgens komt nog een dik element met aan de randen geconcentreerde wapening aan de orde. In dit voorbeeld wordt ingegaan op zowel de vereiste minimum wapening als het scheurgedrag. Aangegeven wordt dat beide verschijnselen worden bepaald door het gedrag van de gewapende randzones.

5

Control of crack width in deep reinforced concrete beams

1 Introduction

1.1 *Scope of the research*

The reinforcement in concrete structures is generally designed to satisfy all the rules presented in the codes. These rules arise from requirements with respect to safety, esthetics, durability and serviceability. So far as safety is concerned, the behaviour of common concrete structures is well known, resulting in widely accepted formulae. With regard to esthetics, durability and serviceability, cracking is one of the major issues. The occurrence of cracks is inherent to most reinforced concrete structures. Therefore, the cracking behaviour has been studied for many years. Most research was restricted to describing crack width and crack spacing in a semi-empirical manner: the cracking behaviour was described on the basis of relatively simple calculation models [e.g. CEB, 1959]. The simplicity of the models led to the introduction of a number of coefficients. When tuned to experimental results, good agreement between experiment and calculation could be obtained for a number of cases. Since laboratory experiments provided the basis for this tuning, most results were restricted to relatively small concrete beams and plates (e.g. 56 of the 58 beams tested by Rehm and Rüsch [1963a-b, 1964] were 625 mm in height, whereas only two beams were 1200 mm deep). Besides, research mostly focused on crack widths and crack spacings at the level of the main reinforcement, see Fig. 1.1 [Rehm and Rüsch, 1964].

dimensions mm
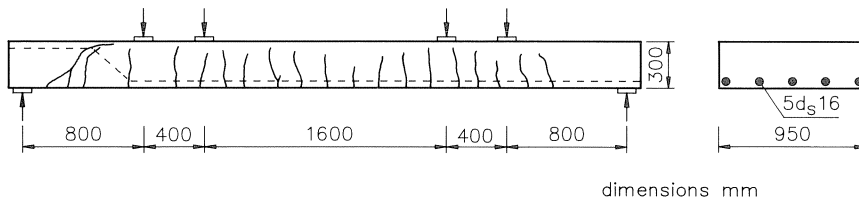
Fig. 1.1   Crack pattern of a reinforced concrete plate [Rehm and Rüsch, 1964].

In the last decade, theoretical models were developed [e.g. Noakowski, 1978, 1985; Fehling and König, 1988]. These models are based on a formulation describing the actual physical behaviour. Fundamental experimental research and finite element (FE) analyses provided the information needed to describe the basic components. However, these theoretical models, too, are mostly still restricted to the cracking behaviour at the level of the main reinforcement.
From experimental results it was obvious that cracking on the side faces of deep beams should also be taken into account, see Fig. 1.2 [Rehm and Rüsch, 1963a].

7
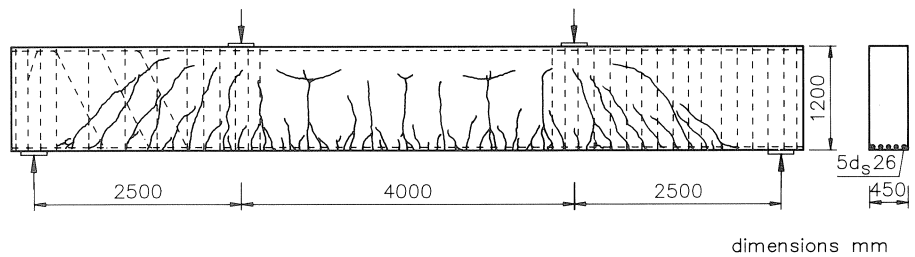
Fig. 1.2 Crack pattern of a deep reinforced concrete beam [Rehm and Rüsch, 1963a].

The amount of experimental research in this field has to date been rather scarce, with the result that there are no rational models to calculate crack widths and crack spacings on the side faces of deep beams. Some rules have been presented for the design of web reinforcement [e.g. Soretz and Colonna-Ceccaldi, 1971; Breen and Frantz, 1978, 1980a and CEB, 1985] but there is still a lack of both fundamental experimental and theoretical information to describe the crack pattern over the entire height of a beam provided with web reinforcement.

1.2   *Aim of the research programme*

Both empirical relations and analytical models describing the cracking behaviour of reinforced concrete structures are mostly restricted to the level of the main reinforcement. In addition, Beeby [1971] presented formulae to predict crack width and spacing over the height of a beam without web reinforcement. The most extensive research was carried out by Breen and Frantz [1978] who presented design formulae for the web reinforcement. However, their formulae are only valid in the specific case of a 0.14 and 0.20 mm maximum crack width at the level of the main reinforcement and in the web respectively. The CEB [1985] related the diameter of the web reinforcement to the web width. The bar spacing was related to the concrete quality and the permissible characteristic web crack width. Moreover, a curve was presented enabling the determination of the distance over which the web reinforcement must be applied. The design rules, however, were empirically based and give very conservative values for the required amount of web reinforcement.

The aim of this research programme is to present a cracking theory describing the cracking behaviour over the entire height of deep beams. Since experimental results presented in the literature are rather scarce, an experimental research programme was aimed at providing the information to verify the theoretical models. Supplementary information will also be provided by FE-calculations. Both experiments and FE-calculations will form the basis for a relatively simple theoretical model. Subsequently, this model can be used to perform parameter studies and to present design rules for engineering practice.

8

2 Cracking behaviour of reinforced concrete tensile members and beams

2.1 *Introduction*

In this chapter attention is focused on existing empirical relations and theoretical models describing the cracking behaviour of tensile members and beams. It should be noted that the tensile members are restricted to specimens with a uniformly distributed reinforcement, resulting in a similar crack pattern along the whole circumference of the specimen.

2.2 *Reinforced concrete tensile members*

2.2.1 Semi-empirical relations and analytical models

The first relations used to predict crack spacing and crack width were based on a relatively simple calculation model [CEB, 1967] which will be explained briefly here. A concrete cross-section A_c, a concrete tensile strength f_{ct}, a circumference of the reinforcing steel u_s and a constant bond stress τ_m between the concrete and the reinforcing steel were assumed. When the concrete cracks, the concrete tensile force must be carried by the reinforcing steel. At a certain distance from a crack, the so-called transfer length [CEB, 1967], the undisturbed situation is again reached, i.e. the bond stress is zero. The transfer length can be calculated with the following formula (see also Fig. 2.1):
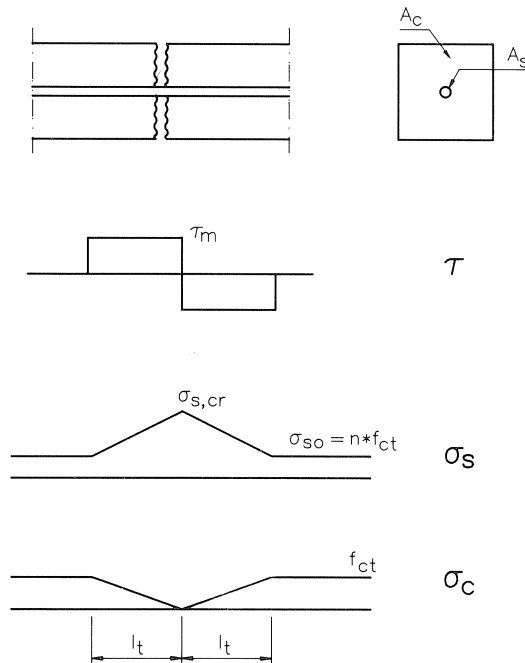
Fig. 2.1 The stresses in a reinforced concrete tensile member just after cracking [CEB, 1967].

9

$$l_t = \frac{A_c f_{ct}}{u_s \tau_m} \quad \text{[mm]} \tag{2.1}$$

It is assumed that at the end of the transfer length, the whole concrete section is in uniform tension so that a new crack can occur. With increasing extension new cracks are formed until the crack pattern is "fully developed", e.g. all the crack spacings vary between l_t and $2l_t$. In this situation there are no parts in which the concrete stress reaches the tensile strength. Thus, the mean crack spacing l_m in a fully developed crack pattern is $1.5l_t$ [CEB, 1967]. Formula (2.1) suggests that the mean crack spacing tends to become zero with an increasing reinforcement ratio. However, from experiments on tensile members it was derived that the mean crack spacing has a lower-bound value l_{min} [Beeby, 1972], see Fig. 2.2. This value is mostly related to the concrete cover [i.e. CEB,
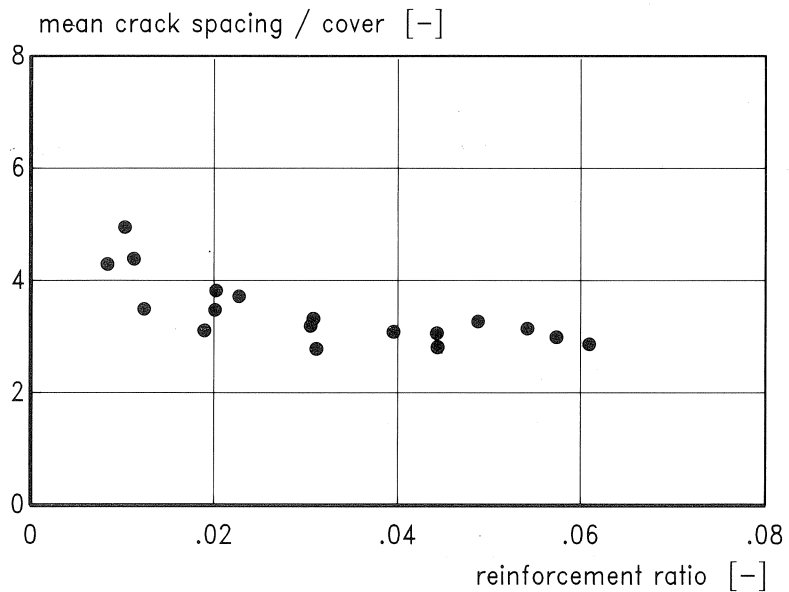
Fig. 2.2   Mean crack spacing in a fully developed crack pattern depending on the concrete cover and the reinforcement ratio [Beeby, 1972].

1967], the concrete cover and the bar spacing [i.e. Leonhardt, 1976] or is assumed to be constant [i.e. Schiessl and Wölfel, 1986]. Rüsch [1956] obtained a similar result for the mean crack spacing at the level of the main reinforcement in beams.
For a specific type of reinforcing bar (defined by the specific rib area f_R [Rehm, 1961]) the bond stress was related to the concrete tensile strength according to:

$$k_2 = \frac{f_{ct}}{\tau_m} \quad \text{[--]} \tag{2.2}$$

Thus, the following semi-empirical relation could be derived for the mean crack spacing in the case of a fully developed crack pattern:

$$l_m = l_{min} + \tfrac{1}{4} k_2 \frac{d_s}{\varrho} \quad [mm] \tag{2.3}$$

The mean crack width was related to the mean crack spacing by:

$$w_m = l_m \, \varepsilon_{sm} \quad [mm] \tag{2.4}$$

In formula (2.4) ε_{sm} is the mean steel strain. This strain was obtained by reducing the steel strain at a crack by a factor depending on the load level $(\sigma_{s,cr}/\sigma_s)$, the bond characteristics of the reinforcement (k_5) and the fact whether or not a sustained or a varying load was applied (k_6):

$$\varepsilon_{sm} = \frac{\sigma_s}{E_s} \left[1 - k_5 k_6 \left(\frac{\sigma_{s,cr}}{\sigma_s} \right)^2 \right] \quad [-] \tag{2.5}$$

In formula (2.5) $\sigma_{s,cr}$ and σ_s are the steel stresses in a crack at the cracking load and the service load respectively. This expression for the mean steel strain was based on research conducted by Rao [1966]. The tensile force – elongation curves of a steel bar and a reinforced concrete tensile member are both presented in Fig. 2.3.

The variation in crack widths was accounted for by the coefficient k_4:

$$w_k = k_4 w_m \quad [mm] \tag{2.6}$$

Combining formulae (2.3) to (2.5) results in a formula for the mean crack width (w_m) containing three coefficients k_i and l_{min}. These coefficients could be defined to obtain
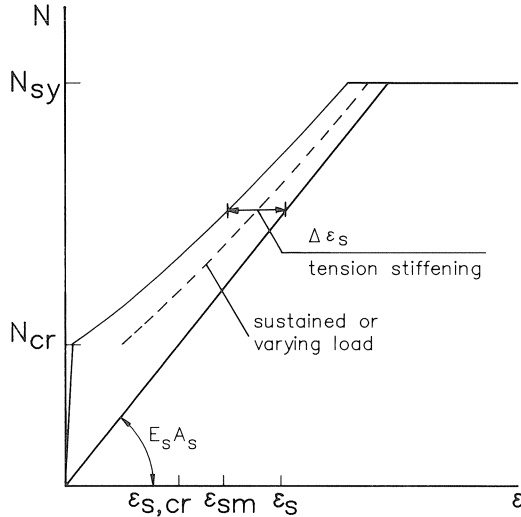
Fig. 2.3 Tensile force – strain curve of a reinforced tensile member [Leonhardt, 1976a].

11

close agreement with experimental results. Table 2.1 presents the values according to several codes and researchers. The Eurocode 1990 formulae were based on research by Schiessl and Wölfel [1986].

Table 2.1 Coefficients in formulae predicting the cracking behaviour of reinforced concrete tensile members

	l_{min}	k_2 plain bars	k_2 deformed bars	k_5 plain bars	k_5 deformed bars	k_6
CEB [1978]	$2(c + s/10)$	0.8	0.4	0.5	1.0	½/1
Martin et al. [1980]	50	1.0	0.5	0.5	1.0	½/1
NEN 3880 [1984]	$2c$ deformed $2.5c$ plain	0.40	0.32	–	–	–
Eurocode [1990]	50	1.6	0.8	0.5	1.0	½/1

In the Dutch code [NEN 3880, 1984] no tension stiffening is taken into account, resulting in an overestimation of the mean steel strain. To ensure a close fit with experimentally observed mean crack widths the theoretical mean crack spacing must be kept artificially small.

The analytical models are based on a model presented by Noakowski [1985]. Noakowski presented an analytical solution for both the transfer length (l_t) and the crack width (w_{cr}) for a not fully developed crack pattern. Use was made of a "power function" to present the bond stress – slip relation:

$$\tau_b = a\delta^b \quad [\text{MPa}] \tag{2.7}$$

At known steel stresses just before (σ_{s0}) and after cracking $(\sigma_{s,cr})$ the crack width and the transfer length were found to be:

$$w_{cr} = 2\left\{\frac{1+b}{2}\frac{d_s}{4}\frac{1}{aE_s}\sigma_{s,cr}(\sigma_{s,cr} - \sigma_{s0})\right\}^{\frac{1}{1+b}} \quad [\text{mm}] \tag{2.8}$$

$$l_t = \frac{w_{cr}E_s}{(1-b)\sigma_{s,cr}} \quad [\text{mm}] \tag{2.9}$$

Noakowski assumed that the crack pattern is fully developed when all the crack spacings vary between l_t and $2l_t$. The mean crack spacing is then:

$$l_m = 1.5l_t \quad [\text{mm}] \tag{2.10}$$

It was assumed that no new cracks form if the load is increased beyond the cracking load, i.e. the mean crack spacing remains unchanged. According to Noakowski's model the tension stiffening is constant:

$$\Delta\varepsilon_s = 0.75\left(\frac{1+b}{2}\right)\varepsilon_{s,cr} \quad [-] \tag{2.11}$$

The mean crack width is:

12

$$w_m = l_m \varepsilon_{sm} = 1.5 l_t (\varepsilon_s - \Delta \varepsilon_s) \quad [\text{mm}] \tag{2.12}$$

However, it should be realized that, strictly speaking, formulae (2.8) and (2.9) are only valid if the crack spacing exceeds twice the transfer length. The calculation of the crack width in the case of loads exceeding the cracking load was no longer based on the bond stress-slip relation; Formula (2.12) was based on the experimentally observed load-elongation behaviour of a reinforced tensile member [Hartl, 1977], see Fig. 2.4.
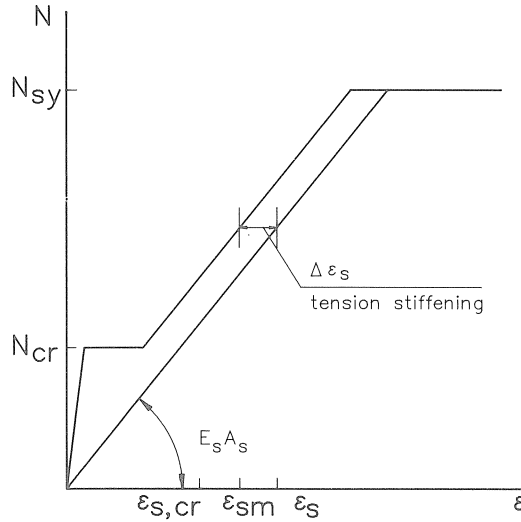
Fig. 2.4   Simplified tensile force-strain diagram of a reinforced concrete tensile member [Noakowski, 1985], based on experimental results by Hartl [1977].

Krips [1985] removed this discrepancy and presented analytical solutions for both the crack width and the crack spacing for loads exceeding the cracking load. The extension of Noakowski's theory led to the introduction of several coefficients which are dependent on the coefficient b of the bond stress-slip relation (see formula (2.7)) and the load level $(\sigma_s / \sigma_{s,cr})$. It should be noted that Krips' model was based on an assumed elastic behaviour of the τ_b-δ relation. From experimental results it can be concluded that the behaviour at unloading is highly non-elastic. For an overview of experimental research on the influence of repeated and cyclic loading on the bond stress-slip relation the reader is referred to Braam [1989].

An analytical model was also presented by Fehling and König [1988]. They used the following linear bond stress-slip relation:

$$\tau_b = a_1 + a_2 \delta \quad [\text{MPa}] \tag{2.13}$$

On the basis of a comparison between theoretically predicted and experimentally observed mean crack widths in tension members and beams, it was concluded that the

13

best results were obtained using $a_1 = 2f_{ctm,0}$ and $a_2 = 0$. Thus, the transfer length (see also formula (2.1)) is:

$$l_t = \frac{1}{8} \frac{d_s}{\varrho} \quad [mm] \tag{2.14}$$

When comparing the constant bond stress used by Fehling and König [1988] with the coefficient $k_2 = f_{ct}/\tau_m$ from Table 2.1, good agreement is found in the case of deformed bars.

By introducing a bond-free length of 15mm at both crack faces, the disturbance of bond in the vicinity of a crack was taken into account. Thus, the maximum crack spacing was:

$$l_{max} = 30 + 2l_t = 30 + \frac{1}{4} \frac{d_s}{\varrho} \quad [mm] \tag{2.15}$$

The mean crack spacing and the mean crack width were found to be:

$$l_m = \frac{l_{max}}{1.7} \quad [mm] \tag{2.16}$$

$$w_m = \frac{1}{1.7}\left[30\frac{\sigma_s}{E_s} + \frac{1}{4}\frac{d_s}{\varrho \cdot E_s}\left(\sigma_s - 0.6\frac{f_{ct}}{\varrho}\right)\right] \quad [mm] \tag{2.17}$$

The factor 1.7, introduced in formulae (2.16) and (2.17), was used for the case of a fully developed crack pattern. When the crack pattern is not fully developed this coefficient equals 1.4. It was mostly assumed that the crack pattern is fully developed in the case where $\sigma_s \geq 1.43\sigma_{s,cr}$ [Martin et al., 1980].

2.2.2 Experimental results versus theory

The semi-empirical relations and the analytical models were compared with experimental results presented by Eligehausen et al. [1976], Hartl [1977], Hartwich [1986] and Van der Veen [1989]. The main conclusions of this study performed by Kruithof [1990] will be briefly presented.

From all four of the research programmes a total of 132 experimentally observed mean crack widths and mean crack spacings were used for the comparative examination. Van der Veen [1987, 1988] not only performed tests on tensile members, but also pull-out tests. These experimental results provided the bond stress-slip relations to be adopted in Noakowski's and Krips' models. For the specimens tested in the other three research projects the following bond stress-slip relationship was assumed [Bruggeling, 1987]:

$$\tau_b = 0.38f_{ccm}\delta^{0.18} \quad [MPa] \tag{2.18}$$

For all the specimens it was assumed that cracking occurs when the concrete tensile stress is equal to the mean short-term tensile strength:

$$\sigma_{cr} = 1.0f_{ctm,0} \quad [MPa] \tag{2.19}$$

14

This assumption will be discussed in more detail in section 2.3.2. The results of the comparative examination are presented in Table 2.2 [Kruithof, 1990].

Table 2.2   Ratio between theoretical and experimental mean crack spacings and mean crack widths

formula/model	mean crack width ratio theory/exp.	mean crack spacing ratio theory/exp.
CEB-FIP Model Code [1978]	0.88	0.92
Martin et al. [1980]	0.77	0.77
NEN 3880 [1984]	1.04	0.71
Eurocode [1990]	1.00	1.04
Noakowski [1985]	1.05	1.07
Krips [1985]	0.59	0.60
Fehling and König [1988]	0.76	0.68

2.3   Reinforced concrete beams

2.3.1   Semi-empirical relations and analytical models

In section 2.2.1 attention was devoted to empirical relations predicting the cracking behaviour of reinforced tensile members. In the present section, attention is focused on reinforced concrete beams.

In formula (2.3) the mean crack spacing was found to depend on, among other factors, the reinforcement ratio ϱ. In the case of a tensile member this ratio is easily defined as $\varrho = A_s/A_c$. For beams several approaches can be distinguished. They are presented in chronological order.

In one of the first generally accepted approaches ϱ was related to the cross-section of a beam, e.g. Martin and Rehm [1968], CEB [1970]:

$$\varrho = \frac{A_s}{bd} \quad [-] \qquad (2.20)$$

In the case of T-beams b is the web width. However, it was felt that with increasing beam height the influence of ϱ is overestimated [Schiessl, 1989]. From the cracking behaviour of deep beams, see Fig. 2.5, Leonhardt [1976a] deduced an approach to treat a
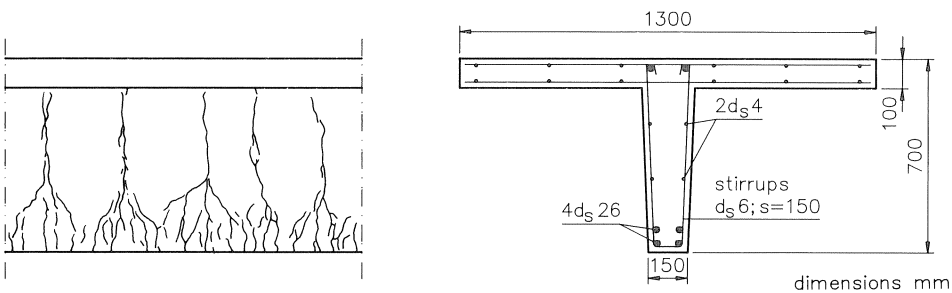
Fig. 2.5   Crack pattern of a deep T-beam [Leonhardt, 1974].

15

concrete beam as a tensile member by defining an "effective concrete area" around the main reinforcement (see Fig. 2.6a):

$$\varrho_{\text{eff}} = \frac{A_s}{bh_{\text{eff}}} \quad [-]$$ (2.21)

Many researchers and codes adopted this approach, e.g. CEB [1978], Martin et al. [1980], NEN 3880 [1984].
Leonhardt [1976a] used the bar diameter as one of the parameters defining the effective area. Schiessl and Wölfel [1986] presented a different approach based on the effective beam depth, see Fig. 2.6b:

$$\varrho_{\text{eff}} = \frac{A_s}{\alpha b(h - d)} \quad [-]$$ (2.22)
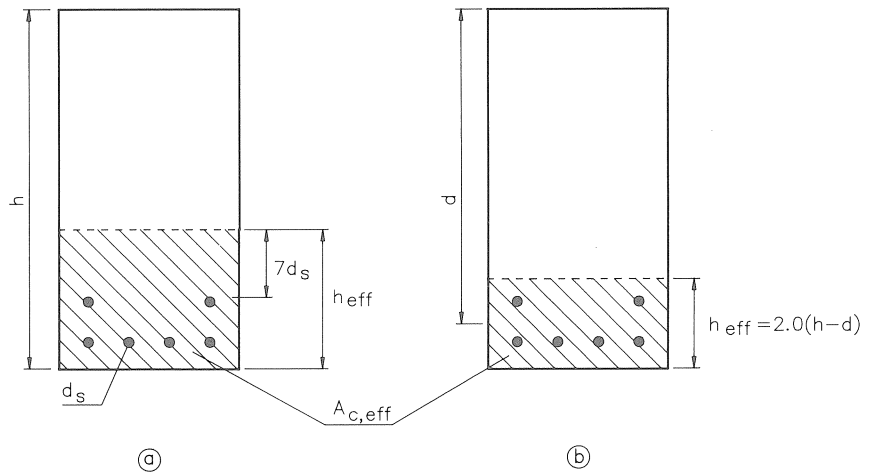
Fig. 2.6 Definitions of the "effective concrete area"
a. Leonhardt [1976a]
b. Schiessl and Wölfel [1986].

This approach had already been introduced earlier, for example by Bjuggren [1948], CEB [1959] and Gergely and Lutz [1968], but until a few years it was not as generally accepted as Leonhardt's approach.
Schiessl and Wölfel assumed $\alpha = 2.0$. In the Eurocode 1990 this value was changed to 2.5.
In formula (2.1) the transmission length was calculated on the basis of the cracking force of a tensile member. A stress gradient is present over the "effective concrete area" of a beam. This results in a mean concrete tensile stress less than f_{ct}:

$$\sigma_{\text{cm}} = k_3 f_{\text{ct}} \quad [\text{MPa}]$$ (2.23)

Formula (2.3) can now be written as:

$$l_m = l_{min} + \tfrac{1}{4} k_2 k_3 \frac{d_s}{\varrho_{eff}} \quad [mm] \tag{2.24}$$

The CEB [1978], Martin et al. [1980] and Schiessl and Wölfel [1986] advised the use of $k_3 = 1$ for tension (see section 2.2.1) and $k_3 = 0.5$ for pure bending. The Dutch code (NEN 3880 [1984]) introduced $k_3 = 0.20$ in the case of bending and 0.16 for plain and deformed bars respectively.

The theory presented by Noakowski (formulae (2.8) and (2.9)) can be used unaltered in the case of beams since the steel stresses just before and after cracking can be calculated easily. The same conclusion holds for Krips' [1985] model.

The model presented by Fehling and König [1988] was based purely on the behaviour of a tensile member. Therefore, a beam had to be translated into a tensile member. The approach presented by Schiessl and Wölfel [1986] was used, see Fig. 2.6b and formula (2.22). The value for α was investigated by means of the FEM. The part of a beam between two cracks was modelled, see Fig. 2.7a. Because of the symmetry only one half was considered. The compressive forces were introduced as a triangular line-load. The steel forces transmitted to the concrete by bond were modelled as a uniform horizontal line-load. It was found that the computational results hardly changed when the bond forces were introduced as a triangular line-load. This finding was also observed by Koch [1976] who performed similar analyses to investigate the linear-elastic state of stress in the part of a beam between two cracks. Fehling and König situated "discrete crack" elements at the axis of symmetry, thus enabling the occurrence of a new crack. These elements had a stress-crack opening ("tension-softening") curve according to Scheidler [1987], see Fig. 2.7b. All the other elements behaved in a linear-elastic way.

The maximum force that could be transferred by bond, N_{ru}, was calculated. In all the analyses the ratio between N_c and N_τ was constant. The beam was translated into a tensile member by using the following formula:
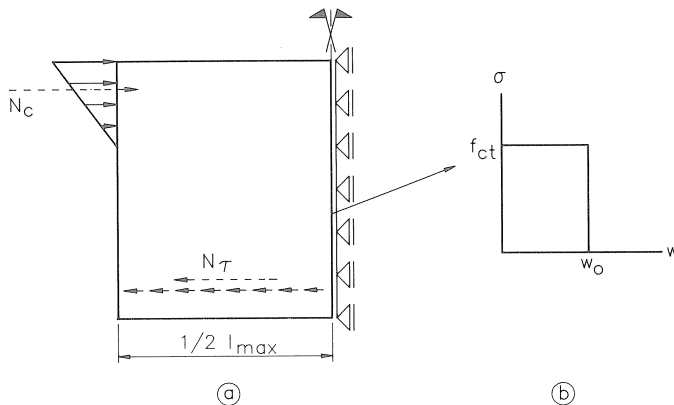
Fig. 2.7 (a) Model of the part of a beam between two cracks [Fehling and König, 1988]; (b) Tension-softening curve of plain concrete as used by Scheidler [1987].

17

$$\alpha = \frac{N_{\tau u}}{b(h-d)f_{ct}} \quad [-] \tag{2.25}$$

The results of the analyses are shown in Fig. 2.8 where α is presented in relation to the ratio between the crack spacing and the beam height and the ratio between the compressive force and the bond force. For bending $\alpha = 3$ was assumed.
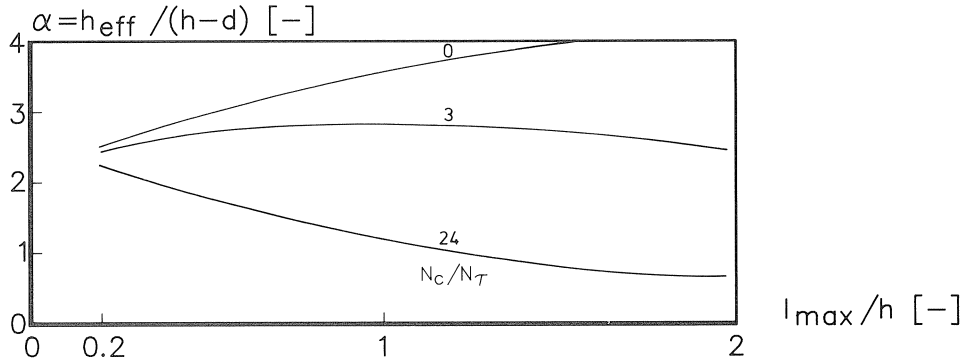
Fig. 2.8   The factor α defining the "effective concrete area" [Fehling and König, 1988].

2.3.2   Experimental results versus theory

For a comparative analysis the experimental results presented by Rehm and Rüsch [1963a, 1963b, 1964] were used. Use was made of all the results for specimens not reinforced with plain bars, viz. 26 rectangular beams, 10 plates and 11 T-beams. In all, over 13600 individual crack widths were used in the analysis. From these measurements 288 mean crack widths and mean crack spacings were deduced. The results are presented in Table 2.3. All the results refer to a fully developed crack pattern. For more detailed information the reader is referred to Smit [1989] and Braam [1990a].

Table 2.3   Ratio between theoretical and experimental mean crack spacings and mean crack widths

formula/model type of specimen number of measurements	mean crack width ratio theory/exp.				mean crack spacing ratio theory/exp.			
	rect. 159	T 78	plate 51	all 288	rect. 159	T 78	plate 51	all 288
CEB-FIP Model Code [1978]	1.18	1.31	0.87	1.16	1.08	1.05	0.69	1.01
Martin et al. [1980]	0.94	1.12	0.87	0.98	0.86	0.89	0.70	0.84
NEN 3880 [1984]	1.07	1.14	0.87	0.98	0.81	0.81	0.55	0.76
Eurocode [1990]	0.92	1.16	0.98	0.99	0.84	0.91	0.79	0.85
Noakowski [1985]	1.19	1.29	1.25	1.23	1.05	1.04	0.99	1.04
Krips [1985]	0.99	1.01	1.20	1.03	0.90	0.85	0.98	0.90
Fehling and König [1988]	1.11	1.17	1.17	1.14	0.99	0.89	1.08	0.98

18

In section 2.2.3 the cracking criterion was presented (formula (2.19)). This criterion was derived from an analysis in which all the reported cracking moments of the specimens were related to the concrete tensile strength [Smit, 1989]. Besides, the specimen height was found not to have any significant influence on this criterion was found. Therefore, it was advised not to take account of the flexural tensile strength.

2.4   *Characteristic and maximum crack width*

From the point of view of serviceability, the calculated crack width must not exceed a certain specified value. For the purposes of this comparison the mean crack width is multiplied by a factor to obtain a characteristic crack width. The 95% upper-bound value is the most commonly used and is calculated by multiplying the mean value by 1.7 (e.g. CEB, 1978; Martin et al., 1980; Schiessl and Wölfel, 1986).

The experiments by Rehm and Rüsch provided the information for a detailed study of this factor. For that purpose the 95% upper-bound crack width $(w_{95\%})$ was calculated from all the individual crack widths for a beam at a certain loading stage. Besides, the maximum crack width (w_{max}) was also registered. In all, a total of 173 characteristic and 291 maximum crack widths were collected. After relating these to the corresponding mean crack widths the results presented in Table 2.4 were obtained [Smit, 1989].

Table 2.4   The characteristic and the maximum crack width related to the mean crack width in the case of a "fully developed crack pattern"

specimen	rect. beam	T-beam	plate	all
number	121	26	26	173
$\dfrac{w_{95\%}}{w_m}$	1.77	1.74	1.77	1.75
number	159	81	51	291
$\dfrac{w_{max}}{w_m}$	1.99	2.22	2.07	2.03

With regard to the factor 1.7 mentioned above good agreement was obtained for the characteristic crack width. It must, however, be emphasized that this is a mean value. This implies that there is a 50% probability of this value being exceeded. As regards the maximum crack width, the factor was found to be about 2.0.

2.5   *Conclusions*

When comparing Tables 2.2 and 2.3 it is clear that, as far as the theoretical models are concerned, the model presented by Fehling and König [1988] gave the best agreement with the experiments. This finding is not surprising since the adopted bond stress-slip curve was tuned to the experimentally observed mean crack widths. In this tuning nearly the same number of results on both tension members and beams were used. This fact might explain the overestimation of crack widths in beams, compensated by the

underestimation for the tensile members. The model not only produces good results; an additional advantage is its relatively simple form, making it appropriate for use in engineering practice.

With regard to the formulae presented in the codes, the Eurocode [1990] gave very good results for crack width and crack spacing, for both the tensile members and the beams. The CEB-FIP Model Code [1978] also gave good results but overestimated the crack width for beams. The modification to this code, presented by Martin et al. [1980] presented a better approximation for the crack widths in beams, but gave an underestimation for the tensile members.

3 Cracking behaviour of concrete structures with concentrated reinforcement

3.1 *Introduction*

In chapter 2 attention was focused on the crack width and crack spacing at the level of the main reinforcement in tensile members and beams. As regards the tensile members specimens with a uniformly distributed reinforcement were analysed (see section 2.2.2 and Kruithof [1990]). Since beams are mostly provided with reinforcement concentrated at the top or bottom of the cross-section, the crack pattern at the main reinforcement (e.g. see Fig. 2.5) is calculated on the basis of an "effective concrete area" (see Figs. 2.6a-b). The semi-empirical relations and theoretical models presented in chapter 2 can not be used to describe the crack pattern in the web of beams. The same conclusion holds for tensile members provided with reinforcement concentrated at the side faces. Fig. 3.1b presents the type of crack pattern to be expected in such a case, whereas Fig. 3.1a presents the situation for a uniformly distributed reinforcement [Fellman and Menn, 1981].

In the following sections attention is focused on the cracking behaviour of deep beams and tensile members provided with reinforcement located at the side faces.

3.2 *Reinforced concrete tensile members*

3.2.1 Experimental results

The following section presents the main results of tests performed on tensile members provided with reinforcement located at the side faces. Attention is focused on the relation between crack widths and crack spacings at the level of the reinforcement and in the unreinforced part of the specimens. For more detailed information the reader is referred to De Groot [1990].

Henning and Rostásy [1990] performed tests on tensile members 1000 mm wide and 160 mm thick. The specimens were provided with reinforcement $6 * d_s$ 12, $4 * d_s$ 12, $2 * d_s$ 20 or $4 * d_s$ 8 + $2 * d_s$ 16 mm, resulting in reinforcement ratios of 0.42, 0.28, 0.39 and $0.38 * 10^{-2}$, respectively. The concrete cover at the side faces was 30 mm. The crack pattern and the crack widths were observed over a measuring length of 4000 mm. From the crack patterns recorded, it was deduced that the ratio between the mean crack
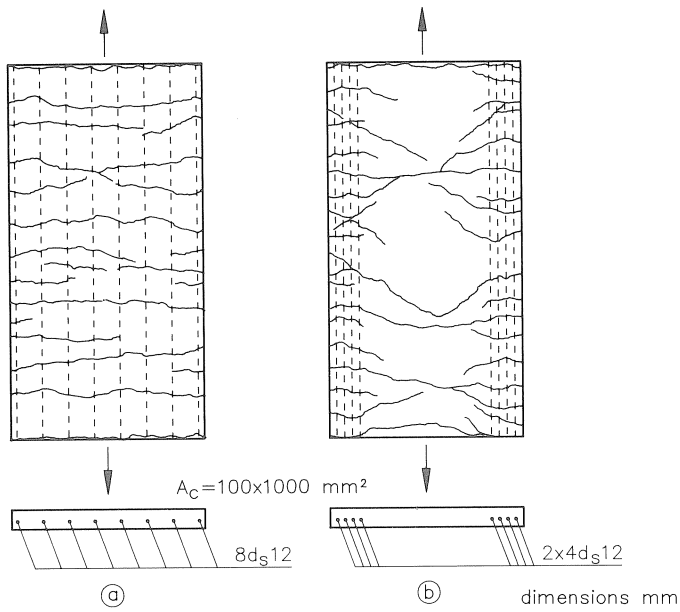
Fig. 3.1 Crack patterns of tensile members with uniformly distributed (a) and concentrated (b) reinforcement [Fellman and Menn, 1981].

spacings in the middle of the specimens and at the side faces was 3.8 (c.v. = 0.37) [De Groot, 1990]. A typical crack pattern is presented in Fig. 3.2 [Henning and Rostásy, 1990]. The crack widths were measured at four locations, see Fig. 3.2.

The mean ratios of $w_{95\%}/w_m$ and w_{max}/w_m were 1.70 and 1.95 (cv = 0.21, fully developed crack pattern) respectively. This is approximately in agreement with the results present-
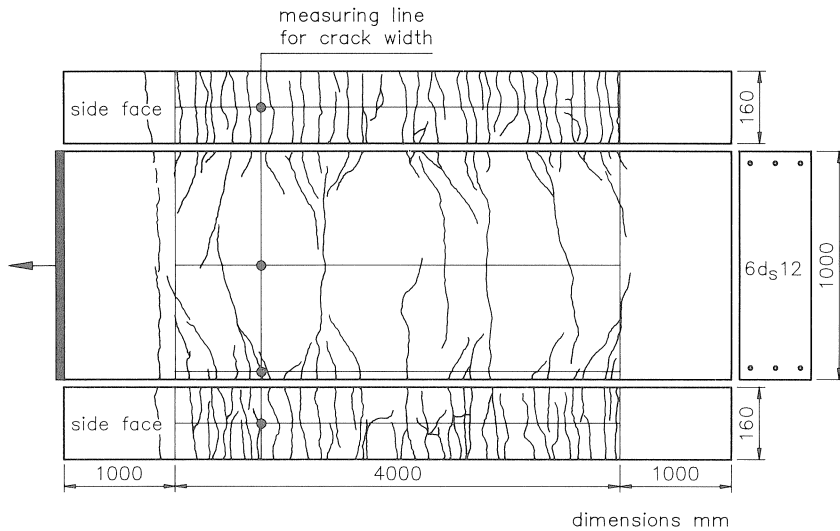

Fig. 3.2 Crack pattern of a tensile member with concentrated reinforcement [Henning and Rostásy, 1990].

ed in Table 2.4. It was also found that at the level of the reinforcement there was no specific difference between the widths of cracks restricted to the side faces (in the following denoted as "secondary cracks") and cracks that penetrated through the whole cross-section ("primary cracks") [Henning and Rostásy, 1990]. This conclusion was also drawn by Beeby [1971] in the case of beams.

Hartwich and Rostásy [1984] investigated the cracking behaviour of steel fibre reinforced concrete tensile specimens. From their research two specimens containing no steel fibres, viz. ZK 10/0 and 20/0, were selected. The cross-sections of both specimens are presented in Fig. 3.3.

The ratio between the mean crack spacing at the middle and at the side faces of the specimens was 4.7 and 4.0 respectively [De Groot, 1990].

dimensions mm
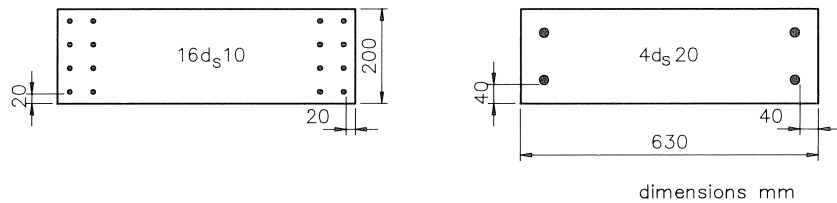
Fig. 3.3 Cross-section of two of the specimens tested by Hartwich and Rostásy [1984].

An extensive investigation into the behaviour of thick-walled concrete structures was conducted by Helmus [1989]. Tests were performed on 12 specimens 400 mm thick and 800, 1200 or 2000 mm wide. The reinforcement ratio ranged from 0.16 to $0.39 * 10^{-2}$ for the whole cross-section. The main object of the study was to set up a model which will enable the reinforcement to be designed to ensure a uniformly distributed crack pattern at the side faces where the reinforcement is located. Helmus' model is presented in section 3.2.2. Fig. 3.4 clearly demonstrates the influence of the detailing of the reinforcement. The figure shows the crack pattern on all four sides of the member. The specimens presented have nearly the same reinforcement ratio, viz. 0.17 and $0.19 * 10^{-2}$ for VK 22 and 24 respectively. At the moment when the concrete cracks a primary crack propagates through the entire cross-section and the steel reaches its yield stress. Since loading was applied in a displacement-controlled way, the decreasing stiffness of the member causes a decrease of the load. At increasing imposed deformation specimen VK 22 demonstrates no further cracking: only widening of the already existing primary crack occurs. However, the reinforcement in specimen VK 24 generates new ("secondary") cracks: an increasing imposed deformation causes the widening of the already existing crack and the formation of new secondary cracks.

22
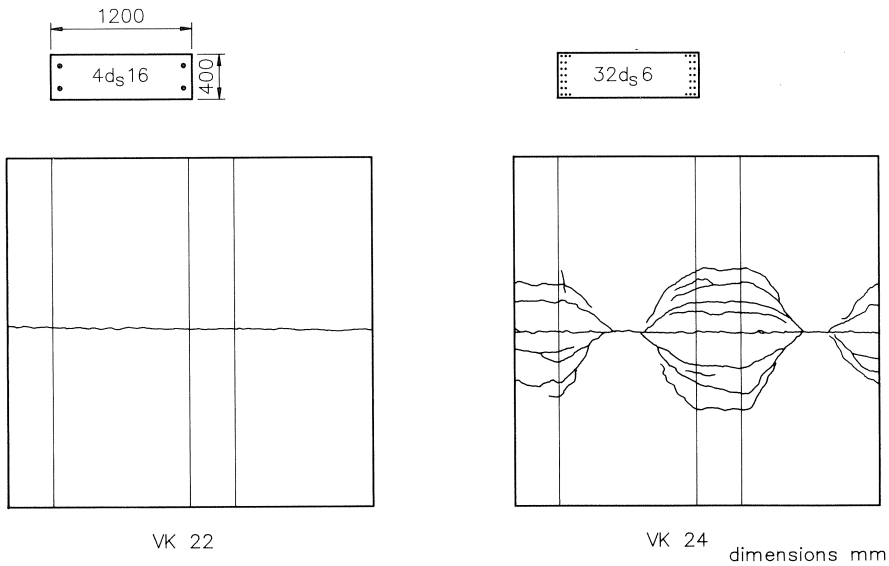
Fig. 3.4   Crack patterns of two specimens tested by Helmus [1989].

3.2.2   Theoretical models

According to Leonhardt [1976a-b, 1985] the theory of the "effective concrete area", as used for the prediction of crack widths and crack spacings at the level of the main reinforcement in beams, can be extended to tensile members, see Figs. 3.5a and b. This figure presents the crack pattern of a concrete wall, 1.5 m thick and 90 m in length. The reinforcement ratio was only $0.30 * 10^{-2}$. The wall was not provided with expansion joints. Fig. 3.5b shows the definition of the "effective concrete area". The crack width at the side faces of the structure can now be calculated according to classical theories for tensile members, see section 2.2.1. The definition of the "effective concrete area" introduced by Schiessl and Wölfel [1986] was also used for these types of structures, see Fig. 3.5c.
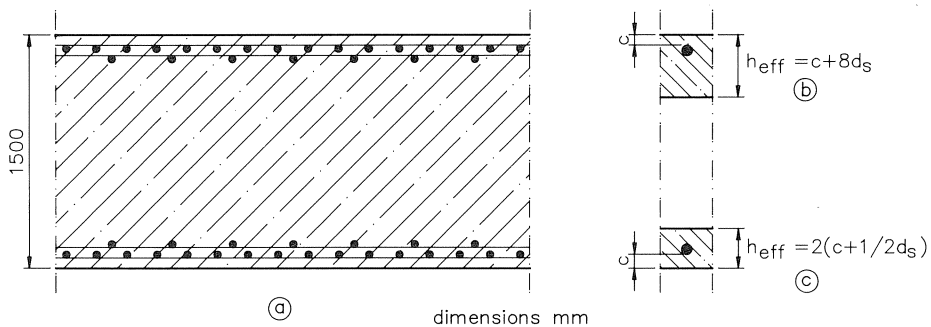
Fig. 3.5   The crack pattern of a 1.5 m thick concrete wall (a) and the definitions of the "effective concrete area" according to Leonhardt [1985] (b) and Schiessl and Wölfel [1986] (c).

23
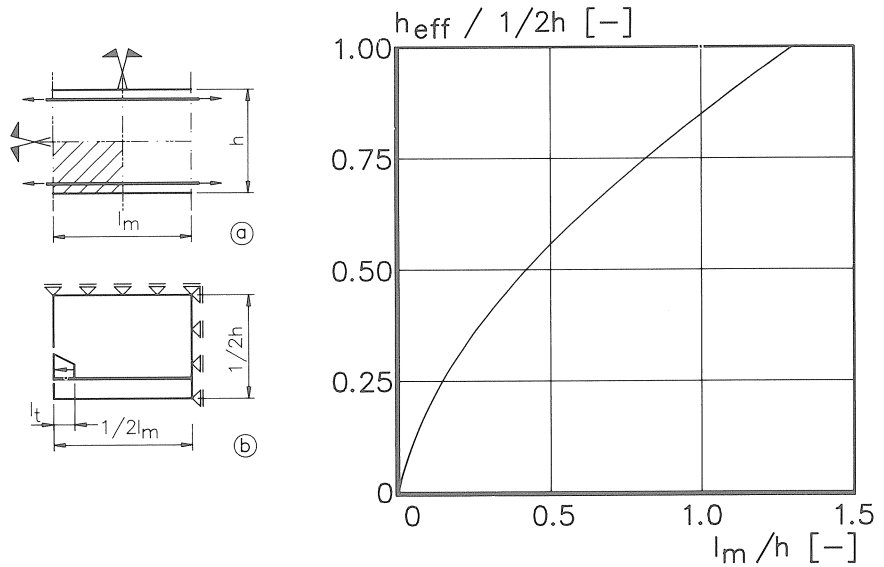
Fig. 3.6 Part of a tensile member analysed (a and b) and the "effective concrete area" depending on the mean crack spacing (c) [Henning, 1987].

Henning [1987] performed FE-analyses to define the "effective concrete area" for tensile members up to 1 m thick. The part of a member located between two cracks was investigated, see Fig. 3.6a. Because of symmetry only one quarter of the specimen was modelled, see Fig. 3.6b. The bond forces were introduced as a linearly varying line load over $l_t = 0.1h$. At the vertical axis of symmetry the part of the section loaded in tension was registered and denoted as h_{eff}. Fig. 3.6c presents h_{eff} in relation to the crack spacing. The curve can be represented by the following formula [Henning, 1987]:

$$\frac{h_{eff}}{\frac{1}{2}h} = 0.42 \left(\frac{l_m}{b}\right)^{0.63} \quad [-] \tag{3.1}$$

for $h \leq 1$ m.

Henning [1987] found that the mean crack widths and spacings at the position of the reinforcement could be calculated by classical theories (eqs. (2.3) to (2.5)) if h_{eff} was calculated in analogy to Leonhardt's approach [CEB, 1978], see Fig. 3.7.

The results of the FE-analyses performed by Fehling and König [1988] (see Figs. 2.7 and 2.8) can also provide information with regard to tensile members since some of the calculations were performed without compressive force $(N_c/N_\tau = 0)$. From the curve presented in Fig. 2.8 the following relation for the height of the "effective concrete area" can be derived:

$$h_{eff} = \left(2.3 + 5.2\,\frac{l_{sec}}{h}\right)(h - d) \leq 4(h - d) \quad [mm] \tag{3.2}$$

24
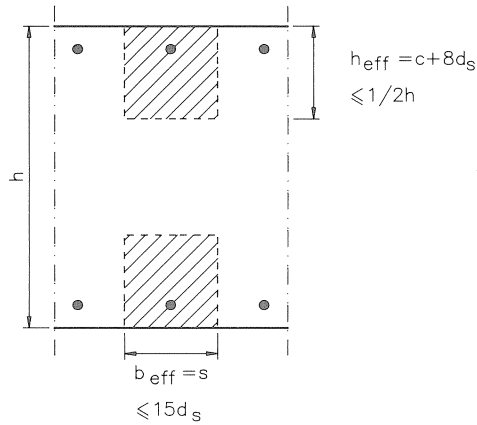
Fig. 3.7   Definition of the "effective concrete area" [Henning, 1987].

Fig. 3.8 presents the principal tensile stresses caused by the transition of bond stresses between the concrete and the reinforcement [Langhout, 1988]. This figure demonstrates that the part of the panel where high tensile stresses occur is restricted to a limited area around the reinforcement. Langhout [1988] found that the total area in tension is defined by an angle $\alpha \simeq 60°$, see Fig. 3.8. This is in accordance with the findings of e.g. Krips [1985] and Henning [1987]. Therefore, Braam and Langhout [1988] assumed that secondary cracking occurs at the end of the transfer length l_t in cases where the mean concrete tensile stress over the concrete area defined by $\alpha = 60°$ equals the mean concrete tensile strength. Helmus [1989] stated that, for the cracking criterion, $\alpha = 30°$ suffices. However, in the following it will be demonstrated that in this way only rather poor agreement with Helmus' [1989] results is obtained. Therefore, a model was introduced that is based on the maximum tensile stresses that occur in a concrete panel loaded by bond forces at the centre of gravity of the main reinforcement, see Fig. 3.9a [Braam, 1990b]. This model will be presented in this section.
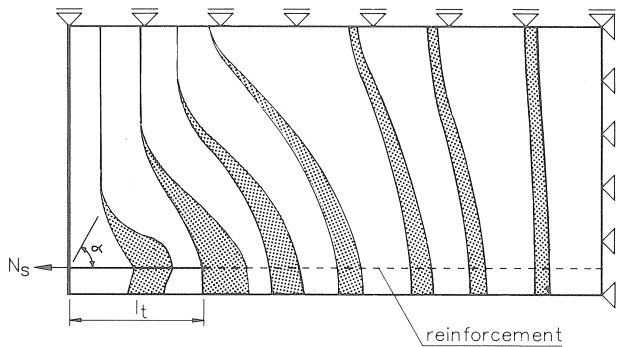
Fig. 3.8   Principal tensile stresses in a concrete panel loaded by bond forces [Langhout, 1988].

25

Linear-elastic FE-calculations demonstrated that the maximum tensile stress $\sigma_{cx,max}$ caused by a force dF_τ at a distance x_1 from the edge, can be calculated according to:

$$\sigma_{cx,max} = \frac{dF_\tau}{b1.5(x - x_1)} \quad \text{[MPa]} \tag{3.3}$$

with $x > x_1$ and $1.5(x - x_1) \leq 2.0(h - d)$.
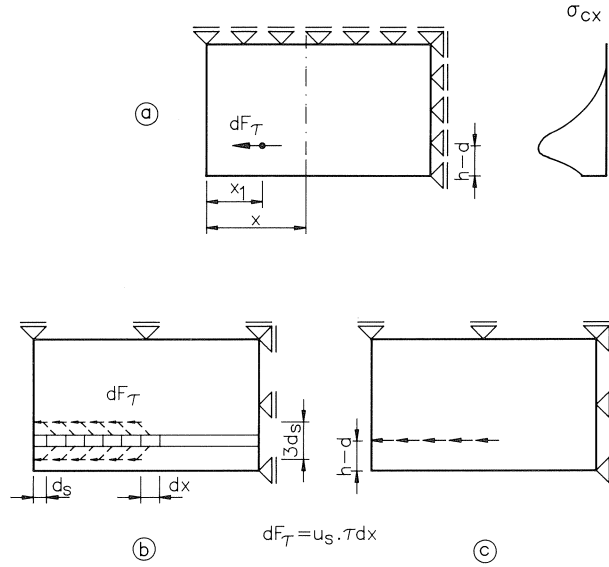
Fig. 3.9 Concrete panel loaded by bond forces: (a) concentrated load, (b) position of the loads outside the slip layer and (c) schematization.

In fact, the bond stresses are transmitted to the concrete by local forces at the bar ribs [e.g. Rehm, 1961; Goto, 1971]. The slip layer where this phenomenon takes place is assumed to be as thick as the bar [e.g. Dragosavic et al., 1981; Vos, 1983]. Therefore, the panel is loaded by two line loads, spaced at $3d_s$, see Fig. 3.9b. A bond-free length of d_s is assumed. When combining the two line loads, the situation presented in Fig. 3.9c is obtained. On the basis of these assumptions the maximum concrete tensile stress at the level of the reinforcement is now calculated by:

$$\sigma_{cx,max} = \frac{dF_\tau}{b\{3d_s + 1.5(x - x_1)\}} \quad \text{[MPa]} \tag{3.4}$$

with $x > x_1$ and $3d_s + 1.5(x - x_1) \leq 2.0(h - d)$.
In the analyses, the two-dimensional state of stress was investigated. In reality, the forces spread three-dimensionally in the structure, which means that the bar spacing

26

must also be taken into account. The bar spacing is incorporated in correspondence with formula (3.5):

$$\sigma_{cx,max} = \frac{dF_\tau}{h_1 b_1} \quad [\text{MPa}] \tag{3.5}$$

with

$$h_1 = 3d_s + 1.5(x - x_1) \leq 2(h - d)$$
$$b_1 = 3d_s + 1.5(x - x_1) \leq s$$
$$x \geq x_1$$

The concrete tensile stress $\sigma_{cx,max}$ at a certain point can now be calculated by the summation of the stresses caused by the individual bond forces dF_τ.
Helmus' [1989] test results were used to make some adjustments in the model.
This resulted in the following two assumptions [Braam, 1990b]:
- a secondary crack occurs if $\sigma_{cx,max} = 2f_{ctm,0}$;
- bond forces dF_τ which are situated at a distance smaller than 30 mm from the position considered must not be used for the calculation of $\sigma_{cx,max}$.

The secondary crack spacing is found by calculating the summation of $\sigma_{cx,max}$ for several values of $x = i * dx$:

$$\sum_{i=\frac{30\text{ mm}}{dx}}^{k} \frac{dF_\tau}{h_1 b_1} = 2f_{ctm,0} \quad [\text{MPa}] \tag{3.6}$$

with:

$$dF = u_s \tau_b \, dx$$
$$\tau_b = 2f_{ctm,0} \quad [\text{Fehling/König, 1988}]$$
$$h_1 = 3d_s + 1.5i * dx \leq 2(h - d)$$
$$b_1 = 3d_s = 1.5i * dx \leq s$$

The secondary crack spacing $l_{sec} = k * dx$ is found if the formula (3.6) is met for a certain "k". In Fig. 3.9 it was assumed that there is only one layer of main reinforcement. If more than one layer is used, then $2(h - d)$ in formulae (3.3) to (3.6) is divided by the number of layers.
It is now possible to distinguish four different approaches with regard to the steel stress initiating secondary cracking, viz:

$$\sigma_{s,sec} = \frac{s h_{eff} f_{ctm,0}}{\frac{1}{4}\pi d_s^2} + n f_{ctm,0} \quad [\text{MPa}] \tag{3.7a}$$

with:

$$l_{sec} = s_0 + \frac{s h_{eff} f_{ctm,0}}{\pi d_s \tau_b} \quad [\text{mm}] \tag{3.8a}$$

$$h_{eff} = c + 8d_s \qquad [\text{Martin et al., 1980}] \quad [\text{mm}] \tag{3.9a}$$

27

$$h_{\text{eff}} = \alpha(h - d) \qquad \text{[Eurocode 1990; Fehling/König, 1988]} \qquad (3.9b)$$
$$\text{[mm]}$$

$$h_{\text{eff}} = h - d + l_{\text{sec}} \tan 30° \quad \text{[Helmus, 1989]} \quad \text{[mm]} \qquad (3.9c)$$

$$\sigma_{\text{s,sec}} = \frac{\pi d_s \tau_b (l_{\text{sec}} - s_0)}{\frac{1}{4}\pi d_s^2} + n f_{\text{ctm,0}} \quad \text{[MPa]} \qquad (3.7b)$$

with:

$$l_{\text{sec}} = k \, dx \quad \text{[mm]} \qquad (3.8b)$$

$$h_{\text{eff}} = \frac{\pi d_s \tau_b (l_{\text{sec}} - s_0)}{s f_{\text{ctm,0}}} \quad \text{[Braam, 1990b]} \quad \text{[mm]} \qquad (3.9d)$$

For all 12 specimens tested by Helmus [1989], h_{eff}, $\sigma_{\text{s,sec}}$ and l_{sec} were calculated according to the four different approaches presented in formulae (3.9a-d), (3.7a-b) and (3.8a-b). The coefficient α in formula (3.9b) was based both on a constant value ($\alpha = 2.5$; Eurocode 1990) and on a value depending on the crack spacing (formula (3.2); Fehling and König).

Table 3.1 presents the results of the four different approaches. In this table no experimental results are presented for specimen VK 22 since the crack patterns reported by Helmus [1989] made it clear that secondary cracking did not occur, see Fig. 3.10. All the experimental results listed in Table 3.1 are deduced from the crack patterns and the experimental data presented by Helmus.

From Table 3.1 it follows that the average crack spacing at the position of the reinforcement can be calculated with good accuracy using all the classical cracking theories (Martin et al. [1980], Fehling and König [1988] and the Eurocode 1990). Helmus' [1989] model produces results with a large coefficient of variation. Braams' [1990b] model fits closest to the experiments. This is not surprising since some of the parameters applied
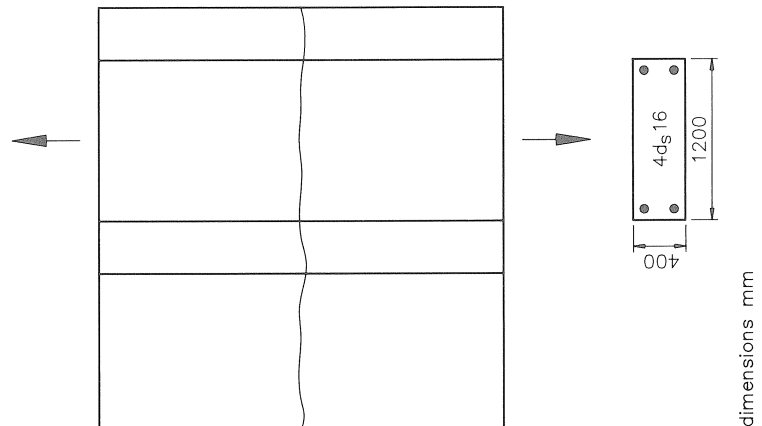

Fig. 3.10   Crack pattern of the specimen VK 22 [Helmus, 1989].

28

Table 3.1 Height of the "effective concrete area" h_{eff}, steel stress initiating secondary cracking $\sigma_{s,sec}$ and secondary crack spacing l_{sec}

specimen	d_s [mm]	s [mm]	h [mm]	$h-d$ [mm]	$f_{ctm,0}$ [MPa]	f_{ccm} [MPa]	h_{eff} [mm] (1)	(2)	(3)	(4)	(5)	$\sigma_{s,sec}$ [MPa] (1)	(2)	(3)	(4)	(5)	l_{sec} [mm] (1)	(2)	(3)	(4)	(5)	experiments $\sigma_{s,sec}$ [MPa]	l_{sec} [mm]
VK 11	12	80	800	70	1.70	22.4	160	231	175	182	291	204	290	222	231	350	220	257	347	193	310	372	280
12	12	100	800	70	1.70	22.4	160	266	175	303	285	252	412	275	468	429	262	365	421	402	380	454	318
13	6	40	800	65	1.70	22.4	125	176	163	94	304	162	223	207	125	366	116	99	188	50	162	380	169
14	6	57	800	65	1.70	22.4	125	189	163	116	292	227	336	291	211	502	145	149	247	88	222	473	176
21	16	100	1200	70	1.92	35.5	190	210	175	165	295	195	214	181	171	281	239	225	329	165	295	389	330
22	16	200	1200	70	1.92	35.5	190	280	175	600	270	376	548	348	1160	516	428	573	607	1194	540	–	–
23	6	57	1200	100	2.17	26.6	245	284	263	149	444	373	430	399	232	649	174	149	262	75	225	425	190
24	6	57	1200	75	2.17	26.6	195	230	213	138	376	389	456	423	280	721	179	158	275	92	250	480	195
31	20	80	2000	80	2.09	31.4	230	208	200	127	342	137	125	121	82	182	196	152	254	81	220	270	410
32	20	200	2000	80	2.09	31.4	230	272	200	1000	309	321	377	281	1346	412	416	453	559	1593	495	398	500
33	20	67	2000	80	1.51	19.7	190	200	200	108	374	95	100	0100	58	167	134	100	191	48	167	196	225
34	12	67	2000	60	1.51	19.7	150	156	150	123	258	145	149	144	120	230	183	150	262	109	230	446	233
theory/exp.:												0.57	0.70	0.60	0.75	0.98	0.77	0.75	1.15	0.75	1.02		
$(n=11)$cv:												0.29	0.31	0.29	1.14	0.31	0.17	0.29	0.21	1.10	0.22		

Specimens according to Helmus [1989]
(1): Martin et al. [1980]
(2): Fehling/König [1988]
(3): Eurocode [1990]
(4): Helmus [1989]
(5): Braam [1990b]

29

in the model were tuned to Helmus' experimental results. However, it is the only model that takes into account the three-dimensional spreading of the stresses. All the other models presented only consider the "effective height", whereas the bar spacing is only accounted for by the condition $s \leq 15d_s$. As early as the seventies, Leonhardt [1976b] had pointed to the influence of the bar spacing. He stated that not only the crack widths and spacings but also the minimum reinforcement in thick concrete members can be calculated on the basis of the "effective concrete area" provided that rather small bar spacings of 50–100 mm are applied. The results presented in Table 3.1 support this statement, since the steel stress initiating secondary cracking $\sigma_{s,sec}$ increases considerably with an increasing ratio of s/d_s.

Taking the experimental results as a basis, Helmus advised the use of

$$h_{eff} = 5.3(h - d) \quad [\text{mm}] \tag{3.10}$$

for tensile members between 800 and 2000 mm thick. This relation presents a mean ratio between the theoretical and the experimental results of 1.27 (cv = 0.30, $n = 11$) and 1.15 (cv = 0.37, $n = 11$) for the secondary crack spacing l_{sec} and the steel stress $\sigma_{s,sec}$ respectively. The correspondence with the experimental results is rather good, but relation (3.10) takes no account of the influence of the bar spacing.

From the experiments performed by Fellman/Menn [1981], Hartwich/Rostásy [1984] and Henning/Rostásy [1990] a total of 8 tensile specimens were selected and analysed with the proposed model. All the specimens selected were provided with reinforcement located at the side-faces. With regard to the secondary crack spacing at the position of the reinforcement, a mean ratio of 1.07 (cv = 0.25) was obtained between the theoretically calculated and experimentally observed values.

3.3   Reinforced concrete deep beams

In this section the main conclusions from experiments on deep beams are presented. Most attention is focused on the crack pattern (i.e. crack spacing and crack width) in the web and at the level of the main reinforcement. The reader is referred to De Groot [1989] for a more extensive survey; in this section only the main results are presented.

3.3.1   Experimental results

Borges and Lima [1960] performed experiments on 14 reinforced concrete beams. The basic type of specimen is presented in Fig. 3.11. The web was provided with 6mm diameter bars, spaced at 200 mm. This web reinforcement was situated in only one half of the beam. The main aim of the research was to investigate the applicability of cracking theories in the case of specimens reduced to scale. For this purpose the beam presented in Fig. 3.11 was reduced to scales 1/2.5 and 1/4. The mean crack spacing was recorded at middle height of the web and at the level of the main reinforcement. From the results of 9 beams the ratio between the two crack spacings was found to be 3.9 (c.v. = 0.5) [De Groot, 1990]. Furthermore, it was observed that the crack pattern was unaffected by the
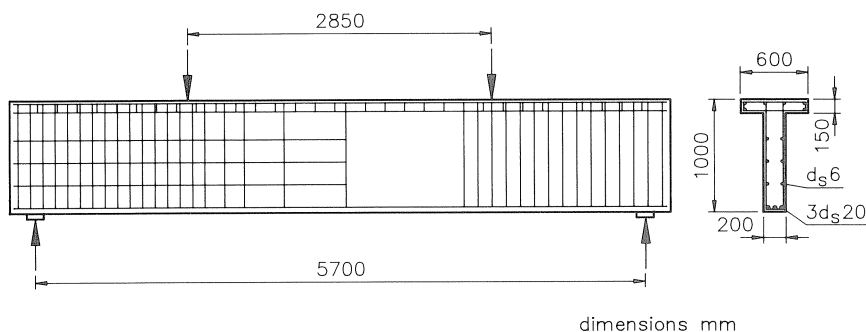
30

Fig. 3.11   Cross-section and loading scheme of basic beam [Borges and Lima, 1960].

web reinforcement. Fig. 3.12 presents a typical crack pattern. The other 5 specimens were used for analysing the influence of bottom concrete cover. It appeared that the ratio between both crack spacings decreased at increasing concrete cover. This finding is not surprising since the increasing height of the "effective concrete area" reduces the part of the web where the crack pattern is unaffected by the main reinforcement.

Beeby [1971] performed tests on 5 T-beams reinforced with two 22 mm diameter bars. The cross-sections of the four types of beams are presented in Fig. 3.13a. The beams were tested upside down in four-point bending, see Fig. 3.13b. The crack widths and crack spacings were measured at 8 different levels, see Fig. 3.14a. Fig. 3.14b shows a typical example of the variation of average crack width down the side of a beam. It was observed that the crack pattern was unaffected by the web reinforcement. However, the stirrups acted as crack inducers. The ratio between the crack spacing halfway down the web and at the main reinforcement was 4.5 (c.v. = 0.9) [De Groot, 1990].

Soretz and Colonna-Ceccaldi [1971] presented the results of tests performed on 6 reinforced concrete beams. The main reinforcement consisted of $2 * d_s$ 40, $5 * d_s$ 25 or $6 * d_s$ 16 + $4 * d_s$ 20 mm bars. The beams were loaded in four-point bending, see Fig. 3.15. The main subject of interest was the amount of web reinforcement required to obtain equal maximum crack widths in the web and at the level of the main reinforcement. It was shown that a web reinforcement amounting to at least 0.25% of the cracked area of concrete above the main reinforcement must be applied at both sides of the web. No definite conclusions could be derived with respect to the bar diameter and the bar
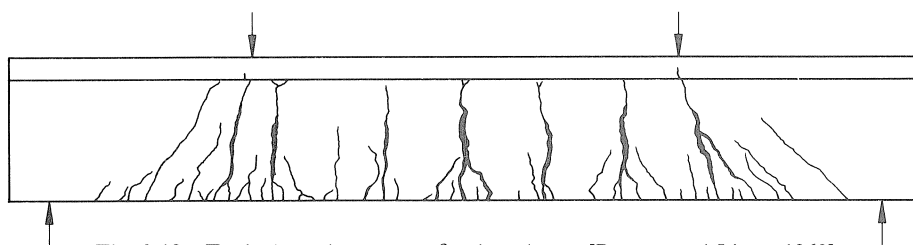
Fig. 3.12   Typical crack pattern of a deep beam [Borges and Lima, 1960].

31
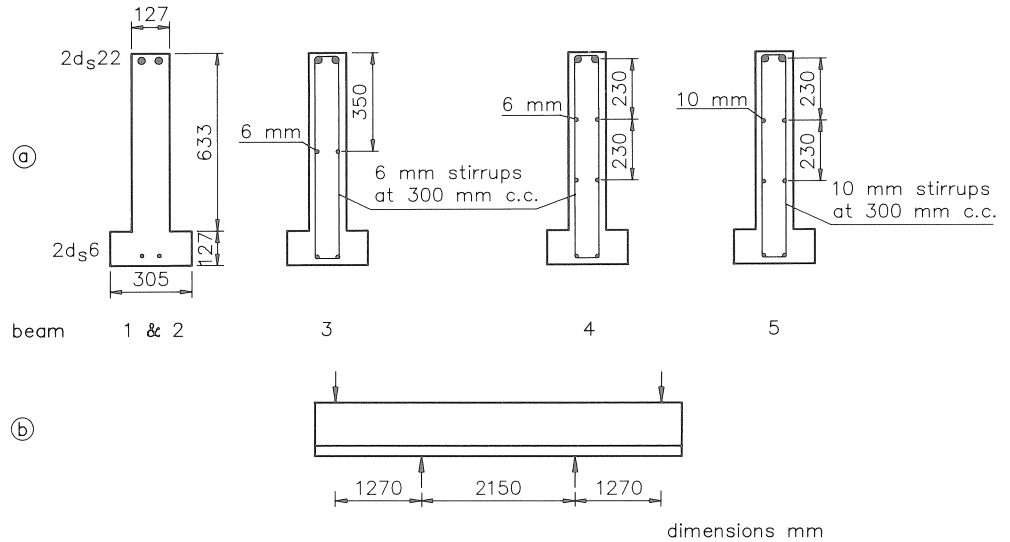
Fig. 3.13 Cross-section (a) and loading scheme (b) [Beeby, 1971].

spacing. However, on the basis of their experimental results, Soretz and Colonna-Ceccaldi [1971] concluded that two bars per side concentrated at the lower third part of the cracked zone will suffice. With regard to the crack spacing they found that where no web reinforcement was applied, the crack spacing at middle-height of the beam amounted 3 to 5 times the crack spacing at the main reinforcement.

Leonhardt [1974] presented the crack pattern of a T-beam loaded by 10 concentrated loads. The loading scheme and the cross-section are presented in Fig. 3.16. The beam was heavily reinforced with $4d_s$ 26 mm bars. A total of 4 bars of only 4 mm diameter were placed in the web. The crack pattern at the side face (see Fig. 2.5) was unaffected by this reinforcement. Leonhardt [1974] stated that in cases where tension zones exceed
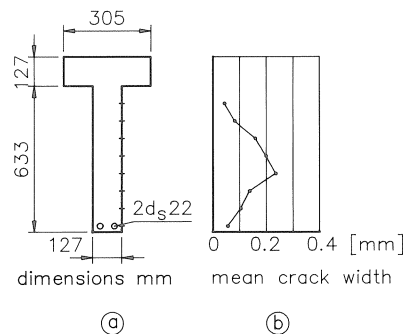
Fig. 3.14 Measuring points for crack width (a) and average crack width down the side face of a beam (b) $\left(\varepsilon_{sm} = 1.34 * 10^{-3}\right)$ [Beeby, 1971].

32
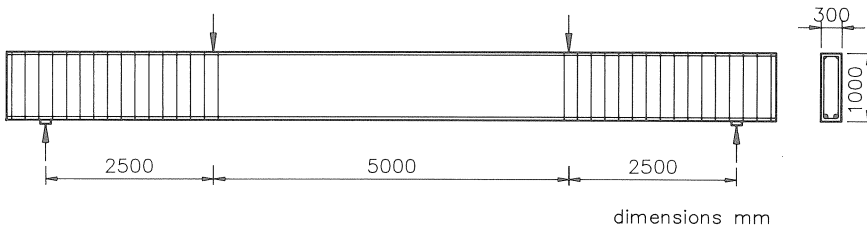
Fig. 3.15   Cross-section and loading scheme [Soretz and Colonna-Ceccaldi, 1971].

500 mm in height, the crack spacing in the web can expected to be 3 to 4 times as large as the crack spacing at the main reinforcement. This statement holds for the case in which no or too little web reinforcement is applied. The T-beam will be analysed in more detail in chapter 4 by using the FEM.

The most extensive research on deep beams was carried out by Breen and Frantz [1978, 1980a]. They performed tests on 44 T-beams ranging from 618 to 1235 mm in height. A 1830 mm long beam segment was cast and loaded by a constant bending moment. This moment was applied by the combination of a tensile force on the main reinforcement and a compressive force on the flange. The main parameters investigated were:

– amount, location and distribution of the web reinforcement;
– web width;
– concrete cover;
– beam height.

Only cracks found in the middle 1220 mm of the specimen were measured. The reason for this was to eliminate possible localized effects of the loading system.

Fig. 3.17 presents the effect of the web reinforcement on the crack profile of four beams with the same main reinforcement. One beam contained only main reinforcement. The other three beams were all provided with the same amount of web reinforcement, viz. 567 mm^2. This figure clearly demonstrates that the reinforcement was most effective when a large number of closely spaced bars were used. This finding is not surprising since it was already known from existing cracking theories.
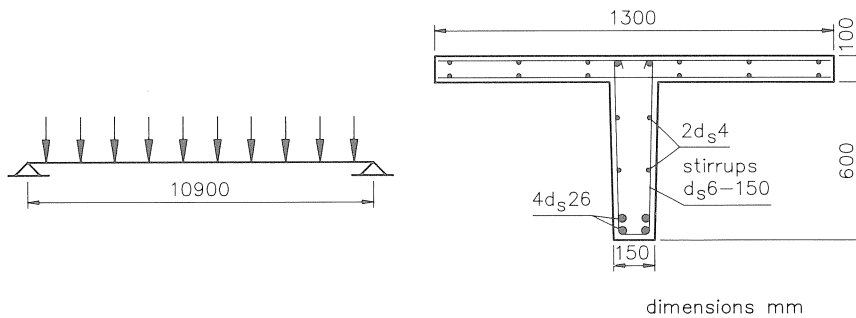
Fig. 3.16   Loading scheme and cross-section of T-beam [Leonhardt, 1974].

33
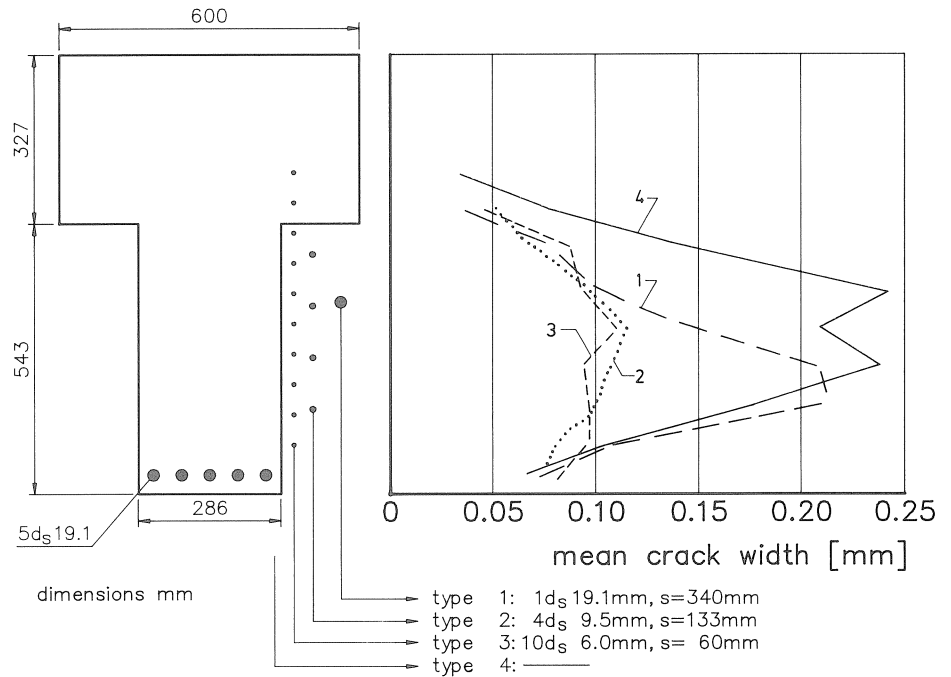
Fig. 3.17 Influence of web reinforcement on the crack width down the side face of a deep beam [Breen and Frantz, 1978].

The web width was 197, 286 or 432 mm. For some of the specimens the main reinforcement was designed to produce the same maximum crack width at this level. Fig. 3.18 presents the effect of web width on the mean web crack width for specimens without web reinforcement and specimens with $2 * 4d_s$ 9.5 mm (bar spacing 105 mm; concrete cover 29 mm). This figure clearly demonstrates that the web width had no significant influence on the web crack width. The same conclusion holds for the crack pattern. It even appeared that web reinforcement along one of the sides does not significantly affect the crack widths on the opposite side face [Breen and Frantz, 1978]. These findings are in accordance with existing cracking theories based on the "effective concrete area", i.e. the reinforcement is only effective in controlling crack widths in a narrow strip of concrete.

In four of the beams with a 286 mm web width, the dimensions and the reinforcement were the same, except for the concrete cover, see Fig. 3.19a. The cover was 19.1, 38.1, 50.8 and 76.2 mm respectively. The ratio between the maximum crack width in the web and at the level of the main reinforcement was found to increase with increasing concrete cover, see Fig. 3.19b. The following relation was derived for steel stresses ranging from 207 to 276 MPa:

$$\frac{w_{\max} \text{ web}}{w_{\max} \text{ bottom}} = 0.50(c)^{0.30} \quad [-] \tag{3.11}$$

34
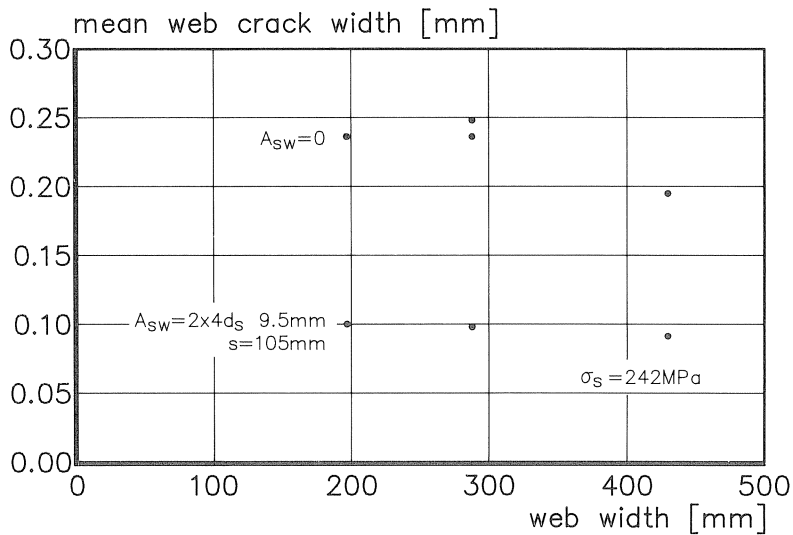
Fig. 3.18   Influence of web width on the web crack width [Breen and Frantz, 1978].

With regard to beam height Breen and Frantz used Beeby's [1971] theory to predict the average web crack width in beams without web reinforcement. Good agreement with experimental results was obtained.

Breen and Frantz derived formulae to calculate the amount of web reinforcement required to obtain a 0.20 mm maximum crack width in the web provided that the crack width at the level of the main reinforcement is 0.14 mm. These formulae are presented in section 3.3.2.
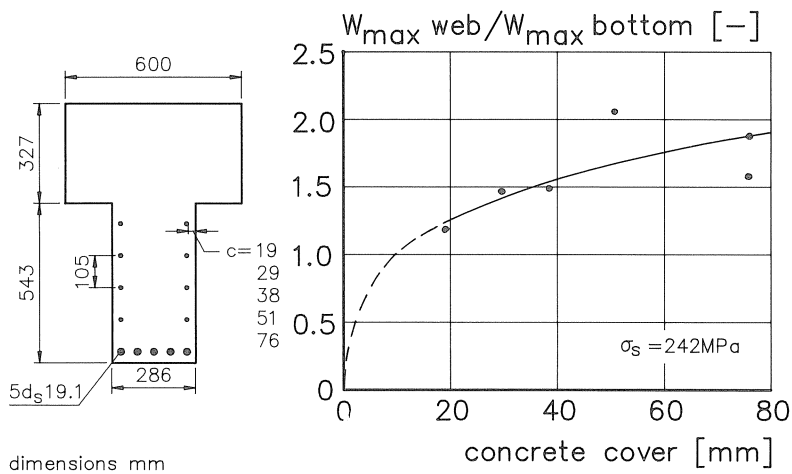
Fig. 3.19   The dimensions of the beams (a) and the influence of concrete cover on the web crack width (b) [Breen and Frantz, 1978].

35

3.3.2 Theoretical models

Beeby [1971] presented formulae describing crack width and crack spacing along the side of deep beams. These formulae were originally derived to present the crack pattern in plates reinforced with widely spaced bars [Beeby, 1972]. Beeby's formulae for deep beams were based on the interpolation between two crack widths, viz. the crack width directly over a reinforcing bar (w_0) and the crack width related to the initial crack height (w_{lim}):

$$w = \frac{a_{\text{cr}} w_{\text{lim}} w_0}{c w_{\text{lim}} + (a_{\text{cr}} - c) w_0} \quad \text{[mm]} \tag{3.12a}$$

in which:

$$w_{\text{lim}} = k_1 h_{\text{cr}} \varepsilon_{\text{m}} \quad \text{[mm]} \tag{3.12b}$$

$$w_0 = \left(k_1 c + k_2 \tfrac{1}{2} c_2 \sqrt{c_1/c_2} \, \frac{c}{d_{\text{s}}} \, e^{-4c/h_{\text{cr}}} \right) \varepsilon_{\text{m}} \quad \text{[mm]} \tag{3.12c}$$

ε_{m} = mean strain at the level considered [−]
c = minimum concrete cover [mm]
h_{cr} = initial crack height [mm]
c_1, c_2 = maximum and minimum average concrete covers surrounding a bar in an equivalent prism of concrete, see Fig. 3.20 [mm]
a_{cr} = distance from the point considered to the surface of the nearest reinforcing bar [mm]

The coefficients k_1 and k_2 depend on the required probability of the calculated crack width being exceeded, see Table 3.2.

Table 3.2   Values of coefficients k_1 and k_2 in equations (3.12b-c).

probability of exceedence	k_1 [−]	k_2 [−]
50%	1.33	0.8
20%	1.59	1.4
10%	1.76	2.1
5%	1.86	2.6
2%	1.94	3.0

Fig. 3.21 presents the average crack width down the side face of a beam. Both experimental [Beeby, 1971] and theoretical results (formulae (3.12a-c)) are shown.
Beeby also presented the following formula for the average crack spacing at a certain level along the side face of a beam:

$$l_{\text{m}} = \frac{w_{\text{m}}}{\varepsilon_{\text{m}}} + \frac{0.05}{\varepsilon_{\text{m}}} \, e^{-0.0135 a_{\text{cr}}} \quad \text{[mm]} \tag{3.13}$$
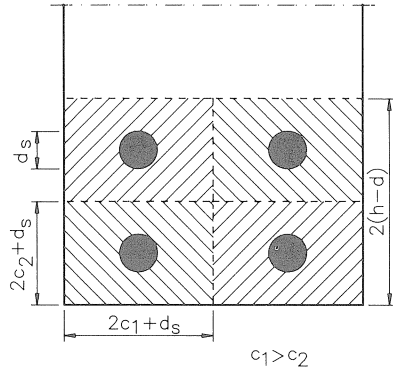
Fig. 3.20 Equivalent prism of concrete surrounding a reinforcing bar [Beeby, 1972].

For the two identical beams 1 and 2 the experimental and the theoretical results are both presented in Fig. 3.22.

It was shown that Beeby's theories are suitable for describing the crack width along the side face of deep beams. However, no information was presented with regard to the amount of web reinforcement required to obtain a well distributed crack pattern.

Breen and Frantz [1978] used their experimental results and FE calculations to derive design rules. From the experiments (see section 3.3.1) it followed that the web reinforcement must be related to an "effective concrete area". In accordance with the findings of Gergely and Lutz [1968] the approach presented in Fig. 3.23 was used. For a maximum crack width of 0.14 and 0.20 mm at the level of the main reinforcement and
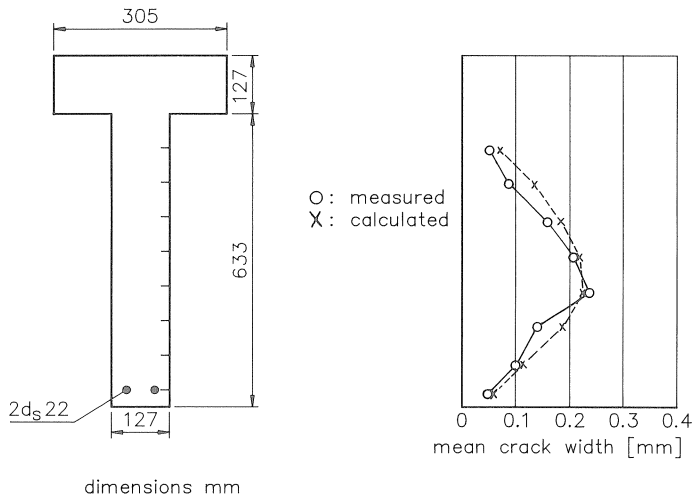
Fig. 3.21 Experimental and theoretical mean crack width at the side face of a deep beam [Beeby, 1971].

37
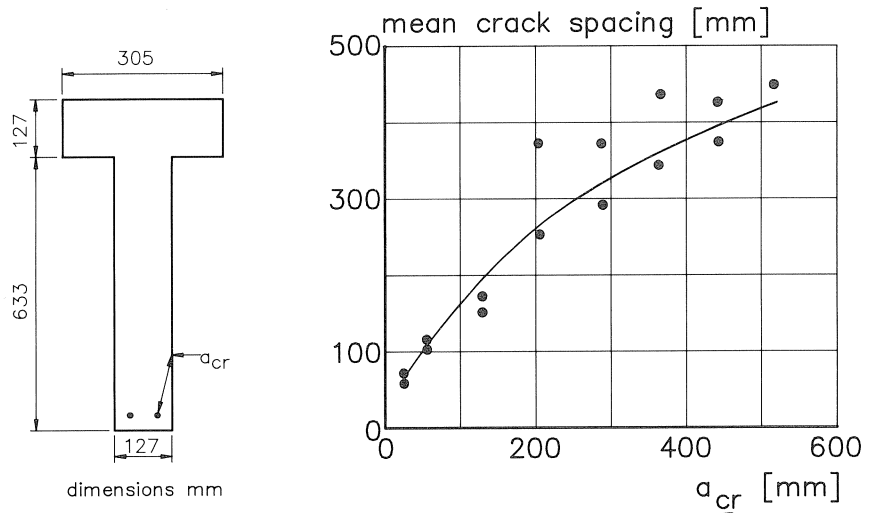
Fig. 3.22 Calculated and experimental mean crack spacing at several levels of a deep beam [Beeby, 1971].

the side face respectively, they derived the following formulae for the web reinforcement ratio:

$$\varrho_{\text{eff}} = 23 * 10^{-6}(h_t - 280) \qquad h_t \leq 1020 \text{ mm} \quad [-] \qquad (3.14a)$$

$$\varrho_{\text{eff}} = 0.0011 + 5.9 * 10^{-6} h_t \qquad h_t \geq 1020 \text{ mm} \quad [-] \qquad (3.14b)$$

h_t = tension depth, i.e. the distance between the neutral axis and the main reinforcement
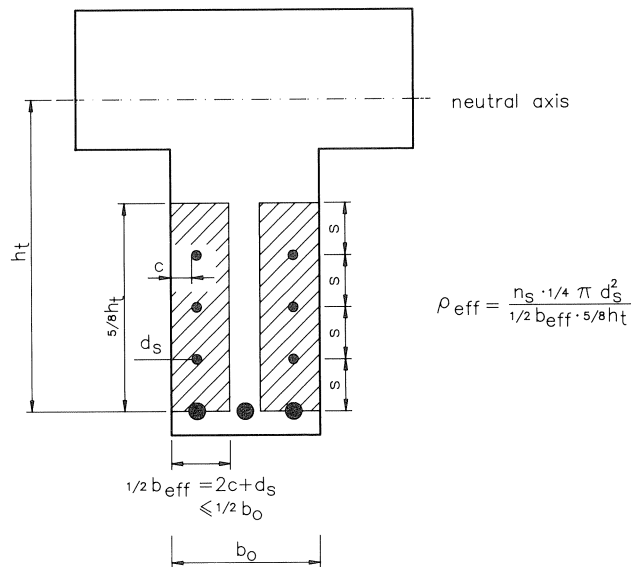
Fig. 3.23 Definition of the web reinforcement ratio [Breen and Frantz, 1978].

38

The web reinforcement is most effective when distributed as small bars. Generally, it is sufficient if four bars are distributed along each side in about 5/8 of the tension zone closest to the main reinforcement. It should be emphasized that formulae (3.14a-b) are only applicable in the case of maximum crack widths at the level of the main reinforcement and in the web of 0.14 and 0.20 mm respectively.

De Groot [1990] analyzed the experimental results with regard to crack spacings. From the results on specimens without or with too little web reinforcement it was concluded that the mean ratio between the mean crack spacing in the web and at the level of the main reinforcement was 3.5 (c.v. = 0.8; 18 results).

The CEB [1985] presented tables from which the amount of web reinforcement can be read off immediately; the bar diameter is related to the web width and the bar spacing depends on the concrete quality and the allowable characteristic crack width, see Table 3.3. If these requirements are met, no detailed crack control is needed. This statement implies that the amount of web reinforcement deduced from Table 3.3 is on the conservative side.

Table 3.3   Web reinforcement according to the CEB [1985]

web width [mm]	≤ 150		150–300		≥ 300
bar diameter [mm]	≥ 10		≥ 12		≥ 16
concrete quality		B25		B45	
char. crack width [mm]	0.2	0.4	0.2		0.4
bar spacing [mm]	150	250	100		150

3.4   *Conclusions*

From the experimental and theoretical results presented in chapter 3 it is clear that the crack pattern at the level of the main reinforcement of deep beams can be calculated according to existing theories. However, in the case of relatively wide bar spacings, i.e. in thick walls, the classical theories present too small values for the "effective concrete area". Therefore, a new theoretical model introduced by Langhout [1988] and Helmus [1989] was presented.

With regard to the crack pattern in the web of deep beams Beeby [1971] presented formulae for the crack width and the crack spacing along the side face for the case in which no web reinforcement was applied.

However, the amount of design rules for the web reinforcement was found to be rather scarce. Though Breen and Frantz [1978] did present rules, these were only applicable for specific cases. The CEB [1985] presented tables for the detailing of web reinforcement. However, the amount of reinforcement required according to these tables is rather conservative. From an economical point of view a more consistent approach seems desirable. With regard to crack spacing it can be concluded that, for the experimental values available, the crack spacing at the concentrated reinforcement is about $\frac{1}{4}$ of the crack spacing in the unreinforced part of the specimen. This conclusion holds for beams and tensile members [De Groot, 1990].

4 FE analysis of deep beams; "smeared crack approach"

4.1 *Introduction*

In the following two sections the cracking behaviour of deep beams is analyzed by the use of the FEM program DIANA [De Borst et al., 1984]. At first a small section of a beam [Leonhardt, 1974] is considered. The influence of web reinforcement on the crack pattern is presented. In the third section attention is focused on the over-all structural behaviour of deep beams. Some conclusions with respect to the crack pattern and steel stresses are also presented.

4.2 *Study in detail*

Leonhardt [1974] presented the crack pattern of a deep T-beam. The cross-section and the crack pattern are presented in Fig. 4.1 (see also Figs. 2.5 and 3.16). From this figure it follows that the mean web crack spacing is 240 mm. Because of symmetry only a part with a length of 120 mm was modelled (Figs. 4.1 and 4.2) and the right edge was kept straight by "tying" the horizontal displacements. The primary crack was modelled as a strip of 10 mm wide elements with a slightly reduced tensile strength. All the concrete elements were eight-noded plane stress elements, numerically integrated by a $3*3$ Gaussian integration scheme. The reinforcement was represented by bar elements connected to the concrete by springs with a multi-linear force-displacement curve according to Bruggeling's [1987] bond stress-slip curve. Over the "primary crack elements" no bond was assumed.

Since no detailed information was available on the material properties, the following realistic material parameters were assumed for the concrete:

$(f_{ccm} = 35$ MPa$)$, $E_c = 30500$ MPa, $f_{ct} = 2.6$ MPa, $G_f = 0.070$ N/mm.

For the "primary crack elements" the last two parameters were reduced to 2.3 MPa and 0.060 N/mm respectively.

Since the "smeared crack approach" was used, the width of the crack band had to be defined [Rots, 1988]. Half the width of the elements was chosen; for the elements on the
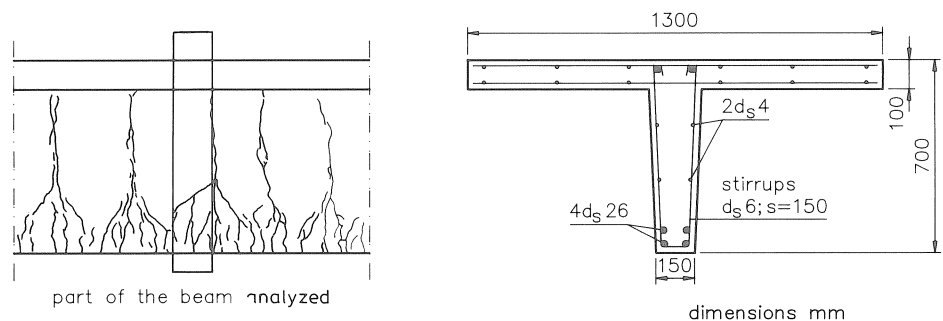
Fig. 4.1   Crack pattern and cross-section of a deep T-beam [Leonhardt, 1974].

40

axes of symmetry this value was doubled. For the softening of concrete in tension the curve presented by Cornelissen et al. [1986] was used.

In the first analysis only the main reinforcement was modelled. Fig. 4.3a presents the crack pattern at several loading stages. The deformed mesh is also presented (500 times enlarged). From the analysis it appeared that at first the primary crack propagated through the web of the beam. At the same instant the reinforcement was stressed. The resulting bond stresses initiated cracking in the concrete at the level of the reinforcement, close to the primary crack. These cracks developed rapidly towards the axis of symmetry where a new dominant crack arose. With increasing load this crack propagated vertically through the web. At some distance from the reinforcement the crack deflected towards the primary crack. This proves that secondary cracking is restricted to a zone of concrete just around the reinforcement. In a second analysis the web rein-
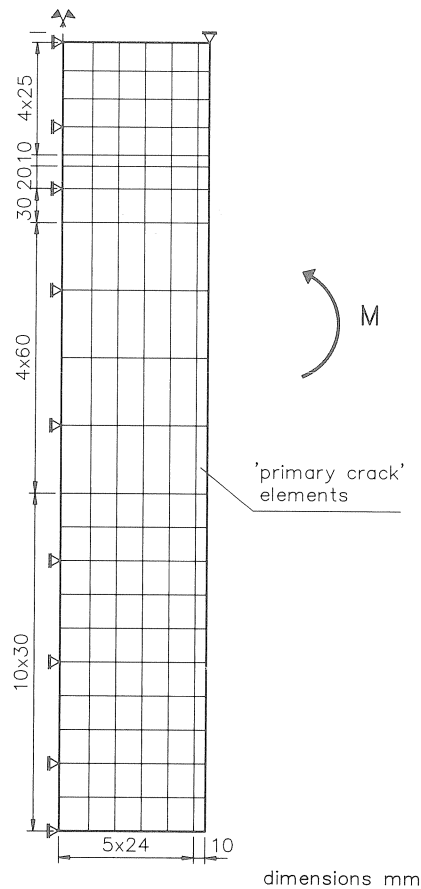
Fig. 4.2   FE mesh of the part of the beam between two primary cracks.

M [10⁶Nmm]	120	234	350	518	350	535
σ_s [MPa]	79	171	260	388	260	394
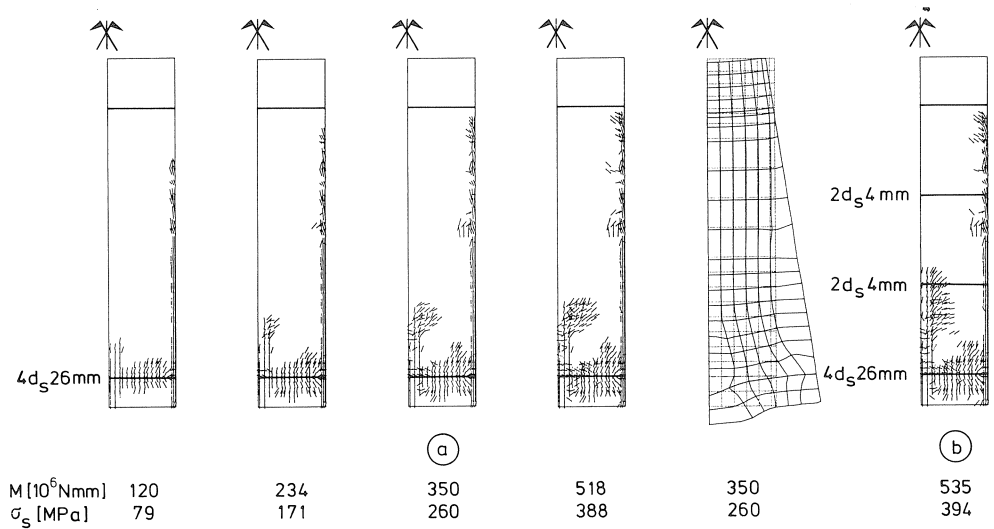
Fig. 4.3   Crack pattern of deep T-beam at several loading stages;
a. no web reinforcement
b. web reinforcement $2*2d_s$ 4 mm; $s = 180$ mm.

forcement was also modelled. Since much too small an amount ($2*2d_s$ 4 mm) was applied it was expected that the secondary crack would hardly be affected. This is confirmed by the crack pattern presented in Fig. 4.3b. The bar spacing of the web reinforcement was 180 mm. It was expected that increasing the bar diameter to 10 mm would result in a "secondary crack" proceeding on to the compression zone, and thus denoted as "primary crack". Fig. 4.4 clearly demonstrates this phenomenon.

M [10⁶Nmm]	91	119	180	227	374
	6	34	116	168	261
σ_s [MPa]^{web}	55	141	225	250	301
	42	68	113	140	261
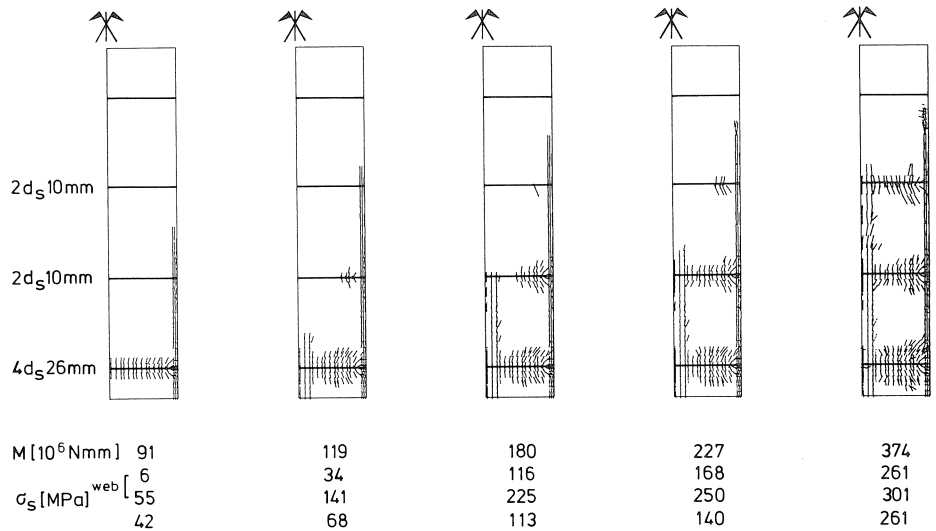
Fig. 4.4   Crack pattern of deep T-beam; web reinforcement $2*2d_s$ 10 mm, $s = 180$ mm.
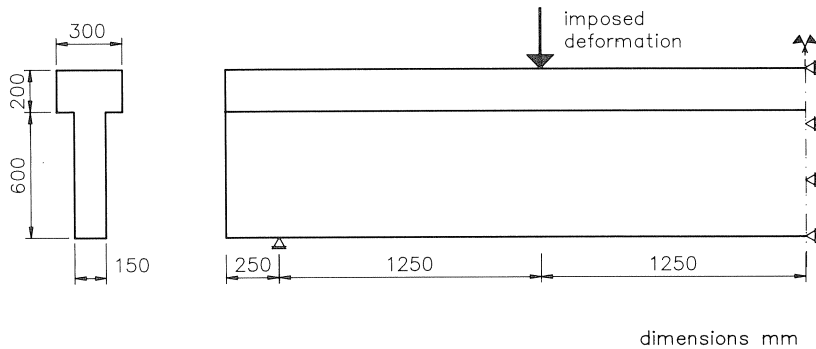
Fig. 4.5   Cross-section and side view of a deep T-beam.

4.3   *Over-all structural behaviour*

In anticipation of the experiments to be presented in chapter 6, FE analyses were performed with respect to the over-all structural behaviour of deep beams. Attention was focused on the cracking behaviour, load-deformation diagrams and steel stresses. In this section a brief overview is presented. For more information the reader is referred to De Groot [1990].

The cross-section and the loading scheme are presented in Fig. 4.5.

Because of symmetry only the left half of the beam was modelled. Loading was applied in a displacement-controlled way. Eight-noded plane stress elements with a $3*3$ Gaussian integration scheme were used. The reinforcement was modelled as bars. Perfect bond between the concrete and the reinforcement was assumed. The main reinforcement ($4 * d_s$ 20 mm) was represented by one bar situated 70 mm from the bottom. The shear zone was provided with 10 mm diameter stirrups, equally spaced at 100 mm. All the stirrups were modelled separately. A total number of 220 elements were applied, viz. 22 in the horizontal direction (125 mm long) and 10 in the vertical direction. The height of the elements was varied provided that at least one layer of unreinforced elements was present between two horizontal reinforcing bars. The main parameters varied were the tension stiffening and the amount of web reinforcement (bar diameter, bar spacing and number of bars).

Fig. 4.6 presents the load-displacement curves of a beam without web reinforcement. Both the force and the displacement are related to the node where the imposed deformation was applied, see Fig. 4.5. The tension stiffening was modelled in two ways. In one case no stiffening was applied (i.e. no stress transfer by the concrete after cracking) and in the other a linear descending branch was assumed. In the latter case the ultimate strain of the stiffening curve was the steel yield strain ($\varepsilon_{sy} = 2.38 * 10^{-3}$). Similar curves were obtained when the mean curvature of the zone with constant bending moment was presented [De Groot, 1990]. The amount of web reinforcement was found to be of minor influence on the calculated load-displacement curves.

43
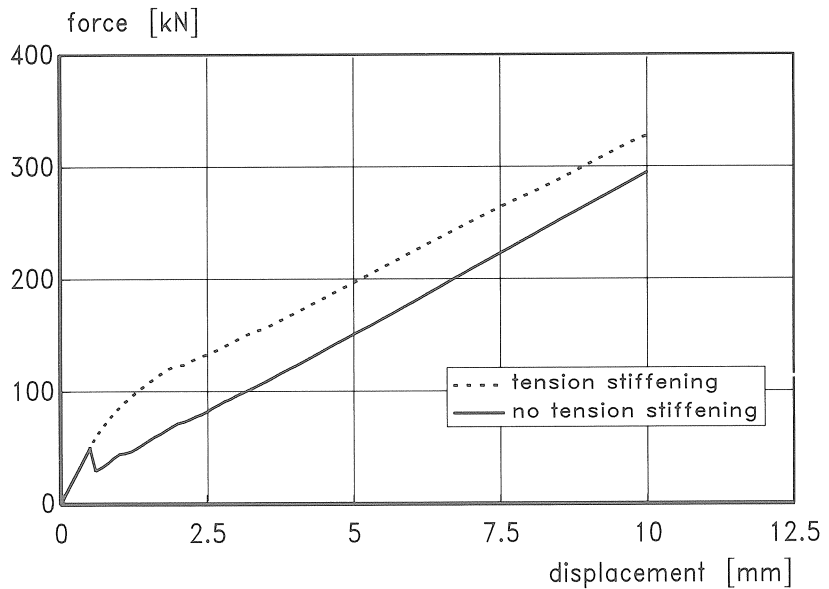
Fig. 4.6   Load-displacement curves for two different ways of modelling the tension stiffening.

With regard to the crack pattern the influence of the web reinforcement was considerable provided that a sufficient amount was applied. Fig. 4.7 presents the crack patterns of several beams with different amounts of web reinforcement. All the figures are presented at an imposed deformation of 7 mm. The corresponding loads are within the range of the loads in the serviceability limit state. All these results and those presented below were obtained by calculations performed with linear tension stiffening. In the "smeared crack approach", the crack width is smeared over a certain length which is dependent on the element size and the direction of the crack [Blaauwendraad et al., 1985; Rots, 1988]. Thus, cracks strains instead of crack widths are calculated. In Fig. 4.7 only cracks with a crack strain in excess of $0.2\varepsilon_{sy}$ are presented. Some of the beams were also investigated assuming no stiffening. However, the crack patterns hardly changed. Fig. 4.7 clearly demonstrates that increasing the amount of web reinforcement results in a higher percentage of cracks extending through the whole web of the beam. In the case where no or too little web reinforcement was applied, a well distributed crack pattern was restricted to the concrete area surrounding the main reinforcement; in the web only a few dominant cracks appeared. With regard to the steel stresses it was expected that local high tensile stresses would appear in the web reinforcement. This is clearly demonstrated in Fig. 4.8a where the stress in the lower web reinforcing bar is presented (web reinforcement: $2 * 2d_s$ 6 mm; bar spacing 200 mm). The displacement refers to the imposed deformation. Three curves are presented, each for one of the integration points of a bar within a concrete element. The concrete element chosen was located at a primary crack. Its position is indicated in Fig. 4.7b. One of the three integration points was unloaded, whereas the other two points were highly stressed, leading to

44
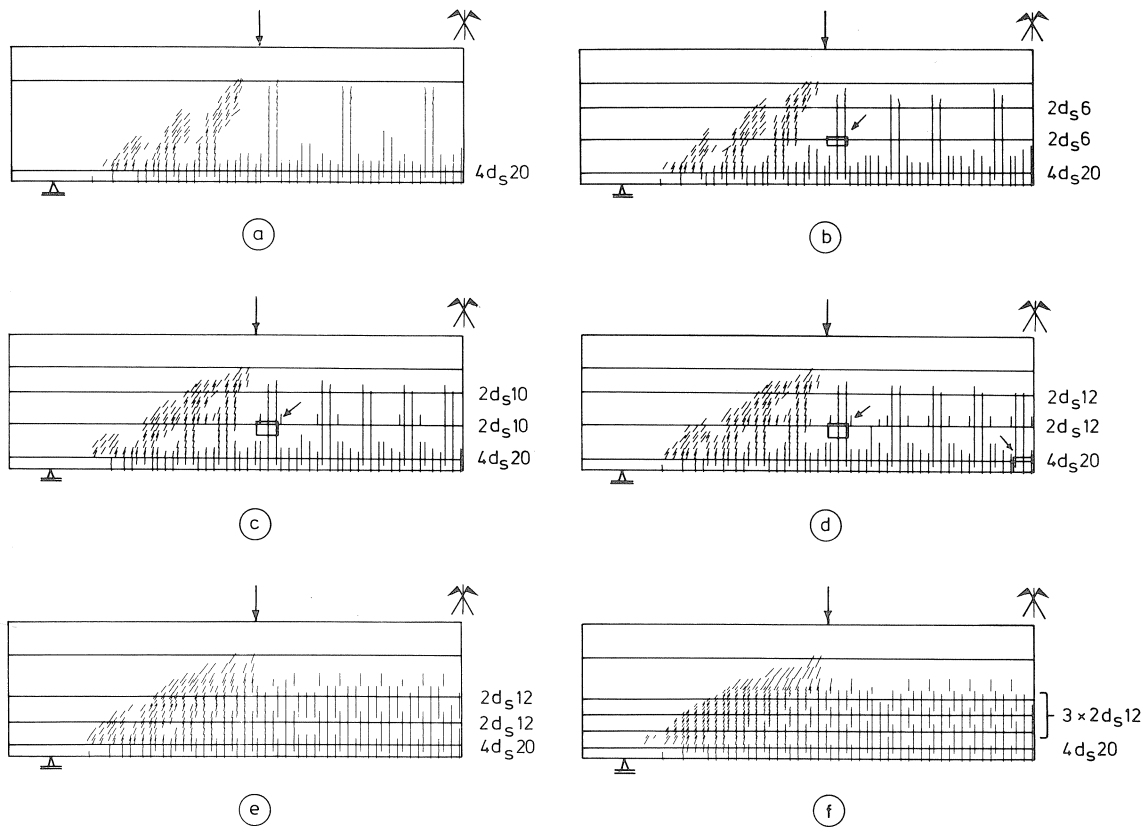
Fig. 4.7 Influence of web reinforcement on the crack pattern in the serviceability limit state
($\varepsilon_{cr} > 0.2\varepsilon_{sy}$, $\varepsilon_{sy} = 2.38 * 10^{-3}$).
a. no web reinforcement
b. $2 * 2d_s$ 6 mm; $s = 200$ mm
c. $2 * 2d_s$ 10 mm; $s = 200$ mm
d. $2 * 2d_s$ 12 mm; $s = 200$ mm
e. $2 * 2d_s$ 12 mm; $s = 150$ mm
f. $3 * 2d_s$ 12 mm; $s = 100$ mm

plasticity in the web reinforcement at loads considerably below loading in the service-
ability limit state. When the diameter of the web reinforcement was increased to 10 mm
plasticity of the web reinforcement still occurred, see Fig. 4.8b. The position of the con-
crete element under consideration is indicated in Fig. 4.7c. A further increase of the
diameter to 12 mm resulted in steel stresses within the range of the stresses in the main
reinforcement (see Figs. 4.8c-d). Both elements considered are shown in Fig. 4.7d.
Fig. 4.9 presents the steel stresses in all three of the beams already presented in Fig. 4.8
plus a beam without web reinforcement. All four figures are related to an imposed
deformation of 7 mm. The stresses are presented as triangles, scaled to the maximum
steel stress. In all four figures the triangles at the main reinforcement represent a steel
stress of about 340 MPa.

steel stress [MPa] vs displacement [mm]
(a)

steel stress [MPa] vs displacement [mm]
(b)
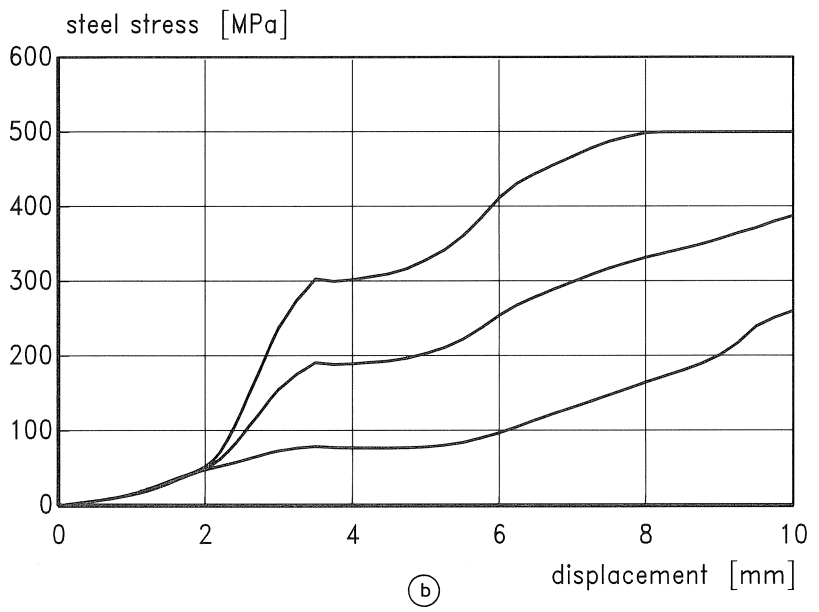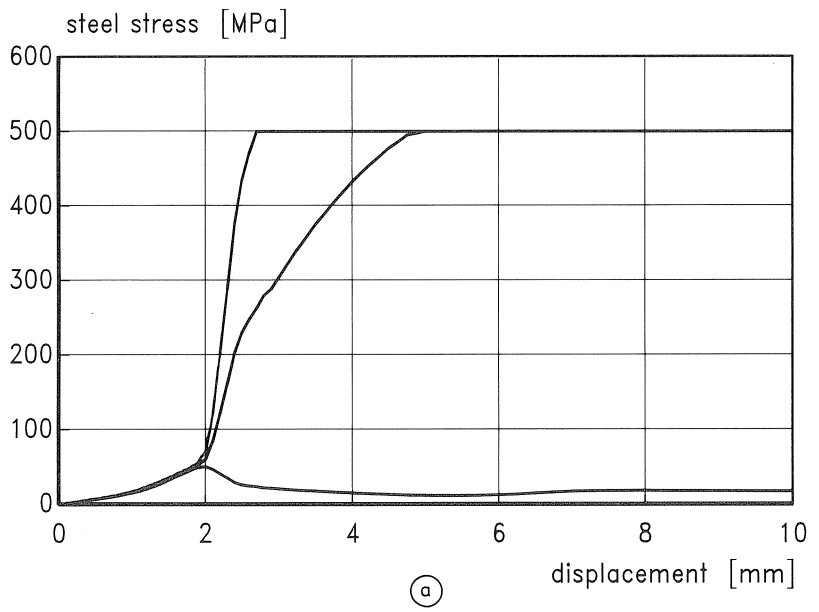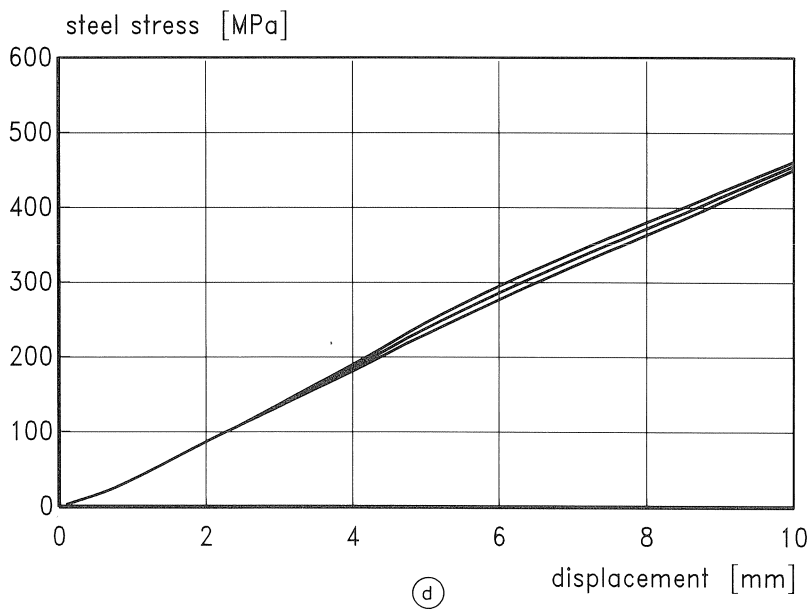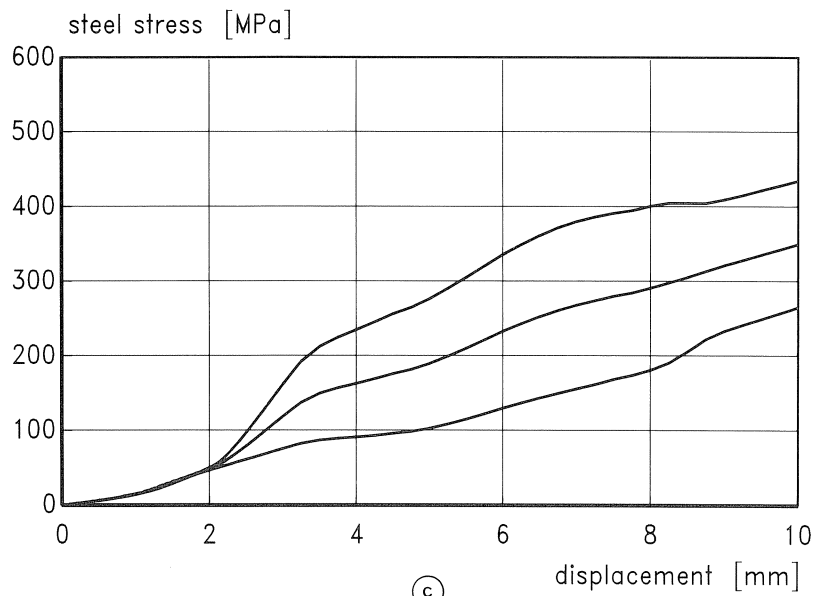
Fig. 4.8   Stresses in the reinforcement:
     a. web reinforcement (web: $2*2d_s$ 6 mm; $s=200$ mm)
     b. web reinforcement (web: $2*2d_s$ 10 mm; $s=200$ mm)
     c. web reinforcement (web: $2*2d_s$ 12 mm; $s=200$ mm)
     d. main reinforcement (web: $2*2d_s$ 12 mm; $s=200$ mm)
     The elements considered are indicated in Figs. 4.7b-d.
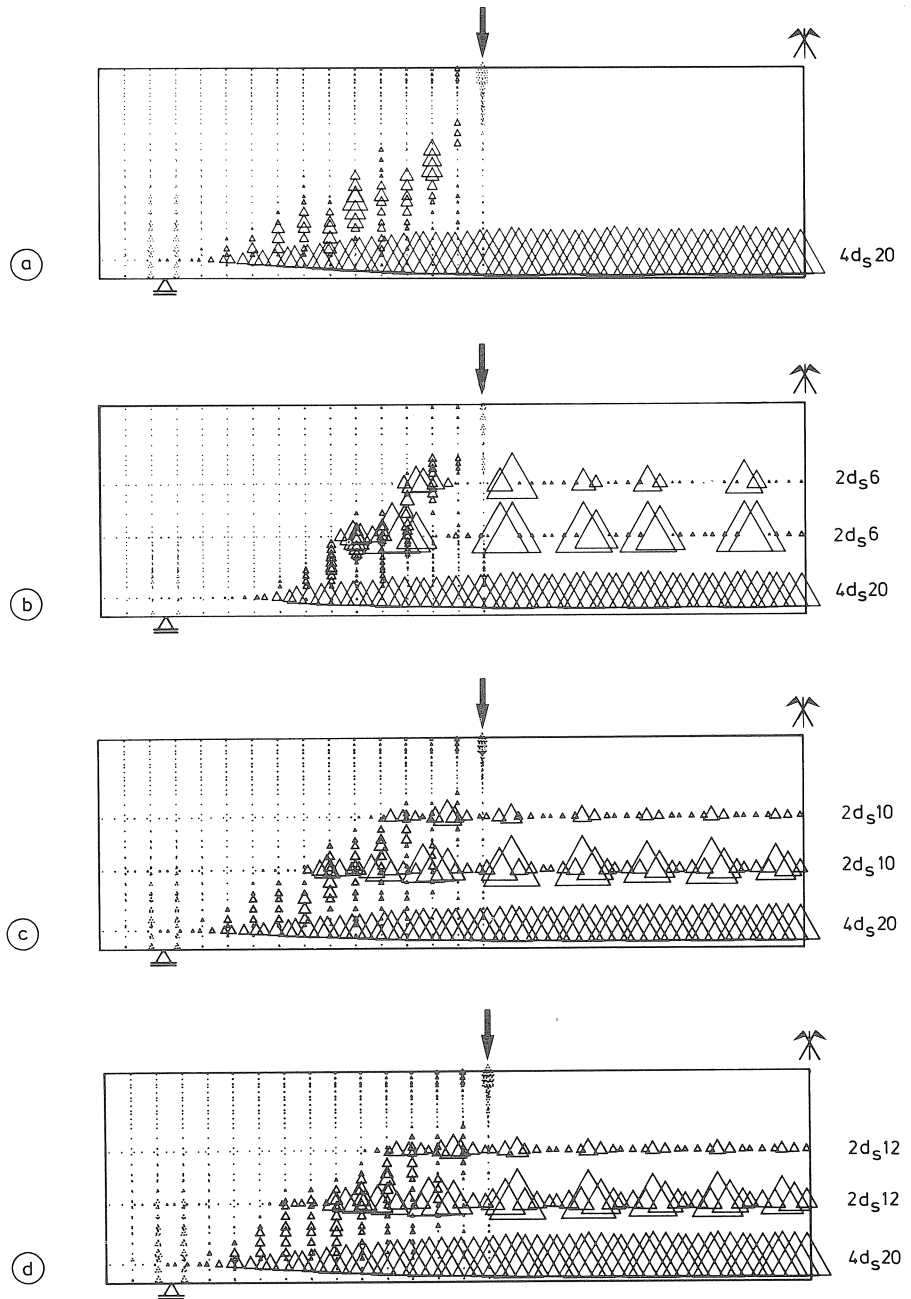
Fig. 4.9 Stresses in the reinforcement for different diameters of the web reinforcement (two layers, bar spacing 200 mm):
a. no web reinforcement
b. $d_s = 6$ mm
c. $d_s = 10$ mm
d. $d_s = 12$ mm

48

4.4 *Conclusions*

In the preceding two sections the main results of FE-analyses on deep beams were presented. In the first section only a small part of a beam was modelled. It was shown that no or just a small amount of web reinforcement results in a small number of wide cracks in the web. This is due to the "bending" of a number of the cracks initiated at the level of the main reinforcement. These "secondary cracks" tend to join the "primary cracks" that reach the compression zone. It was demonstrated that a sufficient amount of web reinforcement ensures that the "secondary cracks" become "primary cracks". In these analyses the "smeared crack approach" was used. The bond between the concrete and the reinforcing steel was modelled by means of non-linear springs.

The overall structural behaviour of deep beams was also investigated. The beams investigated experimentally (see chapter 6) were analysed to obtain an impression of the ability of the "smeared crack approach" to predict the influence of web reinforcement on the cracking behaviour. From these analyses it appeared that, as expected, a well distributed crack pattern is obtained in the vicinity of the main reinforcement. With regard to the web, nearly all the elements cracked. Where no or just a small amount of web reinforcement was applied, the major part of the crack strain was concentrated in a small number of integration points. The web reinforcement yielded at loads far below the load in the serviceability limit state. When the web reinforcement was detailed in conformity with design rules, a well distributed crack pattern was obtained in the web as well. The maximum stresses in the web reinforcement were of the same magnitude as the stresses in the main reinforcement.

The stresses in the web reinforcement are mostly calculated on the basis of the equilibrium of a cracked reinforced cross-section, loaded in bending or combined bending and tension/compression (Bernoulli: "plane sections remain plane") [e.g. Breen and Frantz, 1980b]. Figs. 4.8 and 4.9 clearly demonstrated that this assumption only holds when a large amount of web reinforcement is applied. In most cases the stresses can only be calculated if the beam is regarded as a number of "stacked" tensile members [Krips, 1985; Hordijk and Reinhardt, 1988]. The behaviour of the beam is known when the force-elongation diagrams of the tensile members are defined. Chapter 5 presents a model based on these findings.

5 **Theoretical model for the behaviour of deep beams**

5.1 *Introduction*

In chapter 2 the cracking behaviour at the level of the main reinforcement is investigated for both tensile members and beams. It is demonstrated that the Eurocode 1990 presents the best formulae to predict crack widths and spacings. In the case of deep beams without web reinforcement or tensile members provided with reinforcement concentrated at the side faces, the crack spacing at the level of the reinforcement can be calculated according to existing theories. However, the steel stress required to generate successive cracking is underestimated by the codes. The experimental results presented

49

by Helmus [1990] demonstrated that this steel stress increases considerably at increasing ratio of bar spacing to bar diameter. Therefore, a theoretical model was developed to calculate the secondary crack spacing (l_{sec}) and the corresponding steel stress initiating cracking $(\sigma_{s,\text{sec}})$. Since the ratio of the bar spacing to the diameter of the web reinforcement is rather large (e.g. $s = 100\text{--}200\,\text{mm}$, $d_s = 10\text{--}16\,\text{mm}$; CEB [1985]), this model must be used.

In this chapter a model that presents the overall structural behaviour of deep beams with or without web reinforcement is discussed. Some of the parameters used in this model must be calculated with the "effective concrete area" model. The model presents the curvature, crack height, steel stresses and crack widths as a function of the bending moment. At first, the model is presented for plain concrete. Verification takes place by comparison with the FE program DIANA. Then the model is extended to reinforced concrete. This model will be referred to as the "beam model".

5.2 *Plain concrete beams*

5.2.1 Softening of concrete in tension

When a plain concrete specimen is loaded in pure bending, the ultimate bending moment is larger than the moment that introduces a stress equal to the uniaxial concrete tensile strength in the outer tensile fibres:

$$M_{\text{u}} > W f_{\text{ct}} \quad [\text{Nmm}] \tag{5.1}$$

When the height of the specimens increases, the ratio $M_{\text{u}}/(W f_{\text{ct}})$ decreases. Hillerborg et al. [1976] presented the "fictitious crack model" that defines the stress transfer as a function of the crack opening, see Fig. 5.1.

This phenomenon is mostly denoted as "softening". For an extensive survey of the literature on this subject the reader is referred to Hordijk [1989]. Hillerborg et al. [1976] demonstrated that the existence of the "flexural concrete tensile strength" is caused by this softening. They modelled a beam with one major crack, see Fig. 5.2. After the uni-
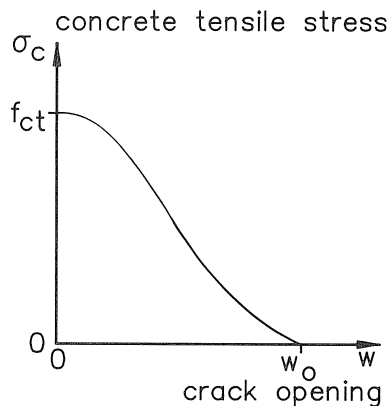
Fig. 5.1   Transfer of stress in a crack in concrete [Hillerborg et al., 1976].

axial tensile strength f_{ct} was reached, the transfer of stress took place according to a linearly descending softening curve. All the elements outside the crack behaved linear-elastically. The "softening" behaviour was introduced by nodal forces. In the FE program DIANA the "discrete crack concept" was introduced by Rots [1988].

5.2.2 Model for plain concrete beams

Hordijk and Reinhardt [1988] presented a model for the analysis of plain concrete specimens loaded in tension or combined tension and bending. The model is based on the behaviour of individual "springs" fixed between two rigid plates, see Fig. 5.3. The force-elongation curve of a spring is easily defined in the case where the concrete strain is less than $\varepsilon_{cr} = f_{ct}/E_c$:

$$N_c = A_c \sigma_c = A_c E_c \varepsilon_c \quad [\text{N}] \tag{5.2}$$
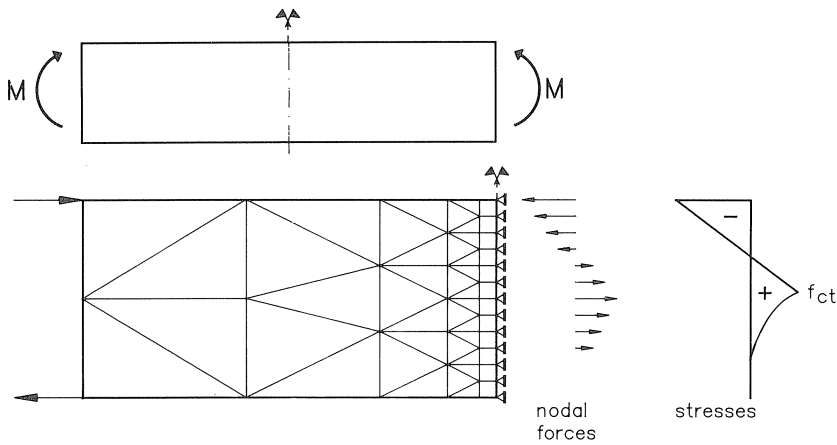
Fig. 5.2   Plain concrete beam loaded in pure bending and corresponding FEM representation [Hillerborg et al., 1976].
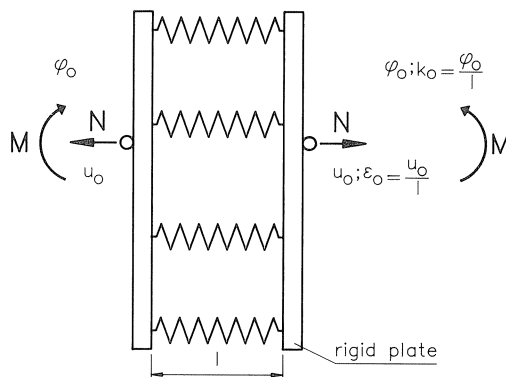
Fig. 5.3   Model for plain concrete loaded in tension and/or bending [Hordijk and Reinhardt, 1988].

51

If the strain exceeds ε_{cr}, softening has to be taken into account. Hordijk and Reinhardt [1988] assumed that the micro crack is "smeared" over the entire length of the spring, see Fig. 5.4.

Leonhardt [1976a] and Beeby [1978] demonstrated that the crack width in a plain concrete member can be calculated according to the following formula:

$$w_m = k_1 h_{cr} \varepsilon_m \quad [\text{mm}] \tag{5.3}$$
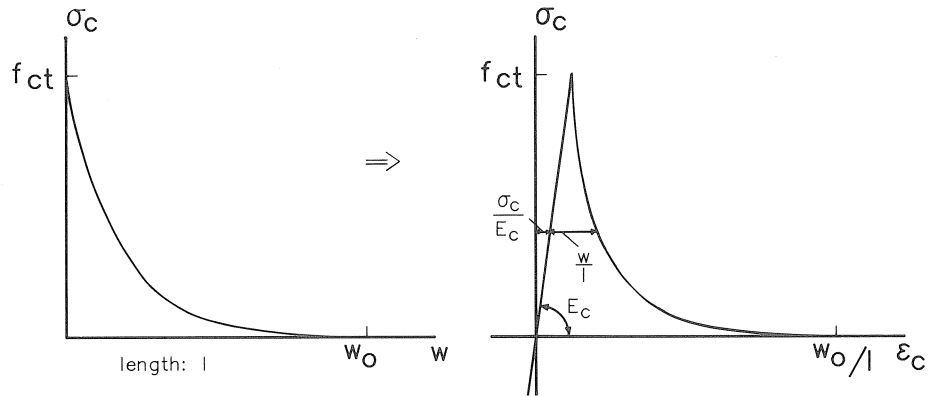
Fig. 5.4   Stress-strain diagram of a plain concrete "spring" [Hordijk and Reinhardt, 1988].
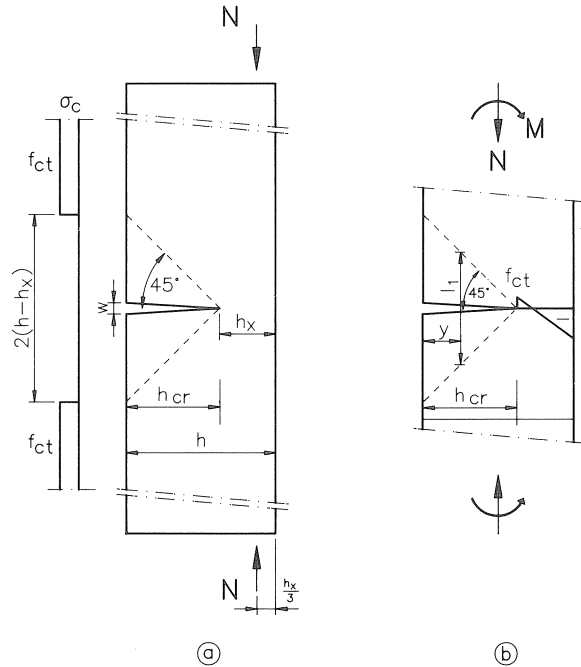
Fig. 5.5   Model to calculate the crack width in a plain concrete member [Beeby, 1978] (a) and the corresponding model to take softening into account (b).

52

In this formula, h_{cr} is the crack height, whereas ε_m is the mean strain at the level considered. According to Leonhardt [1976a], $k_1 = 2$ is assumed. This implies that an area with a length of $2h_{cr}$ can assumed to be unstressed at the concrete surface, whereas in the other parts the concrete tensile strength is reached, see Fig. 5.5a. It is proposed to define a length $l_1 = 2(h_{cr} - y)$ over which the softening curve is smeared, see Fig. 5.5b. The stress-strain curve of the spring is presented in Fig. 5.6. It is emphasized that the crack length h_{cr} depends on the force N and the bending moment M applied.
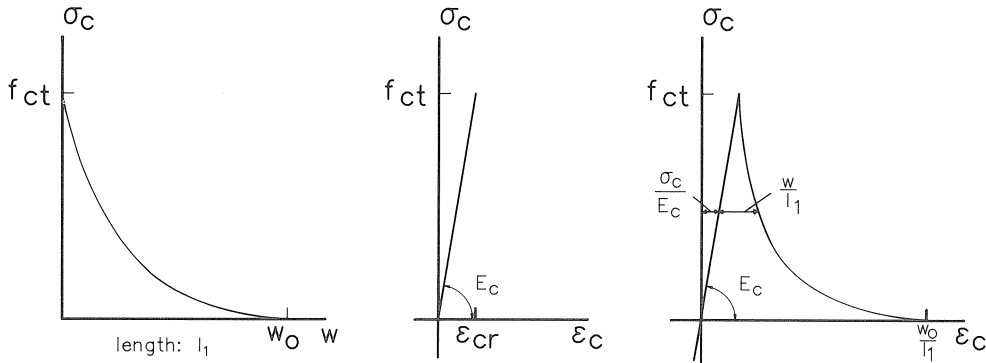
Fig. 5.6   Stress-strain diagram of a plain concrete "spring" including the influence of the crack height.

5.2.3   Comparison between FE calculation and "beam model"

In section 5.2.2 the stress-strain curve of concrete in direct tension was derived. To check the validity of the model a comparison with an FE calculation was made. For this purpose a part of a T-beam was modelled, see Fig. 5.7. The right edge of the mesh was kept "straight" by "tying" the horizontal displacements, thus directly introducing pure bending. The following material properties were used for the concrete: $E_c = 30300$ MPa, $f_{ct} = 2.8$ MPa, $v = 0.2$, $G_f = 0.10$ N/mm.

A linear descending curve was applied for the softening. Since only a part of a beam was modelled, the length of the springs is $l_1 = 2(h_{cr} - y) \leq 300$ mm. In Figs. 5.8a and b a comparison is presented between the DIANA calculation and the results of the "beam model". With regard to the curvature as well as the crack height good agreement was obtained.

5.3   *Model for reinforced concrete beams*

5.3.1   Bond between concrete and reinforcing steel

In section 5.2 a "beam model" is presented for plain concrete beams loaded by a normal force and/or a bending moment. When extending the model to reinforced concrete beams, springs representing the stress-strain curves of steel bars must be implemented.

53

Allowance has to be made for the bond between the concrete and the reinforcing steel. It is assumed that the bond stress is independent of the displacement of the steel bar relative to the outer surrounding concrete [Fehling and König, 1988]:

$$\tau_b = 2f_{ctm,0} \quad [MPa] \tag{5.3}$$
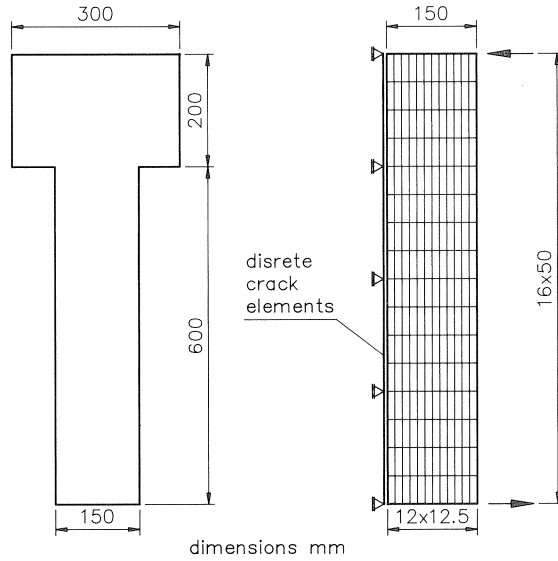
Fig. 5.7   Cross-section and FE mesh of plain T-beam loaded in pure bending.
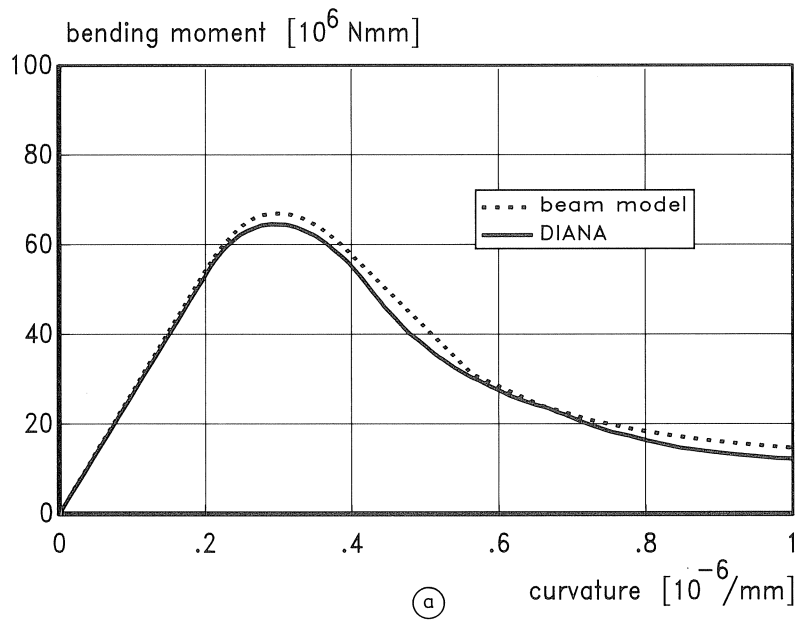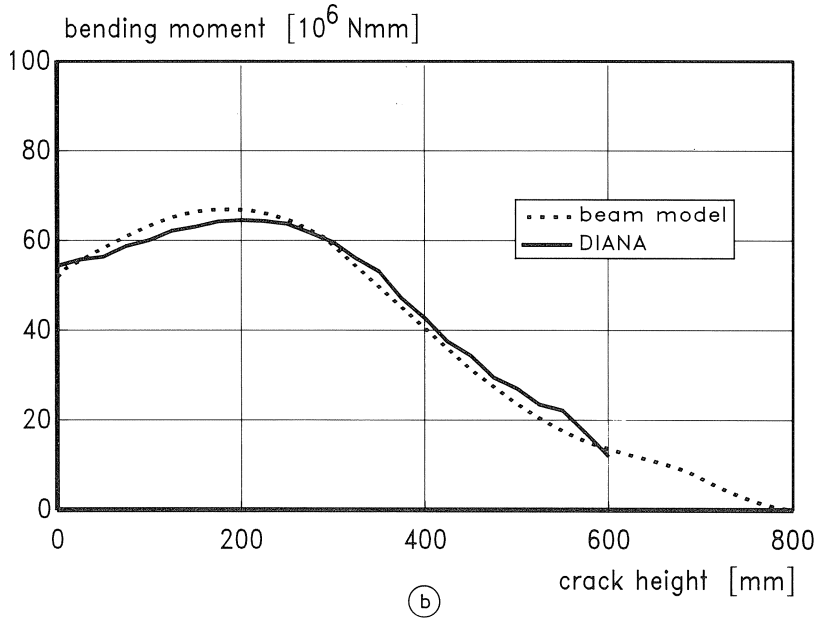
Fig. 5.8   Bending moment-curvature (a) and bending moment-crack height (b) curves for a plain beam loaded in pure bending; a comparison between DIANA and the "beam model".

Just as in the case of the concrete "springs", a steel bar with a length l was modelled. Fig. 5.9 presents the location of the part of the bar in the crack pattern of a beam. In the middle of the bar a discrete crack may occur. At both sides of this crack a bond-free length s_0 is modelled. With regard to the stress-average strain curve of the bar four stages can be distinguished, viz. (also see Fig. 5.9):

a. $\varepsilon_{sm} < \dfrac{f_{ct}}{E_c}$:

$$\varepsilon_{sm} = \frac{\sigma_s}{E_s} \quad [-] \tag{5.4a}$$

b. $\varepsilon_{sm} = \dfrac{f_{ct}}{E_c}$ and $s_0 + l_t \leq \tfrac{1}{2}l : l_t = \dfrac{A_s(\sigma_s - \sigma_{s0})}{u_s \tau_b}$

$$\varepsilon_{sm} = \frac{1}{lE_s} \left\{ 2s_0 \sigma_s + 2l_t \left(\frac{\sigma_s + \sigma_{s0}}{2} \right) + 2(\tfrac{1}{2}l - s_0 - l_t)\sigma_{s0} \right\} \quad [-] \tag{5.4b}$$

c. $\varepsilon_{sm} > \dfrac{f_{ct}}{E_c}$ and $s_0 + l_t = \tfrac{1}{2}l : \sigma_s = \sigma_{s0} + \dfrac{u_s \tau_b}{A_s}(\tfrac{1}{2}l - s_0)$

$$\varepsilon_{sm} = \frac{1}{lE_s} \left\{ 2s_0 \sigma_s + (l - 2s_0) \left(\frac{\sigma_s + \sigma_{s0}}{2} \right) \right\} \quad [-] \tag{5.4c}$$

55

d. $\varepsilon_{sm} > \dfrac{f_{ct}}{E_c}$ and $s_0 + l_t \geq \tfrac{1}{2}l : \Delta\sigma_s = \dfrac{u_s \tau_b}{A_s}\left(\tfrac{1}{2}l - s_0\right)$

$$\varepsilon_{sm} = \frac{1}{lE_s}\left\{2s_0\sigma_s + (l - 2s_0)(\sigma_s - \tfrac{1}{2}\Delta\sigma_s)\right\} \quad [-] \tag{5.4d}$$
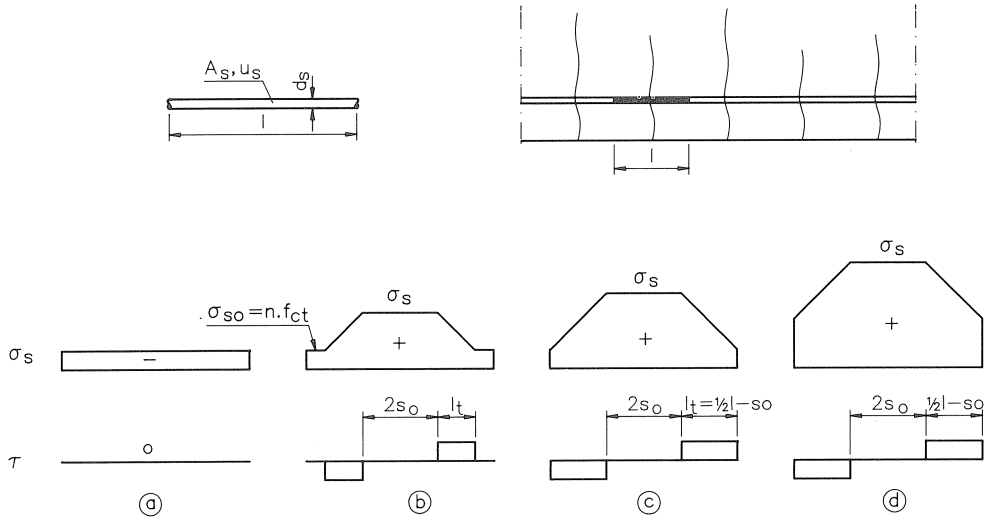
Fig. 5.9. The different stages of a reinforcing bar that define the stress-strain curve.
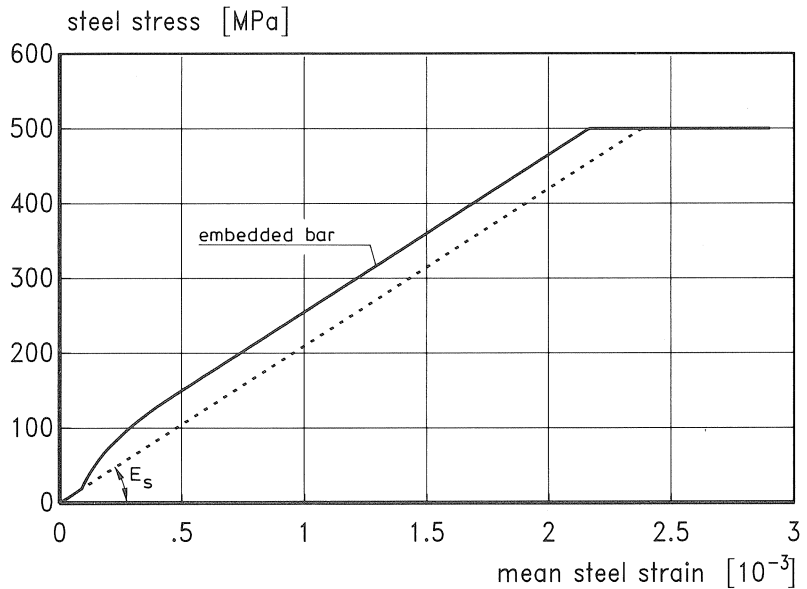
Fig. 5.10   Stress-mean strain curve of an embedded reinforcing bar loaded in tension.

56

At every stage it must be checked whether $\sigma_s \leq f_{sy}$. If $\sigma_s = f_{sy}$ then the force in the bar becomes independent of the mean strain: $N_s = A_s f_{sy}$. The tension stiffening $\Delta\varepsilon_s$ is constant between stages c and d:

$$\Delta\varepsilon_s = \frac{u_s \tau_b}{l E_s A_s} \left(\tfrac{1}{2}l - s_0\right)^2 \quad [-] \tag{5.5}$$

Fig. 5.10 presents the steel stress-mean strain curve of a 20 mm diameter embedded reinforcing bar. The following parameters are used: $E_s = 2.1 * 10^5$ MPa; $f_{sy} = 500$ MPa; $f_{ct} = 2.8$ MPa; $\tau_b = 2f_{ct}$; $d_s = 20$ mm; $A_s = 314$ mm^2; $u_s = 63$ mm; $l = 300$ mm; $s_0 = 2d_s$.

5.3.2 Comparison between FE calculation and "beam model"

The model for the plain concrete beams (see section 5.2.2) can now be extended to reinforced concrete beams by adding springs that represent the force-deformation characteristics of reinforcing bars. Just as in the case of the plain concrete beam, the model was checked by a comparison with a DIANA calculation. Therefore, the beam presented in Fig. 5.7 was provided with reinforcing bars, see Fig. 5.11. In the DIANA-model the reinforcement was modelled by means of 12 truss elements per bar, each 12.5 mm long. Interface elements were used to model the transfer of bond stresses. A very steep ascending bond stress-slip relation was used so that $\tau_b = 2f_{ct}$ was already reached at 0.001 mm slip. All the bars had a bond-free length of 12.5 mm just beside the discrete crack elements. The material properties were: $E_c = 31300$ MPa, $f_{ct} = 2.8$ MPa, $v = 0.2$, $G_f = 0.10$ N/mm (linear softening curve); $E_s = 2.1 * 10^5$ MPa; $f_{sy} = 500$ MPa.
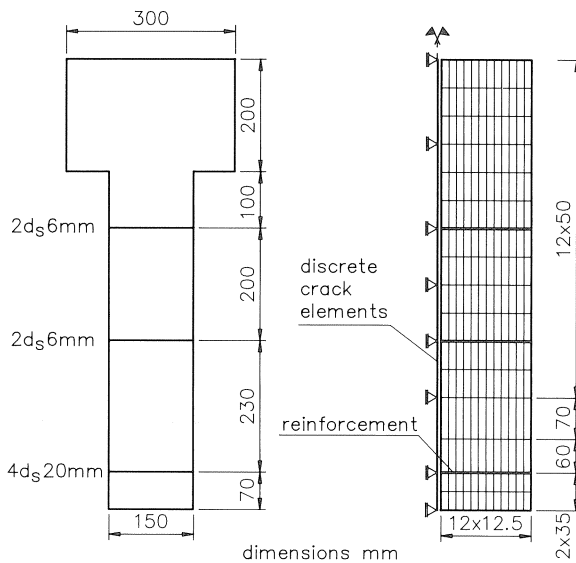
Fig. 5.11 Cross-section and FE mesh of reinforced T-beam loaded in pure bending.

57

In Figs. 5.12a-b the results are compared with the "beam model". In this model the bond-free length was taken as $s_0 = d_s$ to obtain close agreement with the DIANA input. Two other computations were performed: In the first, no web reinforcement was applied and in the second, the diameter of the web reinforcement was increased to 12 mm. In both cases close agreement between both models was obtained.
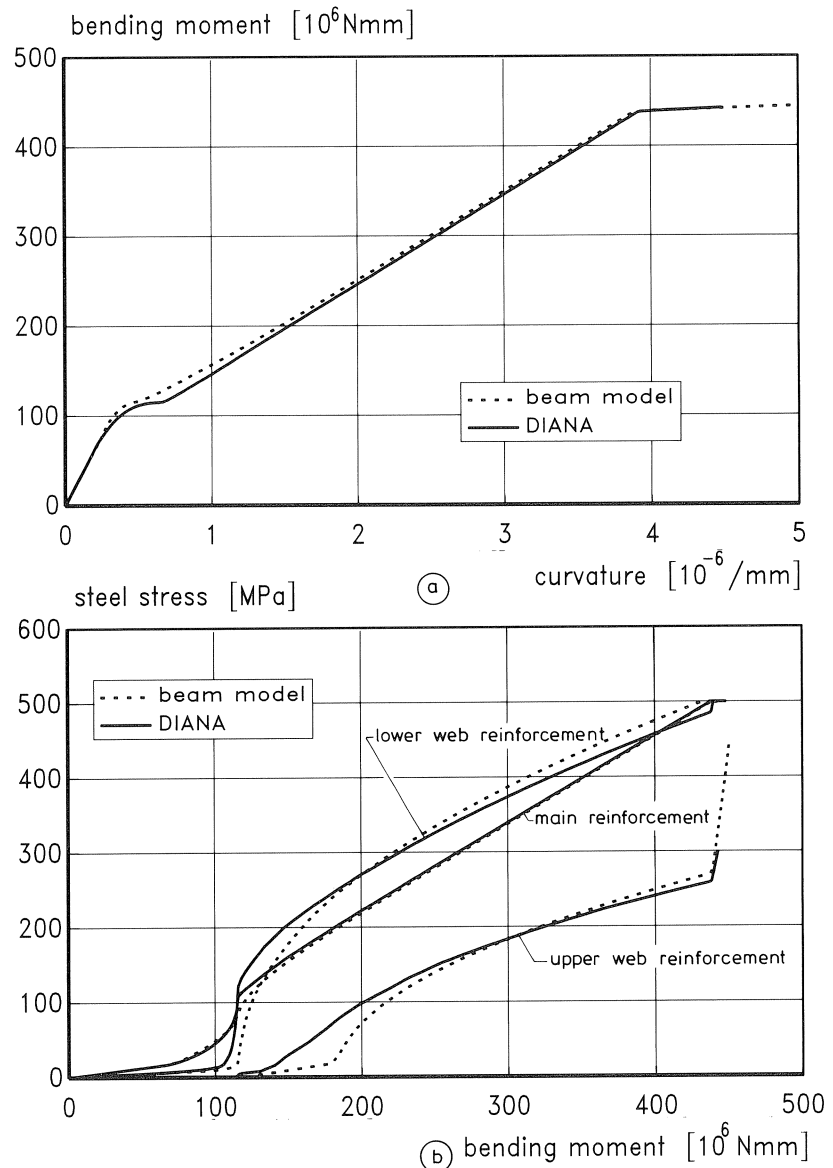
Fig. 5.12 Comparison between DIANA and "beam model":
a. Bending moment-curvature relation
b. Stresses in the main and web reinforcement

6 Experiments

6.1 *Introduction*

In chapter 3 it is concluded that the design rules for the web reinforcement in deep beams presented by the CEB [1985] are not fully supported by experimental investigations. The most extensive experimental research was carried out by Breen and Frantz [1978], but their model is only applicable to specific cases. Therefore, it was decided to perform experiments on deep reinforced concrete beams. In all, 15 beams were tested. In this chapter only a part of the experimental results is presented, since the total amount of experimental data is too extensive to be published in this thesis. For further information, the reader is referred to Braam [1990c].

6.2 *Material properties*

6.2.1 Concrete mix

One mix was used, composed of Portland A and C cement and glacial river gravel aggregates with a 16 mm maximum particle size. The mix composition is given in Table 6.1. The air content and the slump of the mix were 0.8% and 140 mm, respectively. The concrete was delivered by a mixer truck. A 0.3 m^3 skip was used for casting the beams. Each beam was cast in four or five layers. During casting internal vibrators were used to compact the concrete. For standard tests 12 cubes and 6 cylinders were cast together with each beam. The compaction time for the 150 mm cubes was 30 seconds, while this time was 2 * 30 seconds for the ⌀ 150 * 400 mm cylinders. About five hours after casting, the beams and standard specimens were covered with plastic sheets. After two or three days the beams and specimens were demoulded and stored until testing. Six cubes and three cylinders were placed in a fog room (99% R.H. and 20 °C) whereas the beam and the other standard specimens were stored under laboratory conditions (65% R.H. and 15–20° C). The standard specimens which were stored in the fog room were tested at an age of 28 days. The other standard specimens were tested together with the beams.

Table 6.1   Mix proportions and sieve analysis.

components	[kg/m^3]	sieve analysis					
		fraction		sieve opening			
		[mm]	[%]	[kg]	[mm]	[cum. %]	
sand	670	8 –16	28	521	16	0	
glacial river gravel	1191	4 – 8	25	465	8	28	
Portland cement A	170	2 – 4	11	205	4	53	
Portland cement C	170	1 – 2	6	112	2	64	
water	177	0.50– 1	13	242	1	70	
		0.25– 0.50	12	223	0.50	83	
		0.10– 0.25	4	74	0.25	95	
		<0.10	1	19	0.10	99	
calc. density	2378		100	1861			

6.2.2 Reinforcing steel

Use was made of reinforcing bars of 6, 10, 12, 16 and 20 mm diameter respectively. The 6 mm diameter rebars were only used for the stirrups. The specific rib area, f_R, of the 10, 12, 16 and 20 mm diameter bars was 0.79, 0.78, 0.73 and 0.72 respectively. The stress-strain curves of the various bars are presented in Fig. 6.1.
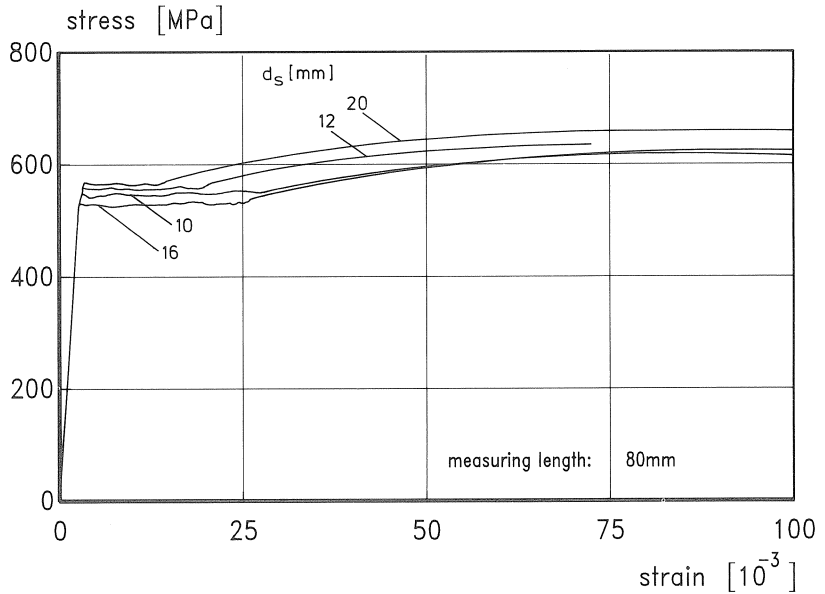
Fig. 6.1   Stress-strain curves of the bars used for the longitudinal reinforcement.

6.3   *Specimens*

In all, 15 beams were cast; 12 T-beams and 3 rectangular beams. The dimensions and cross-sections are presented in Figs. 6.2a-b.

The position of the main reinforcement is presented in Figs. 6.3a-d. The main reinforcement of the beams 1-6 consisted of 4 bars with a 20 mm diameter, placed in two layers of two bars each. The distance from the centre of the layers to the bottom of the beam was 40 and 100 mm respectively.

In the middle 2.5 m of the beams only two stirrups were used. Beams 1-6 and 13 were provided with 10 mm diameter stirrups, whereas this diameter was 6 mm for the other beams. The concrete cover to the stirrups was 20 and 30 mm for beams 1-12 and 13-15 respectively. The bottom cover was equal to the side cover.

The amount of horizontal web reinforcement applied is given by the following code: number of layers – bar diameter [mm] – bar spacing [mm].

Both sides of the web contained the same amount of web reinforcement. Table 6.2 presents the code of the web reinforcement of all 15 beams. Beams 1 and 7 only
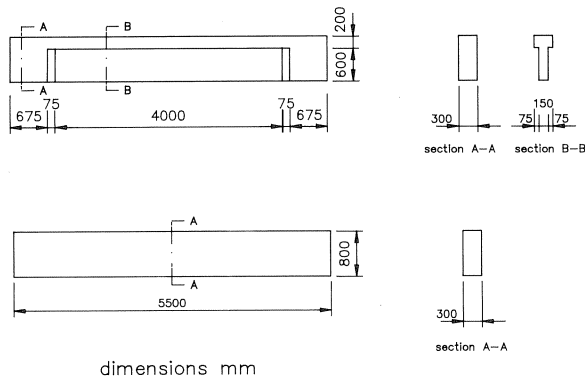
dimensions mm

Fig. 6.2   Dimensions and cross-sections of beams 1-12 (a) and 13-15 (b).

contained main reinforcement. In beams 2 to 6, the bar spacing of the lower web reinforcement is equal to the centre of the upper main reinforcement to the centre of the web reinforcement. Table 6.3 contains all the details of the beams tested.

Table 6.2   Amount of horizontal web reinforcement applied in the experiments

beam	code	beam	code
1	–	9	1–12–200
2	2–12–150	10	1–10–100
3	1–12–200	11	1–10–150
4	1–10–100	12	2–10–100
5	2–10–150	13	1–12–100
6	1–10–200	14	2–16–150
7	–	15	2–12–150
8	2–12–150		

4d$_s$ 20mm   3d$_s$ 16mm   4d$_s$ 20mm   3d$_s$ 16mm

(a)   (b)   (c)   (d)

dimensions mm
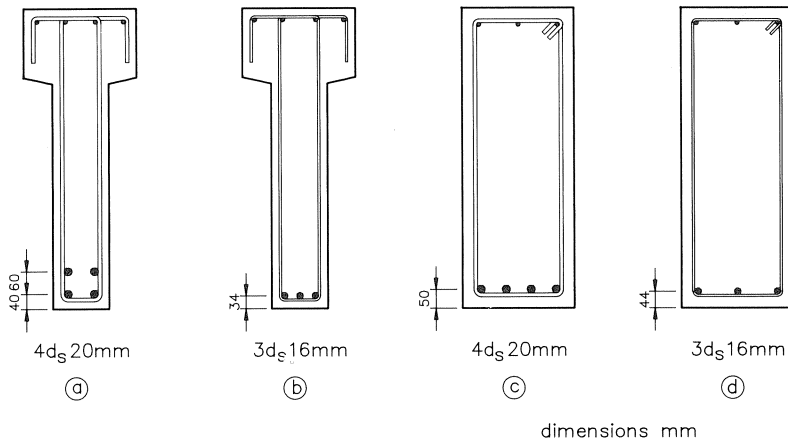
Fig. 6.3   Position of the main reinforcement in the measuring zones of beams 1-6 (a), 7–12 (b), 13 (c) and 14–15 (d).

61

Table 6.3 Details of the 15 beams tested

beam no.	cross-section	h [mm]	d [mm]	web width [mm]	f_{ccm} [MPa]	f_{cspl} [MPa]	main rein-forcement	web reinforcement (per side) d_s [mm]	number of layers	bar spacing [mm]	stirrups d_{ss} [mm]	c [m
1		800	730	150	53.9	3.41	$4d_s$ 20 mm (2 layers)		–		10	20
2		800	730	150	53.0	3.67	$4d_s$ 20 mm (2 layers)	12	2	150	10	20
3		800	730	150	51.4	3.79	$4d_s$ 20 mm (2 layers)	12	1	200	10	20
4		800	730	150	56.4	3.87	$4d_s$ 20 mm (2 layers)	10	1	100	10	20
5		800	730	150	51.8	3.74	$4d_s$ 20 mm (2 layers)	10	2	150	10	20
6		800	730	150	48.9	3.56	$4d_s$ 20 mm (2 layers)	10	1	200	10	20
7		800	766	150	57.6	4.19	$3d_s$ 16 mm (1 layer)		–		6	20
8		800	766	150	54.7	4.07	$3d_s$ 16 mm (1 layer)	12	2	150	6	20
9		800	766	150	56.0	3.92	$3d_s$ 16 mm (1 layer)	12	1	200	6	20
10		800	766	150	55.2	3.72	$3d_s$ 16 mm (1 layer)	10	1	100	6	20
11		800	766	150	48.9	3.02	$3d_s$ 16 mm (1 layer)	10	1	150	6	20
12		800	766	150	43.7	3.20	$3d_s$ 16 mm (1 layer)	10	2	100	6	20
13		800	750	300	51.0	3.72	$4d_s$ 20 mm (1 layer)	12	1	100	10	30
14		800	756	300	50.6	3.66	$3d_s$ 16 mm (1 layer)	16	2	150	6	30
15		800	756	300	40.8	2.99	$3d_s$ 16 mm (1 layer)	12	2	150	6	30

Cross-section diagrams:
- Beams 1–12: T-section, flange 300 wide × 200 high, total height 800, web width 150 (labelled 1–12)
- Beams 13–15: rectangular section, 300 wide × 800 high (labelled 13–15)

h = total height
d = effective depth
f_{ccm} = mean 28-day (150 mm) cube compressive strength
f_{cspl} = mean 28-day (150 mm) cube tensile splitting strength
c = concrete cover to the stirrups (bottom cover = side cover)

6.4 Loading scheme and measuring devices

The 5.5 m long beams were loaded in four-point bending with a span of 5 m. The loading scheme is presented in Fig. 6.4. This figure also presents a view of a T-beam in the test rig.

All the crack width measurements were restricted to the middle 2.3 m of the beams. Only for beam 1 was this zone 2.4 m long. The crack widths were measured on both sides of the beams by means of a microscope with a magnification of 100 and calibrated in 0.01 mm divisions. Nine horizontal lines were drawn on both sides of the beams.
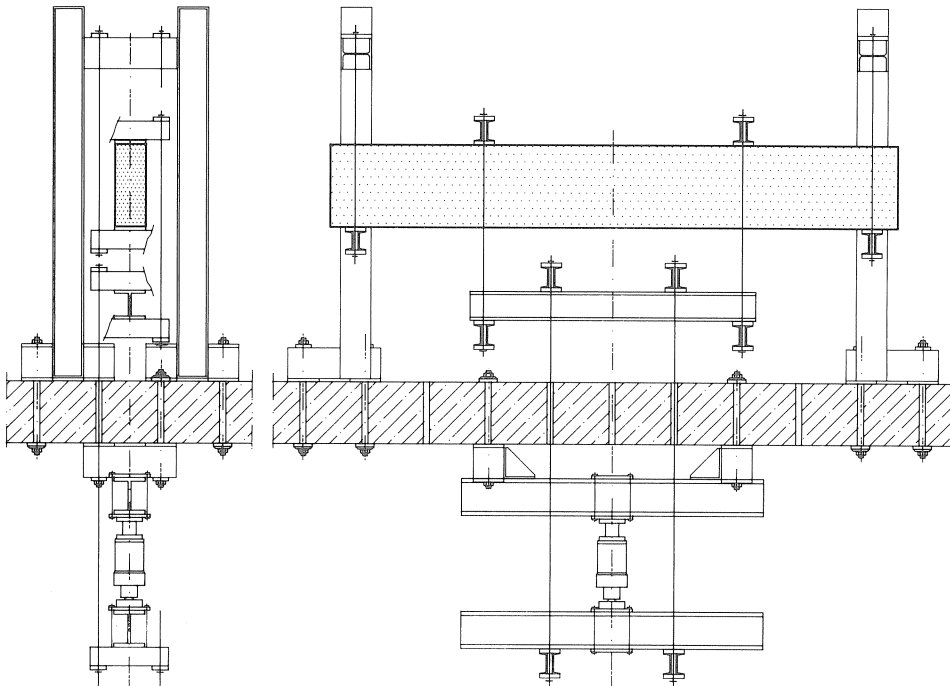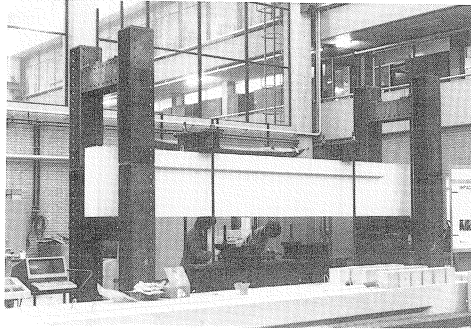
Fig. 6.4 Loading scheme and view of the test rig.

Crack widths were measured at each position where the cracks intersected these lines. The position of these lines is presented in Fig. 6.5. The numbers 1 and 9 are also indicated.

The deflection was measured relative to the supports with LVDTs at mid span and just beside the loading points, see Fig. 6.6. The strains were measured on the surface of the beams with 170 mm extensometers. On both the tension and compression zone 13 extensometers were used, thus covering 2210 mm of the uniform bending moment zone, see Fig. 6.6. The zero-measurements were taken when the beams were only loaded by their dead-weight. Thus, the influence of the dead-weight was not incorporated in the measuring results of the LVDTs and the extensometers.

dimensions mm

Fig. 6.5 Position of measuring lines for crack widths; beams 1–6 (a), 7–12 (b), 13 (c) and 14–15 (b).

At first, the loading frame was applied on the beam, which implies $P = 9$ kN. The actual load was then applied in four to five increments by a hand-operated hydraulic jack with 100-ton capacity. During the crack width measurements the load was kept constant manually. Each test lasted between about 5 hours (beam 15) and 9.5 hours (beam 2).

6.5   *Experimental results*

As mentioned before, only a number of representative experimental results will be presented in this thesis. Each figure will present as much information as possible.

– Results of the control specimens:
Half of the cubes and cylinders were tested at 28 days, whereas the remaining specimens were tested on the same day as the corresponding beams. Table 6.4 presents the

dimensions mm

Fig. 6.6   Position of the measuring devices.

64

results of these tests. Each result is the average of three measurements. Always two values are presented: The first corresponds to 28 days, whereas the second refers to the moment when the beams were tested (ranging from 42 (beam 15) to 83 days (beam 1)).

Table 6.4   Results of the control specimens

beam no.	f_{cc} [MPa]	f_{cspl} [MPa]	E_c [MPa]
1	53.9/61.7	3.41/3.82	31300/28900
2	53.0/56.3	3.67/3.81	34500/30600
3	51.4/52.2	3.79/3.72	33400/31200
4	56.4/61.5	3.87/3.54	35900/30900
5	51.8/50.1	3.74/3.41	32800/28800
6	48.9/53.3	3.56/3.84	34100/30800
7	57.6/64.5	4.19/4.05	34800/32800
8	54.7/56.1	4.07/4.00	33500/30900
9	56.0/61.4	3.92/3.74	34600/32000
10	55.2/58.9	3.72/3.79	33300/32700
11	48.9/49.9	3.02/3.65	34400/30400
12	43.7/49.9	3.20/3.91	31900/31200
13	51.0/55.9	3.72/4.08	33400/31800
14	50.6/53.4	3.66/3.70	34300/31600
15	40.8/41.3	2.99/3.30	31900/28600

– The force-deflection curves:

The vertical displacement of the beams was measured at three positions, see Fig. 6.6. In Figs. 6.7a-b the deflection at mid span is presented as a function of the load P (see Fig. 6.4). The load includes half of the load applied by the hydraulic jack and half the weight of the loading frame $(P = 9kN)$. Fig. 6.7a presents the results of beams 1, 2 and 6 (T-beams; main reinforcement $4d_s$ 20 mm), whereas Fig. 6.7b concerns beams 7, 8, 14 and 15 (2 rectangular and 2 T-beams; main reinforcement $3d_s$ 16 mm). The horizontal branches correspond to the increase of the deflection during the crack width measurements, which took about $1-1\frac{1}{2}$ hours per load step. It is emphasized that the dead-weight of the beams is not included in the load P.

– The bending moment-curvature curves:

The mean surface strains at the tension and the compression faces of the beams were measured by 2 * 13 extensometers (see Fig. 6.6). From these mean surface strains the mean curvature was calculated in the region with constant bending moment. Figs. 6.8a-b present the results of beams 1, 2, 6, 7, 8, 14 and 15. The bending moment was found by multiplying the force P (see Figs. 6.7a-b) by 1250 mm. This implies that the dead-weight is not incorporated. The dead-weight is also not included in the measurements of the extensometers, since all the measuring devices were attached after the beams had been placed in the frame.

65

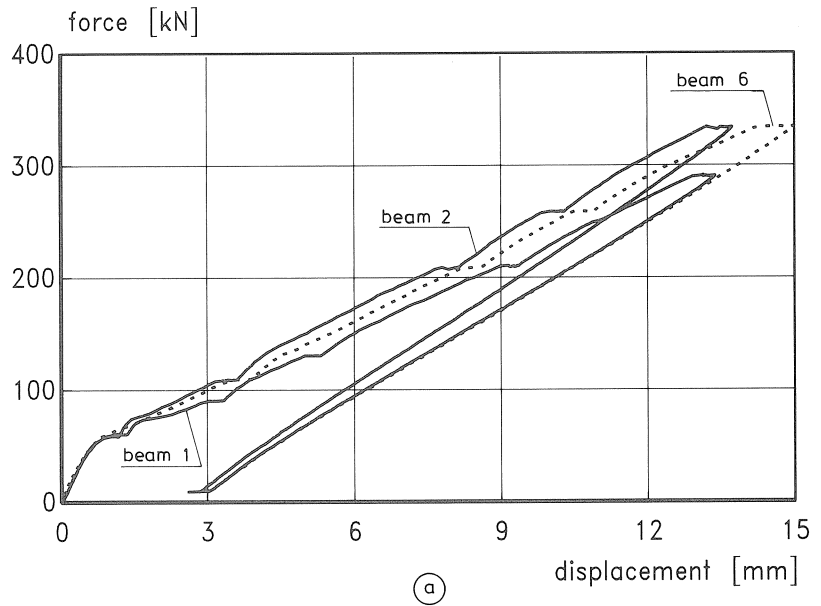Fig. 6.7a   The deflection at mid span as a function of the load applied for T-beams 1, 2 and 6 (main reinforcement $4 * d_s$ 20 mm).
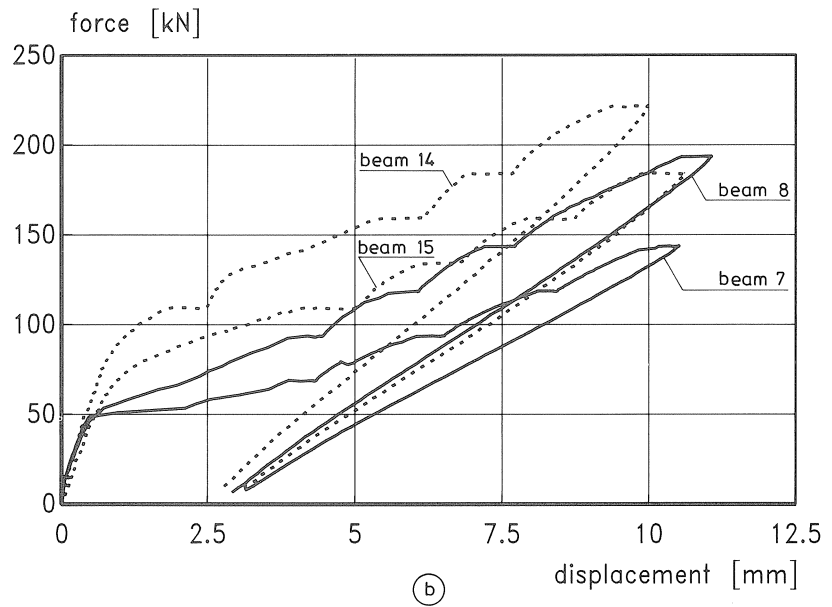

Fig. 6.7b   The deflection at mid span as a function of the load applied for T-beams 7 and 8 and rectangular beams 14 and 15 (main reinforcement $3 * d_s$ 16 mm).
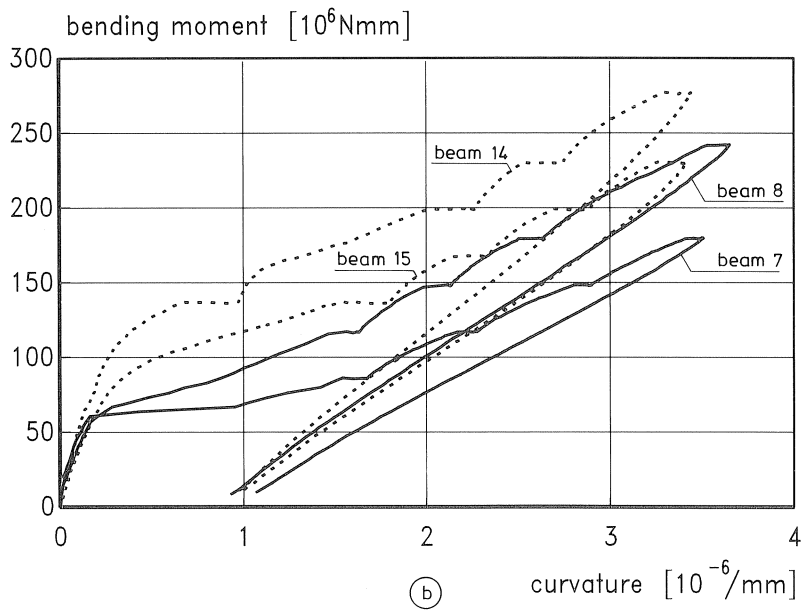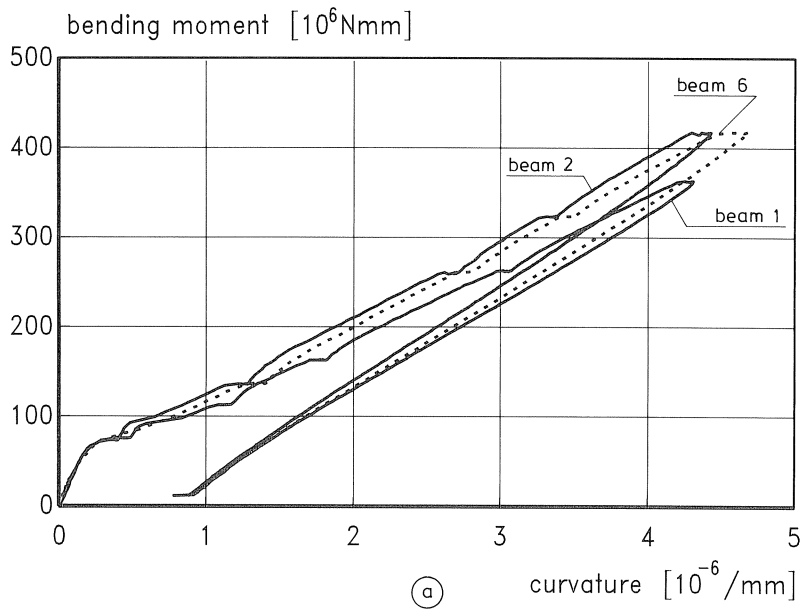
66

Fig. 6.8 The bending moment-curvature relations: Beams 1, 2 and 6 (a) and 7, 8, 14 and 15 (b).

– The mean crack width and the mean crack spacing:
Table 6.5 contains the results of the crack width measurements of beam 4. The first column presents the loading stage. The corresponding load P (see Fig. 6.6) can be calculated by adding the load of the loading frame ($P = 9$ kN) to half of the load applied by the hydraulic jack. The second column gives the number of the measuring lines where all the measurements were taken (see also Fig. 6.5). The third column presents the total number of crack width measurements taken on both sides of the beam. The

Table 6.5 Results of the crack width measurements of beam 4

loading stage	line	no.	l_m [mm]	w_{min} [mm]	w_{max} [mm]	w_m [mm]	c.v. [–]	w_k [mm]	w_k/w_m [–]	w_{max}/w_m [–]
1	1	53	87	0.01	0.10	0.055	0.44	0.09	1.72	1.82
	2	52	88	0.01	0.11	0.045	0.52	0.08	1.86	2.47
$P = 109$ kN	3	34	135	0.01	0.13	0.067	0.50	0.12	1.82	1.94
	4	31	148	0.01	0.15	0.063	0.67	0.13	2.11	2.37
	5	28	164	0.01	0.18	0.068	0.83	0.16	2.36	2.64
	6	20	230	0.01	0.17	0.081	0.66	0.17	2.09	2.11
	7	15	307	0.01	0.15	0.079	0.56	0.15	1.91	1.89
	8	12	383	0.03	0.15	0.091	0.40	0.15	1.66	1.65
	9	11	418	0.01	0.08	0.042	0.58	0.08	1.96	1.91
2	1	63	73	0.01	0.21	0.098	0.54	0.18	1.88	2.14
	2	58	79	0.01	0.20	0.088	0.53	0.17	1.87	2.26
$P = 209$ kN	3	48	96	0.01	0.22	0.106	0.50	0.19	1.82	2.07
	4	47	98	0.02	0.25	0.093	0.67	0.19	2.09	2.70
	5	39	118	0.01	0.26	0.105	0.77	0.24	2.27	2.47
	6	31	148	0.01	0.32	0.106	0.82	0.25	2.35	3.01
	7	20	230	0.02	0.27	0.129	0.65	0.27	2.06	2.09
	8	17	271	0.02	0.28	0.132	0.60	0.26	1.99	2.13
	9	13	354	0.01	0.15	0.090	0.50	0.16	1.82	1.67
3	1	64	72	0.01	0.26	0.118	0.54	0.22	1.89	2.20
	2	59	78	0.01	0.23	0.113	0.48	0.20	1.79	2.03
$P = 259$ kN	3	49	94	0.02	0.26	0.133	0.45	0.23	1.74	1.96
	4	48	96	0.01	0.30	0.114	0.60	0.23	1.99	2.62
	5	41	112	0.01	0.32	0.128	0.78	0.29	2.28	2.51
	6	33	139	0.01	0.35	0.130	0.79	0.30	2.30	2.69
	7	21	219	0.01	0.34	0.157	0.65	0.32	2.07	2.17
	8	17	271	0.03	0.32	0.174	0.55	0.33	1.90	1.84
	9	15	307	0.01	0.20	0.102	0.64	0.21	2.05	1.96
4	1	65	71	0.02	0.32	0.156	0.53	0.29	1.88	2.06
	2	60	77	0.02	0.32	0.147	0.49	0.26	1.80	2.18
$P = 334$ kN	3	51	90	0.03	0.33	0.168	0.44	0.29	1.72	1.97
	4	49	94	0.03	0.35	0.149	0.55	0.29	1.91	2.34
	5	43	107	0.01	0.40	0.155	0.77	0.35	2.27	2.58
	6	36	128	0.01	0.42	0.159	0.85	0.38	2.39	2.64
	7	24	192	0.01	0.42	0.179	0.74	0.40	2.22	2.35
	8	18	256	0.02	0.42	0.222	0.59	0.44	1.97	1.89
	9	15	307	0.01	0.28	0.135	0.61	0.27	2.00	2.08
Measurements:		1300					36		36	36
Mean value:							0.61		2.00	2.21

mean crack spacing is presented in the fourth column and is calculated by dividing the total length of the crack width measuring zone by the number of cracks. For the first beam this length was 4800 mm, whereas for the other 14 beams it was 4600 mm. The following three columns present the minimum, maximum and average crack width respectively. From all the measurements the coefficient of variation was calculated (see the eighth column). The characteristic (95%-upper bound) crack width was calculated as $w_k = w_m * (1 + 1.64 * cv)$. The last two columns contain the ratios of characteristic and maximum to the mean crack width respectively. When considering the results of all the beams the following conclusions can be drawn:
- At the level of the main and the web reinforcement:
  $w_k/w_m = 1.81$ $(cv = 0.07; n = 165)$
  $w_{max}/w_m = 2.12$ $(cv = 0.13; n = 165)$
- At the measuring lines between the reinforcement:
  $w_k/w_m = 1.90$ $(cv = 0.13; n = 390)$
  $w_{max}/w_m = 2.04$ $(cv = 0.17; n = 390)$

The location of the stirrups in the uniform bending moment zone was known precisely. After the tests the cracks initiated by the stirrups were registered. The mean crack width at the stirrups was compared with the mean width of all the cracks. A total (n) of 555 ratios was collected. The mean value was 1.42 $(cv = 0.20)$. This ratio must be interpreted with caution since the crack width at the stirrups is the mean value of at most four measurements (two stirrups; measurements at both sides of the beams).

Figs. 6.9a-c present the mean crack width over the height of several beams. In Fig. 6.9a the influence of the diameter of the web rebars is shown. All three beams contain the same amount of main reinforcement, viz. $4 * d_s$ 20 mm. Beam 1 contains no web reinforcement, whereas beams 3 and 6 contain one bar at each side of the web. The diameter of these bars is 12 and 10 mm respectively. The load P (including half the weight of the loading frame) is presented in the right upper corner of the figure. On the vertical axis, y is the distance to the bottom of the beam.
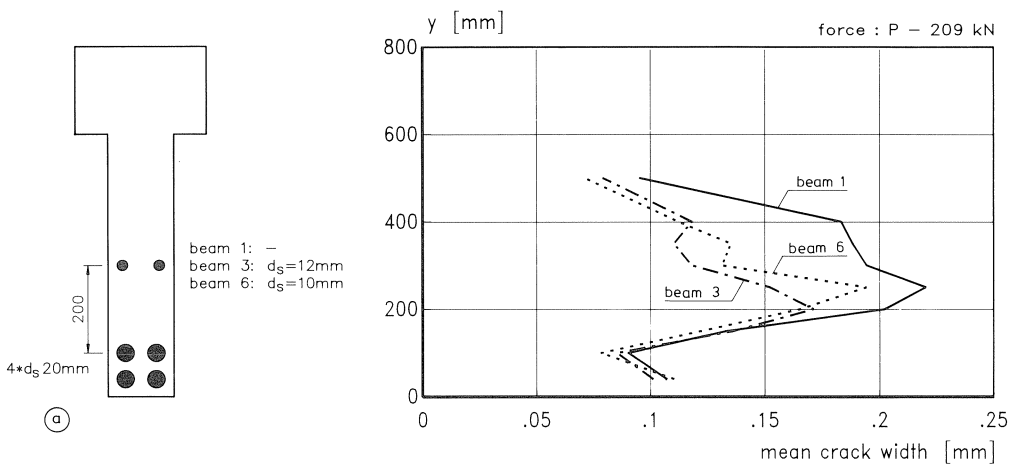
The influence of the bar spacing is shown in Fig. 6.9b. Just as in Fig. 6.9a, the load is $P = 209$ kN. In each side of the web of beams 4 and 6, one reinforcing bar with a 10 mm diameter is placed. The distance from the centre of the upper main rebars to the web rebar is 100 and 200 mm for beams 4 and 6 respectively.

Fig. 6.9c presents the influence of the number of layers of web reinforcement. Also in this figure, one curve refers to a beam without web reinforcement, viz. beam 7. All three
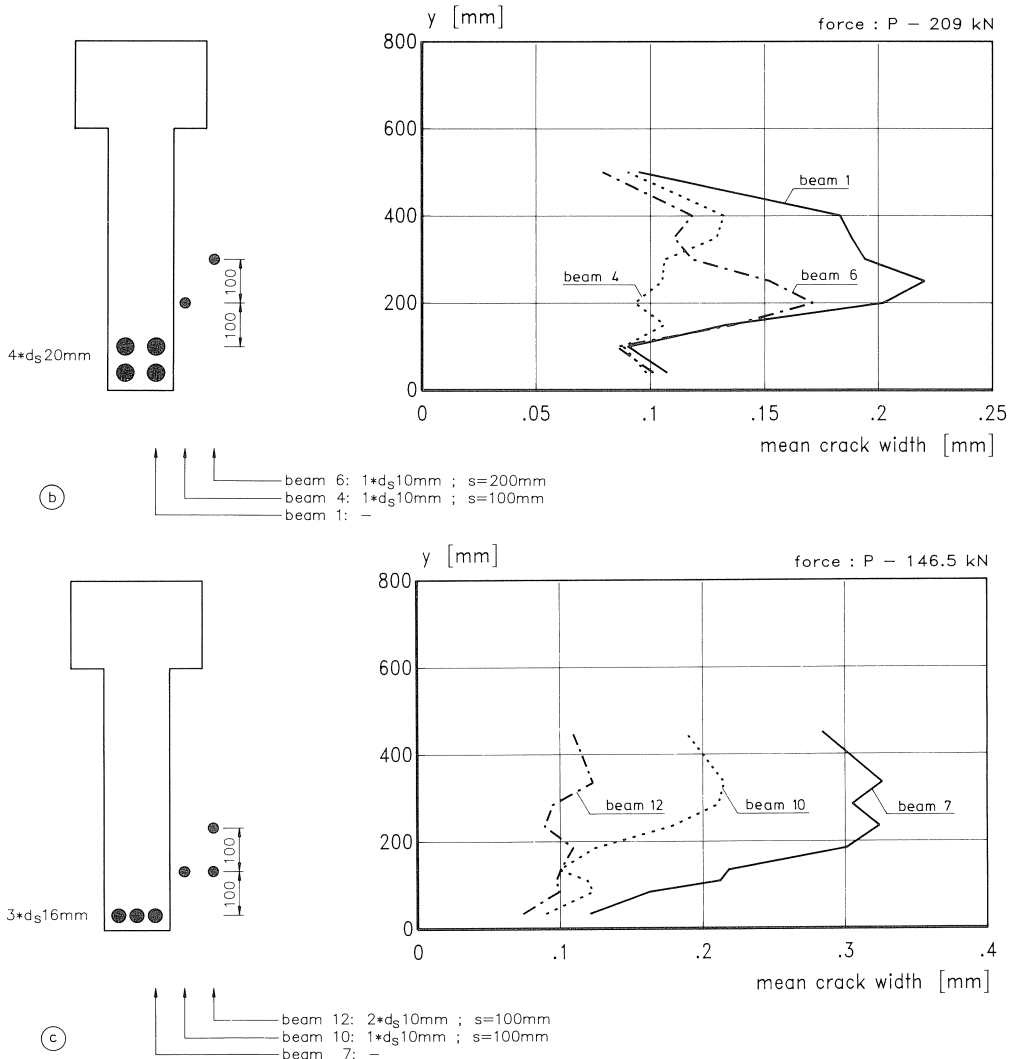
Fig. 6.9   The mean crack width over the height of several beams. This demonstrates the influence of:
a. the diameter of the web rebars
b. the spacing of the web rebars
c. the number of layers of web reinforcement

beams contain $3 * d_s$ 16 mm as main reinforcement. Beams 10 and 12 contain 1 and 2 layers of web reinforcement respectively. The diameter of the rebars in the web is 10 mm, whereas the bar spacing is 100 mm.

Figs. 6.9a-c clearly demonstrate that, as expected, the crack widths decrease as the amount of web reinforcement increases. Furthermore, the widest cracks in the un-reinforced part of the web occur about half way between the neutral axis and the upper web reinforcement.

Fig. 6.10 presents the crack patterns of beams 7 to 12. All the patterns were recorded at the maximum load applied, viz. $P = 146.5$ (beam 7), 171.5 (beams 9–11) and 196.5 kN (beams 8 and 12). It is clearly demonstrated that cracks are initiated by the web rein-forcement. This leads to a well distributed crack pattern over a larger part of the beam.

71
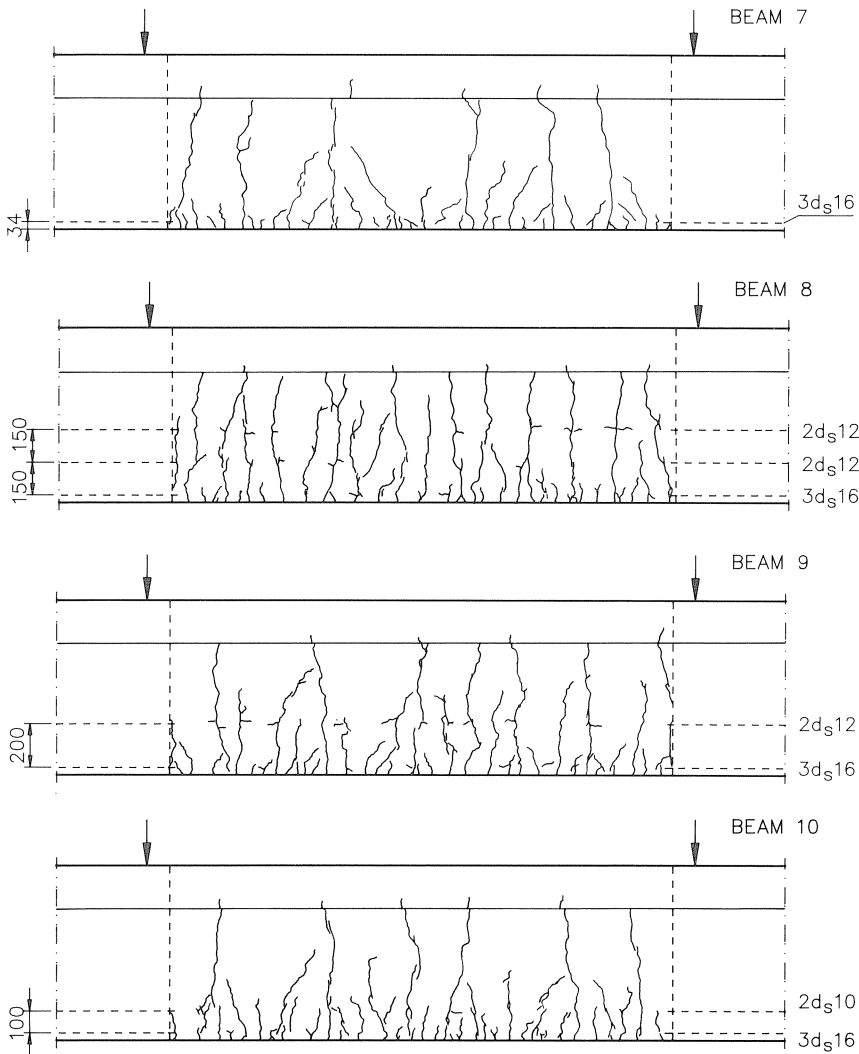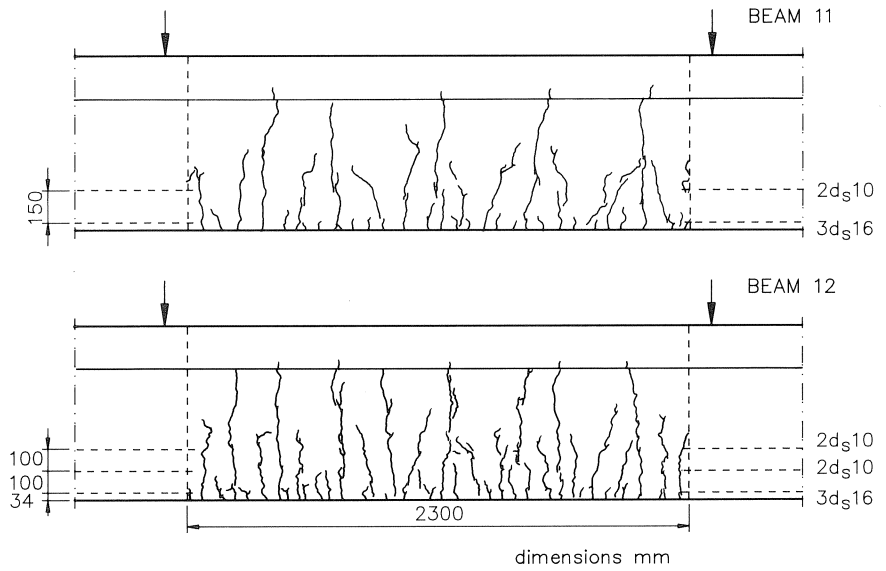
Fig. 6.10   The crack patterns of beams 7 to 12 after completion of the experiments.

The development of the crack patterns was also recorded. Fig. 6.11 presents the crack pattern on both side faces of beam 13 at several loading stages. These stages refer to a load P of 109, 184, 234 and 334 kN respectively. In the figure the stages are indicated by the Roman numerals I to IV. Beam 13 is a rectangular beam, provided with a main reinforcement consisting of 4 bars of 20 mm diameter. One layer of 12 mm diameter rebars
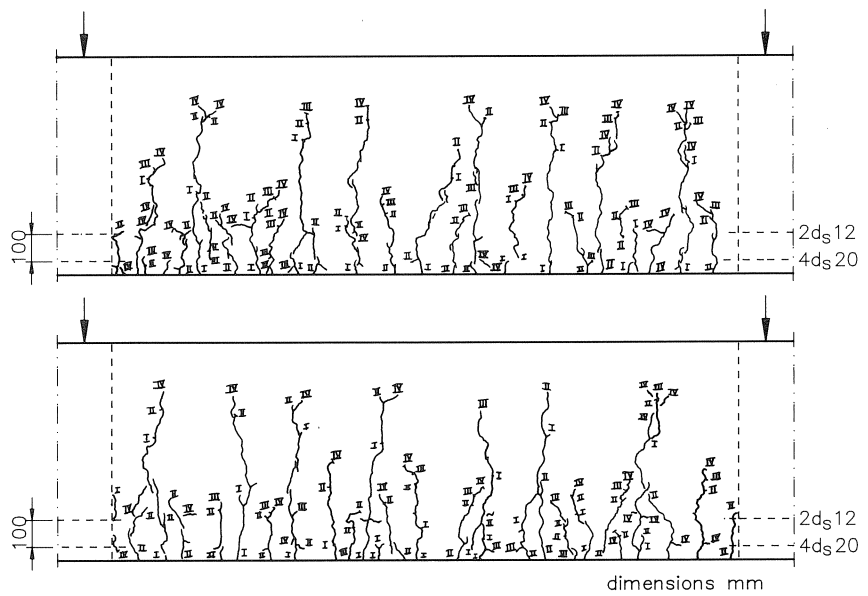
Fig. 6.11   The development of the crack pattern of beam 13.

72

is placed at both sides of the web. The bar spacing is 100 mm. From the figure it can be seen that in the first stage a rather limited number of cracks occur. These cracks penetrate through a relatively large part of the web. Between these primary cracks some secondary cracks also appear. However, they are restricted to the level of the main reinforcement. In the following loading stages the already existing cracks extend further into the web. The secondary cracks remain restricted to the part of the beam provided with reinforcement.

– The cracking moments:

Of all the 15 beams tested, the cracking load was registered. Table 6.6 contains the cracking moments, including the bending moment caused by the dead-weight of the beams. The average concrete tensile splitting strength on the day of testing f_{cspl} is also presented. The moment of inertia of the beams was calculated (including the influence of the reinforcement) and the concrete cracking stress was determined. When relating these stresses to f_{cspl}, it was observed that, on average, $\sigma_{cr} = 0.97 f_{cspl}$ (cv = 0.18) (see last column in Table 6.6). In nearly all the beams the first cracks were initiated at the stirrups. At increasing load the number of cracks increased rapidly. In this stage, the crack spacing was relatively large and all the cracks extended to the compression zone. The further increase of the load caused the formation of new cracks between the already existing ones. These new cracks were restricted to the level of the main reinforcement if no web reinforcement had been applied. By adding web reinforcement these cracks can be forced to extend into the web.

Table 6.6 The cracking moments and the cracking stresses related to the tensile splitting strength

beam no.	M_{cr} [10^6 Nmm]	σ_{cr} [MPa]	f_{cspl} [MPa]	σ_{cr}/f_{cspl} [–]
1	75	3.46	3.82	0.91
2	79	3.64	3.81	0.96
3	100	4.61	3.72	1.24
4	85	3.92	3.54	1.11
5	85	3.92	3.41	1.15
6	82	3.78	3.84	0.98
7	73	3.58	4.05	0.88
8	82	4.02	4.00	1.01
9	79	3.87	3.74	1.03
10	79	3.87	3.79	1.02
11	75	3.68	3.65	1.01
12	82	4.02	3.91	1.03
13	111	3.21	4.08	0.79
14	86	2.54	3.70	0.69
15	86	2.56	3.30	0.78

7 Verification and comparison of the experimental results

7.1 *Introduction*

In section 3.2 a model is presented to predict the crack spacing l_{sec} and the steel stress initiating secondary cracking $\sigma_{s,sec}$ in thick concrete tensile members provided with reinforcement concentrated at the side-faces. It is demonstrated that good agreement with the experimentally observed cracking behaviour is obtained. The codes tend to underestimate l_{sec} and $\sigma_{s,sec}$. In this chapter the model presented is used in the case of deep beams to calculate the crack spacing at the level of the main reinforcement. Subsequently, the same model is used for the crack spacing at the web reinforcement. If the crack spacing is known over the entire height of the beams, the "beam model" presented in chapter 5 can be used to investigate the overall structural behaviour, i.e. the bending moment-curvature relations.

7.2 *The mean crack width and spacing at the main reinforcement*

7.2.1 The mean crack spacing

In section 3.2 a model is introduced to calculate the secondary crack spacing l_{sec}. The model is based on the three-dimensional spreading of the bond stresses in a concrete structure, see Fig. 3.9. If the detailing of the reinforcement and the concrete quality are known, all the parameters are defined, viz. d_s, s, $h - d$ and f_{ct}.

Table 7.1 gives an overview of a comparison between the theoretical model and the experiments. It must be emphasized that it is assumed that the mean short-term concrete tensile strength $(f_{ctm,0})$ to be used in the model is equal to the splitting strength (f_{cspl}) as presented in Table 6.4. This is in accordance with Heilmann [1969], who stated that at an age of 90 days, both strengths can be assumed to be equal. With regard to the age of the beams at the time of testing (42 to 83 days), this assumption seems to be permitted. In Table 7.1 the experimental results are only presented in the case where the crack pattern is fully developed. The corresponding load P (see Fig. 6.6) is given in the fifth column. The load is equal to half of the load applied by the hydraulic jack and half the weight of the loading frame (9 kN). Thus, the dead-weight of the beams is not included. With regard to the mean strain in the case of a fully developed crack pattern, the following can be stated: Just before the secondary crack arises, the steel stress in the primary crack is $\sigma_{s,sec}$. Over the bond-free length l_0 the steel stress is constant, whereas the stress decreases linearly along the transfer length l_t because of the bond stresses between the concrete and the reinforcement (Fig. 7.1a). After the formation of the secondary crack (Fig. 7.1b), the steel stress in the secondary crack is also $\sigma_{s,sec}$. The mean strain is now:

$$\varepsilon_{sm} = \varepsilon_{s,sec} - \tfrac{1}{2}\Delta\varepsilon_s \left(1 - \frac{2l_0}{l_{sec}}\right) \quad [-] \tag{7.1a}$$
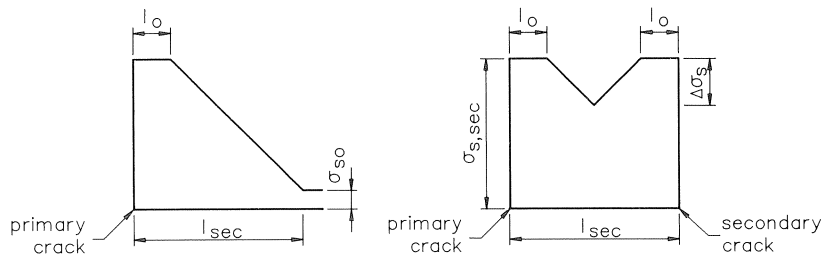
with:

74

Fig. 7.1   The steel stress just before (a) and after (b) secondary cracking.

$$\Delta \varepsilon_s = \frac{1}{E_s} \tfrac{1}{2}\left(l_{sec} - 2l_0\right) \frac{4\tau_b}{d_s} \quad [-] \tag{7.1b}$$

The combination of both formulas gives the following expression:

$$\varepsilon_{sm} = \varepsilon_{s,sec} - \frac{1}{E_s} \frac{\tau_b}{d_s} \frac{\left(l_{sec} - 2l_0\right)^2}{l_{sec}} \quad [-] \tag{7.1c}$$

In most cases it can be assumed that $\varepsilon_{sm} \simeq 0.9\varepsilon_{s,sec}$.

In beams 1–6 the main reinforcement was applied in two layers (see Fig. 6.3). The results for both layers are presented in Table 7.1. The first result refers to the rebars

Table 7.1   The mean crack spacing at the level of the main reinforcement. Comparison between theoretical model and experiments

beam no.	d_s [mm]	s [mm]	$h-d$ [mm]	experiments		theory	
				load [kN]	l_m [mm]	l_m [mm]	$\sigma_{s,sec}$ [MPa]
1	20	75	70	89-129-209-289	109- 89- 84- 84	96	143
					107- 89- 86- 84		
2	20	75	70	109-209-259-334	105- 92- 88- 88	96	142
					105- 82- 81- 82		
3	20	75	70	109-209-259-334	82- 75- 74- 74	96	139
					82- 68- 68- 67		
4	20	75	70	109-209-259-334	87- 73- 72- 71	96	132
					88- 79- 78- 77		
5	20	75	70	109-209-259-334	81- 69- 69- 69	96	128
					78- 68- 65- 65		
6	20	75	70	109-209-259-334	78- 71- 68- 67	96	144
					77- 66- 65- 65		
7	16	50	34	72- 97-122-147	72- 69- 66- 65	83	164
8	16	50	34	97-122-147-197	70- 70- 70- 70	83	162
9	16	50	34	97-122-147-172	70- 70- 66- 66	83	151
10	16	50	34	97-122-147-172	68- 66- 64- 64	83	153
11	16	50	34	97-122-147-172	70- 69- 68- 68	83	148
12	16	50	34	97-122-147-197	73- 69- 67- 66	83	158
13	20	75	50	184-234-334	105- 98- 92	126	202
14	16	100	44	159-184-222	124-112-115	174	318
15	16	100	44	109-134-159-184	139-139-135-131	174	284

situated closest to the tension face. The mean ratio between the theoretically predicted and experimentally observed crack spacings is 1.25 $(n = 82, cv = 0.11)$. In accordance with the codes a coefficient k_3 (see formula (2.23)) was used to account for the stress gradient over the "effective concrete area", $2(h - d)$. In the analyses this coefficient was assumed to be constant for the main reinforcement (viz. $k_3 = 0.85$), since it was found that the detailing of the reinforcement has little influence.

7.2.2 The mean crack width

In all the experiments presented in chapter 6, the surface strains were measured by means of extensometers (see Fig. 6.6). By linear interpolation between the strains at the tension and compression face of the beams, the average strain at every level along the height of the beams can be determined. According to existing cracking theories (see chapter 2), the mean crack width is calculated by multiplying the mean strain by the mean crack spacing. In section 7.2.1 it was demonstrated that good agreement between theory and experiment was obtained. Therefore, the theoretical mean crack spacing will be used to calculate the mean crack width. The results of the analysis are presented in Table 7.2. Just as in the preceding section, only the measurements related to a fully developed crack pattern are considered. The mean ratio between the theoretically predicted and experimentally observed crack widths is 1.67 $(n = 82, cv = 0.11)$.

Table 7.2   The mean crack width at the level of the main reinforcement. Comparison between theoretical model and experiments

beam no.	experiments w_m [mm]	theory w_m [mm]	$w_m \dfrac{\text{theory}}{\text{experiments}}$
1	0.04-0.06-0.11-0.15	0.07-0.10-0.18-0.24	1.60-1.62-1.64-1.63
	0.03-0.06-0.09-0.13	0.06-0.09-0.16-0.22	1.91-1.68-1.75-1.73
2	0.05-0.10-0.12-0.15	0.07-0.15-0.18-0.24	1.36-1.52-1.57-1.63
	0.04-0.07-0.09-0.12	0.06-0.13-0.16-0.21	1.71-1.86-1.86-1.79
3	0.04-0.09-0.11-0.15	0.07-0.15-0.18-0.24	1.62-1.66-1.66-1.67
	0.03-0.06-0.08-0.11	0.06-0.13-0.16-0.22	2.04-2.16-2.10-2.05
4	0.06-0.10-0.12-0.16	0.07-0.15-0.19-0.24	1.28-1.52-1.57-1.55
	0.05-0.09-0.11-0.15	0.06-0.13-0.17-0.22	1.41-1.52-1.47-1.47
5	0.05-0.09-0.11-0.14	0.07-0.15-0.18-0.24	1.43-1.71-1.67-1.70
	0.04-0.07-0.09-0.11	0.06-0.13-0.16-0.21	1.58-1.92-1.87-1.91
6	0.04-0.08-0.10-0.14	0.08-0.15-0.19-0.25	1.70-1.88-1.89-1.86
	0.04-0.07-0.09-0.11	0.07-0.14-0.17-0.22	1.72-1.95-2.01-1.97
7	0.05-0.07-0.10-0.12	0.09-0.12-0.15-0.18	1.68-1.59-1.57-1.91
8	0.05-0.06-0.08-0.12	0.08-0.10-0.13-0.18	1.61-1.60-1.54-1.53
9	0.06-0.08-0.10-0.11	0.10-0.13-0.16-0.19	1.51-1.55-1.62-1.65
10	0.06-0.08-0.09-0.11	0.10-0.13-0.16-0.18	1.71-1.64-1.73-1.66
11	0.06-0.08-0.10-0.12	0.10-0.13-0.16-0.18	1.58-1.60-1.62-1.56
12	0.05-0.06-0.07-0.10	0.08-0.10-0.13-0.18	1.64-1.74-1.75-1.81
13	0.09-0.11-0.16	0.13-0.18-0.26	1.45-1.56-1.64
14	0.13-0.14-0.17	0.21-0.25-0.33	1.62-1.86-1.90
15	0.12-0.15-0.19-0.21	0.16-0.21-0.26-0.32	1.34-1.41-1.40-1.48

mean: 1.67 $(n = 82, cv = 0.11)$

From Table 7.2, it appears that the theory overestimates the measured values, although the crack spacing is in correspondence with the experimental results and the average strain was measured during the tests. An explanation for this finding is the fact that the crack pattern is "frayed" at the level of the reinforcement: The elongation is not concentrated only in the major cracks. Mostly, one major crack is accompanied by several small cracks. These cracks might be internal cracks that spread from the ribs of the rebar and reach the concrete surface [Goto, 1971]. In most of the beams tested, all these small cracks were within 1 cm of the major crack. Fig. 7.2 presents typical examples of a "frayed" crack pattern in beam 13. Major cracks at the level of the main reinforcement are shown. The minor cracks are also indicated. The load on the beam is $P = 150$ kN. The distance from the tension face of the beam to the horizontal measuring line is 50 mm.
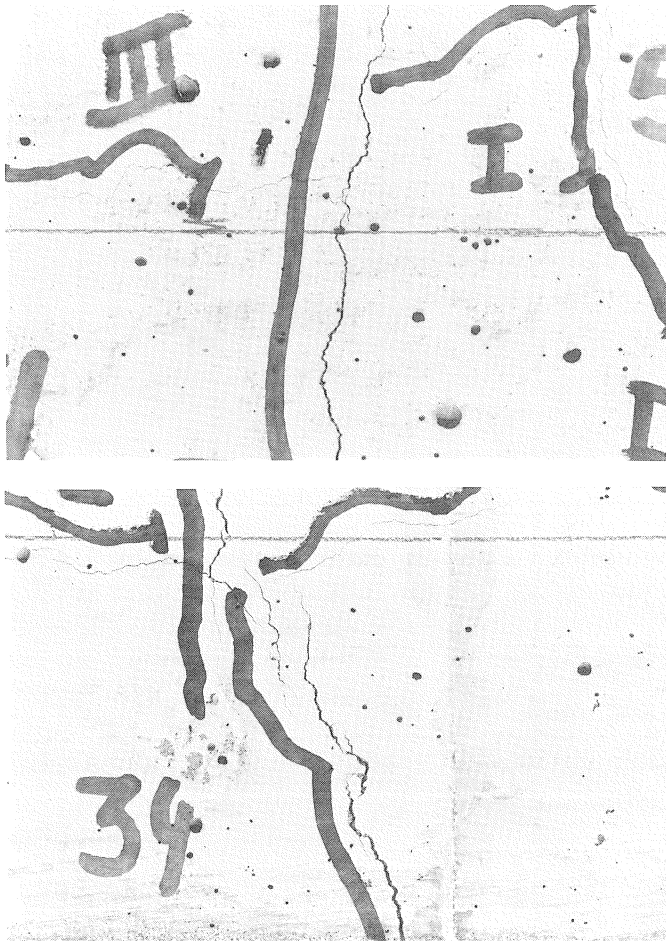

Fig. 7.2   Major cracks at the level of the main reinforcement accompanied by several minor cracks (beam 13; $P = 150$ kN).

In the measurements, attention was focused on the major cracks, and therefore the total width of the cracks considered will be less than the total elongation. The same phenomenon was observed by Breen and Frantz [1978]. Van Mier [1990] also observed it in the case of plain concrete. A comparison between the sum of the crack width and the elongation is made in Table 7.3. The same loading stages as in Table 7.2 are considered. It appears that 74% of the elongation can be found in the crack width measurements $(n = 82,\ cv = 0.11)$.

Table 7.3   The sum of the measured crack widths compared to the recorded elongation

beam no.	sum of crack widths [mm]	elongation [mm]
1	1.80-3.42-6.08- 8.56	3.28-5.12-8.75-12.22
	1.38-2.96-5.06- 7.32	2.96-4.61-7.88-10.99
2	2.16-4.87-6.04- 7.57	3.20-7.06-8.75-11.44
	1.54-3.97-5.02- 6.64	2.87-6.33-7.83-10.23
3	2.35-5.39-6.70- 9.01	3.27-7.02-8.76-11.61
	1.67-3.97-5.02- 6.64	2.93-6.30-7.86-10.40
4	2.92-6.17-7.55-10.12	3.37-7.15-8.89-11.58
	2.32-5.13-6.67- 8.81	3.03-6.42-7.98-10.38
5	2.74-5.69-7.30- 9.34	3.28-6.98-8.70-11.34
	2.28-4.63-6.16- 7.91	2.95-6.27-7.80-10.16
6	2.60-5.25-6.85- 9.33	3.58-7.31-9.16-12.02
	2.31-4.93-6.04- 8.12	3.22-6.55-8.20-10.76
7	3.29-4.98-6.75- 8.57	4.76-6.52-8.37-10.13
8	3.16-4.25-5.46- 7.71	4.28-5.69-7.10- 9.93
9	4.16-5.34-6.74- 7.91	5.28-6.96-8.63-10.30
10	3.93-5.38-6.50- 7.90	5.51-7.01-8.61-10.10
11	4.19-5.27-6.56- 8.05	5.51-7.02-8.62-10.22
12	3.03-4.05-5.12- 7.01	4.37-5.78-7.16-10.01
13	3.92-5.26-8.06	4.70-6.39-9.62
14	4.65-5.57-6.83	5.41-6.68-8.61
15	3.93-4.92-6.43- 7.49	4.20-5.55-6.99- 8.38

Beeby [1978] also pointed to a similar observation, see Fig. 7.3: The measured mean crack width is smaller than the mean crack spacing multiplied by the mean surface strain. Therefore, Beeby presented a formula which introduces a factor to take account of this finding [Beeby, 1971]:

$$w_m = l_m \varepsilon_m - 0.05 e^{-0.0135c} \quad [\text{mm}] \tag{7.2}$$

In this formula the last term is 0.029 and 0.038 mm, for a concrete cover (c) of 40 and 20 mm respectively.

7.2.3   Comparison with existing theories

In chapter 2 it was shown that several codes and models are very well able to predict the average crack width and spacing at the level of the main reinforcement in beams and in tensile members provided these have a uniformly distributed reinforcement. In this
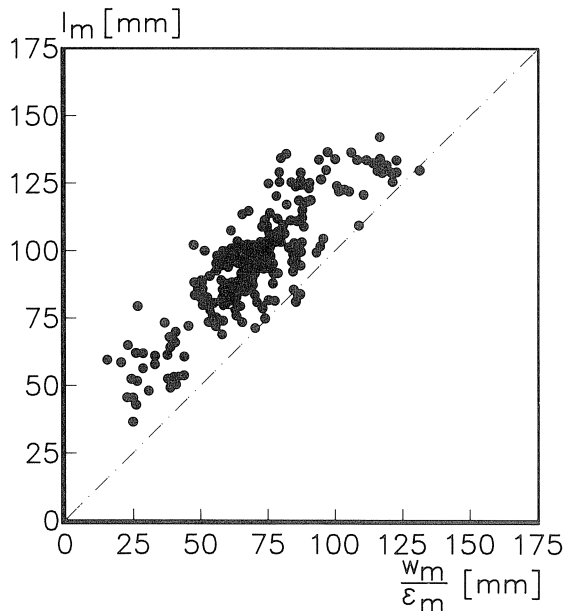
Fig. 7.3 Comparison between the mean crack width and the average crack spacing multiplied by the average surface strain measured [Beeby, 1978].

section attention will be focused on the mean crack spacing. The crack width is disregarded since it is easily calculated by multiplying the mean spacing by the mean strain. In the codes a coefficient k_3 (see formula (2.23) and Fig. 7.4) is introduced to account for the fact that, in the elastic stage, the mean concrete tensile stress over the "effective concrete area" is less than f_{ct}. In the case of the deep beams tested, the stress gradient is rather small. Just as in section 7.2.1, $k_3 = 0.85$ was used. Table 7.4 presents the mean crack spacing to be expected according to five relations. Two values are given, one in the case where the parameters according to "pure bending" are used $(k_3 = 0.5)$, whereas the second value refers to the case in which $k_3 = 0.85$ is used.

Only the model presented by Fehling and König has no specific input parameters in the case of pure bending: The beam is translated into a tensile member (by the "effective
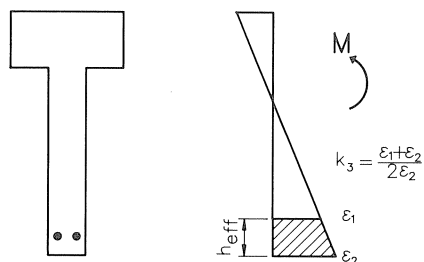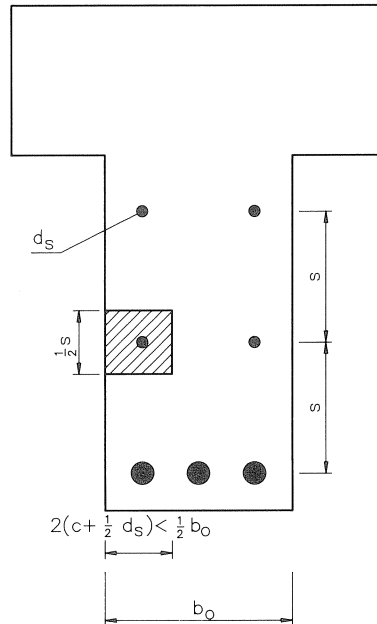

Fig. 7.4 The definition of the coefficient k_3.

Fig. 7.5 The "effective concrete area" used to calculate the crack pattern at the web reinforcement.

concrete area") and is further treated just the same way as a tensile member. The mean value of the experimental results is also presented. The number of values from which the results are derived is also given (n). The loading stages considered are the same as in Tables 7.1–7.3.

Table 7.4 The mean crack spacing at the main reinforcement: Experiments versus theory

beam no.	mean crack spacing [mm] bending/tension			
	1–6	7–12	13	14–15
CEB [1978]	97/103	106/113	143/151	157/188
Martin et al. [1980]	125/177	146/242	169/253	213/397
NEN 3880 [1984]	84/101	91/112	118/125	124/171
Eurocode 1990	92/121	92/122	110/152	138/236
Fehling/König [1988]	91	77	123	211
proposed model	96	83	126	174
experiments	79	68	98	128
n	48	24	3	7

From Table 7.4 it follows that the average crack spacing can be calculated accurately with existing codes provided that $k_3 = 0.5$. This was also concluded by Smit [1989] (see Table 2.3), who used $k_3 = 0.5$ independent of the height of the beams and plates analysed.

7.3 The mean crack width and spacing in the web

7.3.1 The mean crack spacing

In this section the same procedure as in section 7.2.1 will be followed. In section 3.2.2 a model to calculate the secondary crack spacing is developed for tensile members. It is shown in section 7.2.1 that the model can be extended to deep beams if the coefficient k_3 is included in the calculation. This coefficient takes account of the stress gradient in the linear elastic stage over the height of the "effective concrete area". The height is $2(h-d)$ if the main reinforcement is considered. In section 7.2.1 $k_3 = 0.85$ was used, since the coefficient of all the 15 beams tested differs only slightly from this value. With respect to the crack spacing at the web reinforcement the same procedure as in the case of the main reinforcement is followed. This procedure is explained in Fig. 7.5 and is given by the following formula, which is only a minor modification of formula (3.6):

$$\sum_{i=\frac{30\text{ mm}}{dx}}^{k} \frac{dF_\tau}{h_1 b_1} = k_3 2 f_{\text{ctm},0} \quad [\text{MPa}] \tag{7.3}$$

in which:

$$dF_\tau = u_s \tau_b \, dx$$
$$\tau_b = 2 f_{\text{ctm},0} \; [\text{Fehling/König, 1988}]$$
$$h_1 = 3 d_s + 1.5 i * dx \le 2(c + 0.5 d_s) \le 0.5 b_0$$
$$b_1 = 3 d_s + 1.5 i * dx \le \tfrac{1}{2} s$$

The coefficient k_3 is now defined by the hatched area in Fig. 7.5. If $k_3 \simeq 0.85$ for the main reinforcement, a value of about 0.75 can be assumed for the web reinforcement. As can be seen in Fig. 7.5, the height of the "effective concrete area" is defined by only the half of the bar spacing s. This was derived from the experimental results. The reason why the whole bar spacing is not used is because the main reinforcement induces cracks that penetrate in the web over a certain height, thus reducing the height of the concrete area stressed by the web reinforcement.

Where no web reinforcement is applied, the crack pattern is in accordance with the pattern that occurs in a concrete wall cast after the floor slab has hardened. Fig. 7.6a presents the schematized crack pattern of a wall without longitudinal reinforcement, cast on an infinitely stiff slab [CUR, 1978]. It was observed that the stiffness of the slab has minor influence on the type of crack pattern [CUR, 1978]. Therefore, the same procedure can be followed in the case of a deep beam, see Fig. 7.6b. The average crack spacing in the unreinforced web depends on the level considered. About half way down the beam, the mean crack spacing is:

$$l_m = h - h_x - (h - d) \quad [\text{mm}] \tag{7.4}$$

In section 3.3.1 it was concluded that, for the experiments under consideration, the ratio between the average crack spacing in the web and at the level of the main reinforcement is about 4. This finding can be explained with the aid of formula (7.4): In the case of
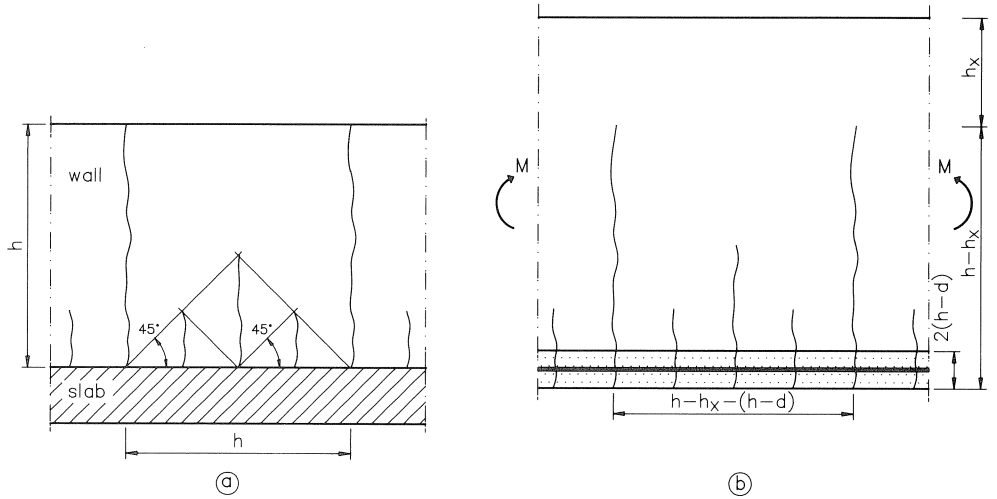
Fig. 7.6 The crack pattern of an unreinforced wall cast on a hardened slab [CUR, 1978] (a) and the corresponding model of a deep beam without web reinforcement (b).

a rectangular beam, h_x is calculated by formula (7.5).

$$\frac{h_x}{d} = -n\varrho_d + \sqrt{(n\varrho_d)^2 + 2n\varrho_d} \simeq 1.05(n\varrho_d)^{0.45} \quad [-] \tag{7.5}$$

The effective depth d is assumed to be $0.9h$. According to the Eurocode 1990, the average crack spacing at the main reinforcement is:

$$l_m = 50 + 0.1 \frac{d_s}{\varrho_{eff}} \quad [mm] \tag{7.6}$$

with:

$$\varrho_{eff} = \frac{d}{2.5(h-d)} \varrho_d \simeq 3.6\varrho_d$$

The Eurocode presents good agreement with the experimental results provided that $k_3 = 0.5$ is used in formula (7.6) (see sections 2.3.1 and 2.3.2). Thus, the following formula for the ratio between both crack spacings can be derived:

$$\frac{l_{m\,web}}{l_{m\,reinf}} = \frac{h\{0.90 - 0.94(n\varrho_d)^{0.45}\}}{50 + 0.028 \frac{d_s}{\varrho_d}} \quad [-] \tag{7.7}$$

Formula (7.7) is graphically presented in Fig. 7.7 where the ratio is shown as a function of the reinforcement ratio, for several combinations of bar diameter and beam height. It is demonstrated that in the case where combinations used in the experiments presented in chapter 3 are considered, good correspondence with the experimentally observed mean value of 4 is obtained. In these experiments the beam height was in the range of 700–1000 mm, and the reinforcement ratio $\varrho_d = 0.003$–0.010.
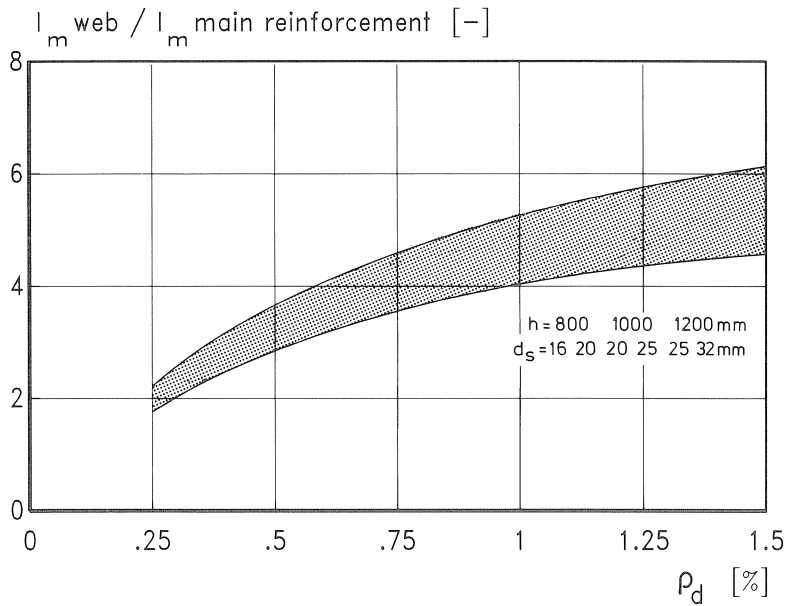
Fig. 7.7 The ratio between the mean crack spacing in the web and at the main reinforcement of beams without web reinforcement.

Now, the experimentally observed crack spacings at the web reinforcement will be compared with results obtained by the model presented. Table 7.5 contains the mean web crack spacing of 13 of the beams tested. Beams 1 and 7 are disregarded since they were not provided with web reinforcement. The load P is also presented. Several loading stages are not considered since the crack pattern is in general fully developed at

Table 7.5 The mean crack spacing at the level of the web reinforcement. Comparison between theoretical model and experimental results

| beam no. | theory | | experiments | | $l_m \dfrac{\text{theory}}{\text{experiments}}$ |
	$\sigma_{s,sec}$ [MPa]	l_{sec} [mm]	load P [kN]	l_m [mm]	
2	334	133	259-334	135-131	0.99-1.02
3	410	167	259-334	184-159	0.91-1.05
4	305	109	209-259-334	98- 96- 94	1.11-1.14-1.16
5	406	150	334	135	1.11
6	574	188	–	–	–
8	316	120	122-147-197	135-128-118	0.89-0.94-1.02
9	370	150	122-147-172	159-153-153	0.94-0.98-0.98
10	246	99	122-147-172	96- 94- 94	1.03-1.05-1.05
11	327	136	147-172	131-131	1.04-1.04
12	254	99	97-122-147-197	112-107-100-100	0.88-0.93-0.99-0.99
13	311	116	184-234-334	107-102-100	1.08-1.14-1.16
14	226	124	159-184-222	139-131-124	0.89-0.95-1.00
15	327	150	159-184	148-148	1.01-1.01

mean: 1.02
$(n=31, \; cv=0.08)$

83

higher strains than in the case of the main reinforcement. This is due to the relatively high steel stress initiating secondary cracking. Moreover, the web reinforcement is situated closer to the neutral axis, which implies that a certain desired average strain is reached at rather high load levels. Therefore, only the lower bars of the beams provided with two layers of web reinforcement are considered. The average ratio between the calculated and the measured crack spacings is 1.02 ($n = 31$, $cv = 0.08$). For beam 6 no experimental results are presented since the crack pattern in the web was not fully developed.

7.3.2 The mean crack width

Table 7.6 presents the mean crack widths at the level of the lower web reinforcement for the beams and loads from Table 7.5. The measured mean surface strain was used as input for the theoretical crack width.

The same finding is observed as for the main reinforcement, viz. the theory over-estimates the mean crack width measured. Also for the web reinforcement the sum of the measured crack widths can be compared to the elongation as derived from the mean surface strains. If the same loading stages as in the Tables 7.5 and 7.6 are considered, it is found that the crack widths present only 72% of the total elongation ($n = 31$, $cv = 0.14$). This is in agreement with the result for the main reinforcement, see Table 7.3.

Table 7.6   The mean crack width at the level of the web reinforcement. Comparison between theoretical model and experiments

beam no.	experiments w_m [mm]	theory w_m [mm]	$w_m \dfrac{\text{theory}}{\text{experiments}}$
2	0.12-0.14	0.16-0.22	1.31-1.63
3	0.13-0.16	0.17-0.23	1.32-1.44
4	0.09-0.11-0.15	0.12-0.15-0.20	1.30-1.32-1.33
5	0.16	0.24	1.51
6	–	–	–
8	0.08-0.10-0.13	0.14-0.18-0.23	1.75-1.77-1.86
9	0.11-0.13-0.14	0.15-0.19-0.23	1.36-1.46-1.57
10	0.08-0.10-0.12	0.10-0.13-0.18	1.27-1.29-1.50
11	0.14-0.17	0.19-0.23	1.35-1.33
12	0.06-0.08-0.10-0.14	0.10-0.13-0.16-0.18	1.56-1.51-1.56-1.31
13	0.07-0.09-0.15	0.10-0.13-0.20	1.36-1.39-1.33
14	0.09-0.11-0.13	0.11-0.13-0.17	1.13-1.20-1.27
15	0.12-0.14	0.17-0.20	1.41-1.40

mean: 1.42
($n = 31$, $cv = 0.16$)

7.4.   *The bending moment-curvature diagram*

7.4.1 Introduction

In the previous sections 7.2 and 7.3, it is demonstrated that the average crack spacing can be calculated over the entire height of deep beams, either with or without web reinforcement. In the analyses, the mean surface strains measured during the experiments

84

are used to calculate the crack widths. To complete the cracking theory, the calculation of the mean surface strain is now presented. For that purpose, the "beam model" presented in chapter 5 is used.

7.4.2 Input parameters for the "beam model"

In the "beam model", a part of a beam is modelled. The length of this part is one of the input parameters. In chapter 5 it was demonstrated that tension stiffening can be accounted for by the stress-average strain curve of a reinforcing bar. Thus, the stiffening is implemented in the reinforcement instead of the concrete. The latter schematization was used in the DIANA calculations presented in section 4.3. In the "beam model" another approach was chosen, since the stress-strain curve of the concrete can now be used to model the softening of plain concrete in tension. For the rebars, the major parameters are the secondary crack spacing l_{sec} and the stress initiating secondary cracking $\sigma_{s,sec}$. The model to calculate both these parameters is discussed in sections 7.2 and 7.3. With regard to the softening of plain concrete a model is presented in section 5.2.2: The length over which the softening is "smeared" depends on the crack height and the length of the part of the beam analysed. With regard to the crack pattern presented in Fig. 7.6b, it is decided to "smear" the softening over (also see Fig. 5.5):

$$l_1 = 2(h_{cr} - y) \le h - h_x \quad [\text{mm}] \tag{7.8}$$

Using the "beam model" four of the beams tested were analysed. Both the measured and calculated bending moment-mean curvature curves of four bars are presented in Figs. 7.8a-d. To test the validity of the model, beams with considerably varying parameters were chosen. Beams 1 and 8 have a T-shaped cross-section, whereas 14 and 15 are rectangular. Furthermore, beam 1 contains no web reinforcement. With regard to the main reinforcement, beam 1 is provided with $4 * d_s$ 20 mm, while the other beams contain $3 * d_s$ 16 mm. In the experiments, the dead-weight of the beams is not incorporated in either the bending moment or the curvature. Therefore, the measured values were adjusted, so that the curves can be compared directly. Moreover, in the experiments the curvature increased during the time required for the crack width measurements. In the curves presented in the Figs. 7.8a-d, the increase of the concrete compressive strain during these measurements was eliminated in the calculation of the curvature. It is emphasized that the influence was found to be relatively small. From the figures presented, it appears that the "beam model" is well able to predict the behaviour. The figures also present the curves in the cases where no tension stiffening and softening are taken into account. Thus, these curves correspond to the behaviour calculated on the basis of a cracked cross-section, i.e. the concrete tensile strength is assumed to be zero. The mean curvature can be calculated accurately by using the following well-known formula from the codes:

$$\varkappa_m = \varkappa \left[1 - \left(\frac{M_{cr}}{M} \right)^2 \right] \quad [\text{mm}^{-1}] \tag{7.9}$$

for $M > M_{cr}$.

The curvature $\varkappa$ refers to a cracked cross-section. Formula (2.5) and Fig. 2.5 present the same approach for a tensile member. It is emphasized that the tension stiffening according to formula (7.9) must be reduced if a sustained or varying load is applied. With regard to the strains the same procedure can be followed. From the steel strains ε_s in a crack, the mean steel strain ε_{sm} can be calculated if the curvature in formula (7.9) is
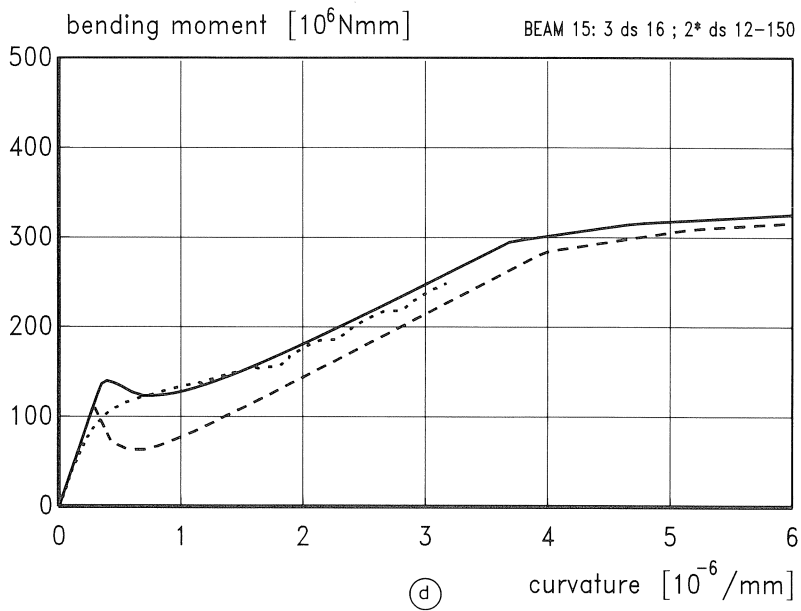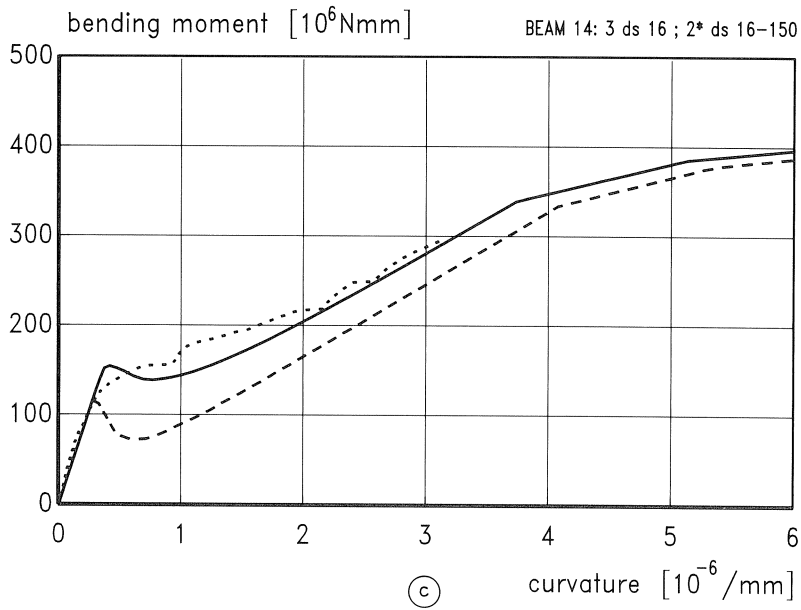

(a)

(b)
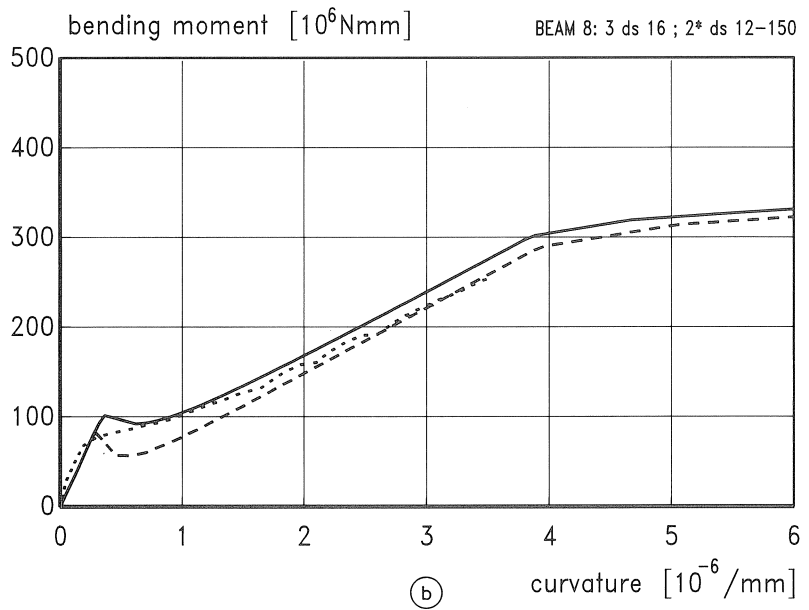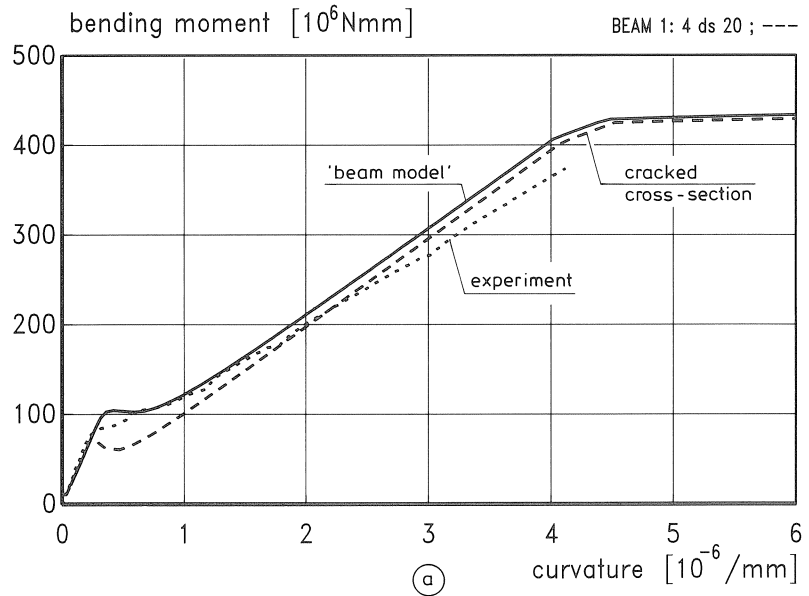
Fig. 7.8 Bending moment-mean curvature relations of four beams:
a. beam 1: $4 * d_s$ 20 mm, - - -
b. beam 8: $3 * d_s$ 16 mm, 2 layers d_s 12 mm ($s = 150$ mm)
c. beam 14: $3 * d_s$ 16 mm, 2 layers d_s 16 mm ($s = 150$ mm)
d. beam 15: $3 * d_s$ 16 mm, 2 layers d_s 12 mm ($s = 150$ mm)

replaced by a strain. Thus, the mean strain in the main and the web reinforcement can be calculated. If the mean strain is less than about $0.9\varepsilon_{s,sec}$, the crack pattern at the level of the relevant reinforcement is not fully developed. The steel stress in a crack is then equal to $\sigma_{s,sec}$. If the mean strain exceeds $0.9\varepsilon_{s,sec}$, the crack pattern is fully developed. The mean steel strain is then about $\varepsilon_{sm} = 0.9\varepsilon_s$. Thus, the steel stress in a crack is $1.1E_s\varepsilon_{sm}$.

7.5 Conclusions

In this chapter, the experimental results are analysed and compared with computational results obtained using models presented in chapters 3 and 5. With regard to the cracking behaviour of the beams, it is found that the model based on the "effective concrete area" around the reinforcement is well able to calculate the crack spacing at the main and the web reinforcement of beams. For the calculation of crack widths the average surface strain is also required. In section 7.4 it is demonstrated that the average curvature can be calculated accurately with the beam model. For practical use, it is advisable to perform a calculation on the basis of the behaviour of a cracked cross-section. The tension stiffening is then accounted for by existing theories.

The average strains can be derived from the mean curvature. Then, it can be judged whether the crack pattern is fully developed. As long as the crack pattern is not fully developed, the steel stress in a crack is equal to the steel stress that initiates secondary cracking. If the crack pattern is fully developed, the steel stress is directly related to the mean steel strain.

Thus, a calculation based on the behaviour of a cracked cross-section is only suitable for calculating the mean curvature and the mean strains. This was already demonstrated in chapter 4. If the stresses in the reinforcement are required, the mean strain must be related to the steel stress that initiates secondary cracking in order to judge whether the crack pattern is fully developed or not.

The crack widths are overestimated if they are calculated on the basis of the average crack spacing and the average strain at the level considered. This phenomenon was already observed by several other investigators. From the experimental results, it was derived that about 75% of the elongation is concentrated in the major cracks. The rest of the elongation is found in minor cracks that accompany the major cracks.

8 Design curves and working examples

8.1 Introduction

In chapter 7 it is demonstrated that the cracking theory developed in chapter 3 can be used to predict the cracking behaviour at the level of both the main and the web reinforcement. The mean surface strain can be calculated according to existing theories based on the behaviour of a cracked cross-section. The tension stiffening is accounted for by reducing the strain in a crack by a factor that depends on the load level and the type of loading. If both the mean crack spacing and the surface strain are known, the

crack widths can be calculated. However, the formula that defines the mean crack spacing (see chapters 3 and 7) is complicated and not suitable for the use in engineering practice. Therefore, attention is focused in this chapter on design curves for the detailing of the reinforcement. These curves are presented in section 8.2. In section 8.3, the theory developed will be applied to a deep beam and a tension member with reinforcement located at the side-faces. The results will be compared with the present design rules.

8.2 *Diagrams for the detailing of the reinforcement*

The secondary crack spacing l_{sec} is calculated with formulae (3.6)/(3.8b) and (7.3)/(3.8b) for the main and the web reinforcement respectively. If the crack pattern is fully developed, the mean crack spacing is $l_m = l_{sec}$. The secondary crack spacing depends on the bar diameter d_s, the bar spacing s and the "effective concrete area" $2(h - d)$. The concrete tensile strength has no influence on the crack spacing, since f_{ct} is used in both the bond stress and the cracking criterion as a linear function. The steel stress initiating secondary cracking $\sigma_{s,sec}$ can be calculated if the secondary crack spacing is known (see formula (3.7b)). Furthermore, the coefficient k_3 that takes account of the stress gradient in the uncracked stage must be used. This coefficient is 0.5 and 1 in the case of a triangular and rectangular stress distribution over the "effective concrete area" respectively. Since the formulae are complicated, both l_{sec} and $\sigma_{s,sec}$ are presented in diagrams, see Fig. 8.1. This figure presents the results for $f_{ct} = 2.5$ MPa, $k_3 = 1.0$ and $2(h - d)/n_s = 100$ mm. n_s is the number of layers of reinforcement.

With regard to the web reinforcement, the following remarks must be made: For the web reinforcement, $h - d$ is equal to the sum of the concrete cover, the diameter of the stirrups and half the bar diameter. With regard to the bar spacing, only the half of the actually applied spacing must be used in the diagrams. This was concluded in chapter 7 (see formula (7.3)) and is explained by the reduction of the "effective concrete area" around the web reinforcement by cracks initiated by bars located lower down in the cross-section.

If the parameters differ from the assumed values, the following formulae can be used to calculate l_{sec} and $\sigma_{s,sec}$:

$$l_{sec} = l_{sec}^d \left(0.875 * 10^{-2} \frac{2(h - d)}{n_s} + 0.125 \right) k_3 \quad \text{[mm]} \tag{8.1}$$

$$\sigma_{s,sec} = \sigma_{s,sec}^d \left(0.875 * 10^{-2} \frac{2(h - d)}{n_s} + 0.125 \right) k_3 \frac{f_{ct}}{2.5} \quad \text{[MPa]} \tag{8.2}$$

In formulae (8.1) and (8.2) the superscript "d" refers to the "diagrams" (Figs. 8.1a-b). The crack pattern is fully developed if the mean strain ε_{sm} exceeds about $0.9\varepsilon_{s,sec}$, see section 7.2.1. The mean crack width is:

$$w_m = 0.75 l_m \varepsilon_{sm} = 0.75 [l_{sec} \varepsilon_s - \tfrac{1}{2}(l_{sec} - 2l_0) \Delta \varepsilon_s] \quad \text{[mm]} \tag{8.3}$$

In this formula, ε_s is the strain at the level considered, calculated on the basis of a

cracked cross-section. $\Delta \varepsilon_s$ is the tension stiffening term, and is calculated according to (see formula (7.1b)):

$$\Delta \varepsilon_s = \frac{1}{E_s} \frac{1}{2} (l_{\text{sec}} - 2l_0) \frac{4\tau_b}{d_s} \quad [-] \tag{8.4}$$

secondary crack spacing [mm]
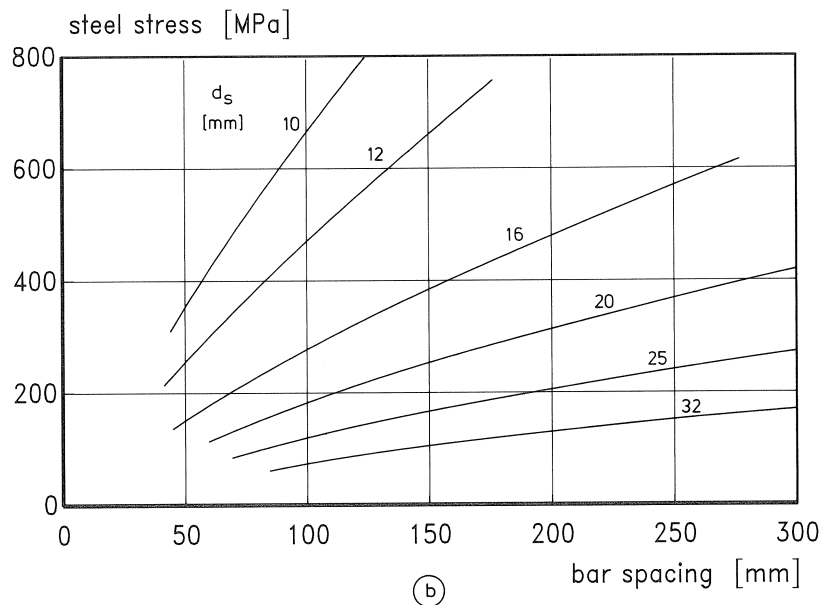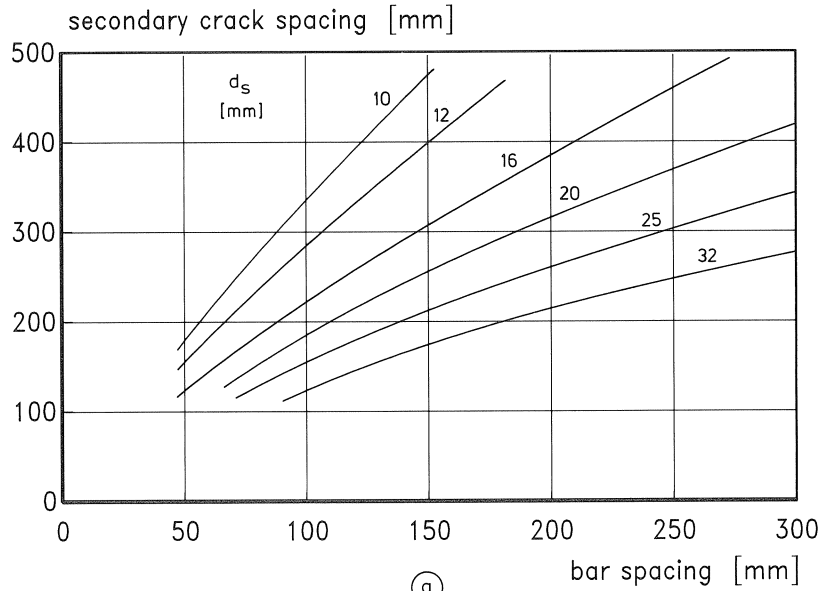
(a)

steel stress [MPa]

(b)

Fig. 8.1. Secondary crack spacing (a) and steel stress initiating secondary cracking (b) for $f_{ct} =$ 2.5 MPa, $k_3 = 1.0$ and $2(h-d)/n_s = 100$ mm.

90

The factor 0.75 in formula (8.3) is introduced in correspondence with the experimental results, as discussed in sections 7.2.2 and 7.3.2. The 95%-upper bound crack width is calculated according to:

$$w_k = 1.7 w_m \quad [\text{mm}] \tag{8.5}$$

The factor 1.7 is used in most of the codes, and the experimental results presented in chapter 6 are in close agreement with this value.

In the case of a not fully developed crack pattern, the characteristic crack width is [Fehling and König, 1988]:

$$w_k = 0.75 * 2l_{sec}\varepsilon_{sm} = 0.75\left[2l_{sec}\varepsilon_{s,sec} - \tfrac{1}{2}(2l_{sec} - 2l_0)\Delta\varepsilon_s\right] \quad [\text{mm}] \tag{8.6}$$

in which:

$$\Delta\varepsilon_s = \frac{1}{E_s}\left(l_{sec} - l_0\right)\frac{4\tau_b}{d_s} \quad [-] \tag{8.7}$$

The mean crack width is:

$$w_m = w_k/1.4 \quad [\text{mm}] \tag{8.8}$$

For the bond-free length $l_0 = d_s$ is assumed.

Formulae (8.3–8.5) and (8.6–8.7) can be approximated as follows:

Not fully developed crack pattern:

$$w_k = 0.75 * 2l_{sec}0.6\varepsilon_{s,sec} = 0.9l_{sec}\varepsilon_{s,sec} \quad [\text{mm}] \tag{8.9a}$$

Fully developed crack pattern:

$$w_k = 1.7w_m = 1.7 * 0.75l_{sec}0.9\varepsilon_s = 1.15l_{sec}\varepsilon_s \quad [\text{mm}] \tag{8.9b}$$

In the case where a long-term or varying load is applied, the relations (8.9a-b) must be adjusted since the bond stress decreases. This is incorporated by reducing the bond stress by 30%, thus $\tau_{b\infty} = 1.4f_{ctm,0}$. In the case of a not fully developed crack pattern, the transfer length increases by about 40%, which means that $1.4l_{sec}$ instead of l_{sec} must be used in the formulae. When the crack pattern is fully developed, the mean steel strain increases, i.e. ε_{sm} is $0.95\varepsilon_{s,sec}$ instead of $0.9\varepsilon_s$. Thus:

Not fully developed crack pattern:

$$w_k = 1.3l_{sec}\varepsilon_{s,sec} \quad [\text{mm}] \tag{8.10a}$$

Fully developed crack pattern:

$$w_k = 1.2l_{sec}\varepsilon_s \quad [\text{mm}] \tag{8.10b}$$

It is not necessary to place reinforcement along the side of the whole web, since the mean strain is small close to the neutral axis. Now, the position of the upper web rebars will be discussed.

The widest cracks occur half way down the unreinforced part of the web, see chapter 6.

The mean crack spacing at this level is h_{w0}, see Fig. 8.2. This assumption is in accordance with Fig. 7.6b. The characteristic crack width is:

$$w_k = 1.7 h_{w0} \frac{1}{2} \left(\frac{h_{w0}}{h - h_x} \right) \varepsilon_m \quad [mm] \tag{8.11}$$
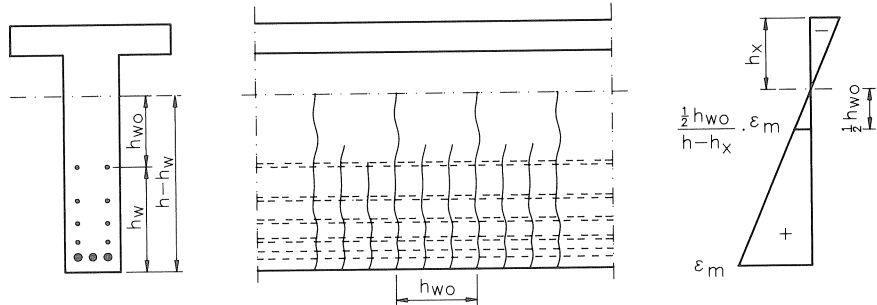
Fig. 8.2. The crack pattern in the part of the web not provided with reinforcement [CEB, 1985].

This formula was also presented by the CEB [1981]. In this formula, ε_m is the mean strain at the tension face of the beam. The part of the beam where reinforcement must be applied is:

$$h_w = h - h_x - \sqrt{\frac{w_k(h - h_x)}{0.5 * 1.7 \varepsilon_m}} \quad [mm] \tag{8.12}$$

The CEB [1981] assumed $\varepsilon_m = 0.8 * 10^{-3}$ and presented Fig. 8.3 to determine h_w. If the mean strain ε_m exceeds $0.8 * 10^{-3}$, h_w must be increased by the values according to Table 8.1.

Fig. 8.3. The distance over which web reinforcement must be applied [CEB, 1981].

92

Table 8.1.   The increase of h_w in mm at increasing mean surface strain

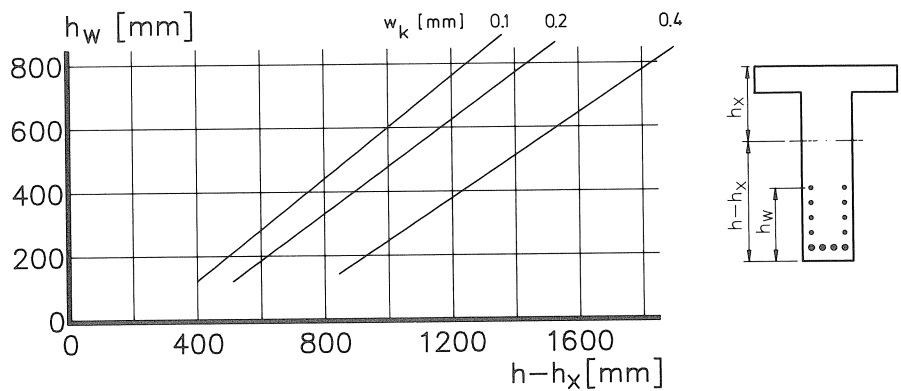| ε_m [–]	w_k [mm]		
	0.1	0.2	0.4
0.0012	75	100	150
0.0016	100	150	250

8.3   Working examples

8.3.1   Introduction

In this section the theory is illustrated by two working examples. The first example concerns a deep T-beam analysed by Leonhardt [1976a]. Leonhardt used this beam to demonstrate the use of the "effective concrete area" for the calculation of crack widths and spacings. The web reinforcement was likewise detailed on this basis. In the second example a tensile member provided with reinforcement at the side-faces is presented. This structure was also analysed by Helmus [1989]. Thus, the difference between the various approaches can be demonstrated.

8.3.2   Deep reinforced concrete T-beam

The cross-section and the main reinforcement are presented in Fig. 8.4a. The strains in a crack under the bending moment for which the crack widths must be checked are given in Fig. 8.4b.

The following material properties are used: $f_{cck} = 25$ MPa, $f_{sy} = 400$ MPa. The concrete cover $c = 20$ mm and the beam is provided with stirrups $d_{ss} = 12$ mm. The main rein-
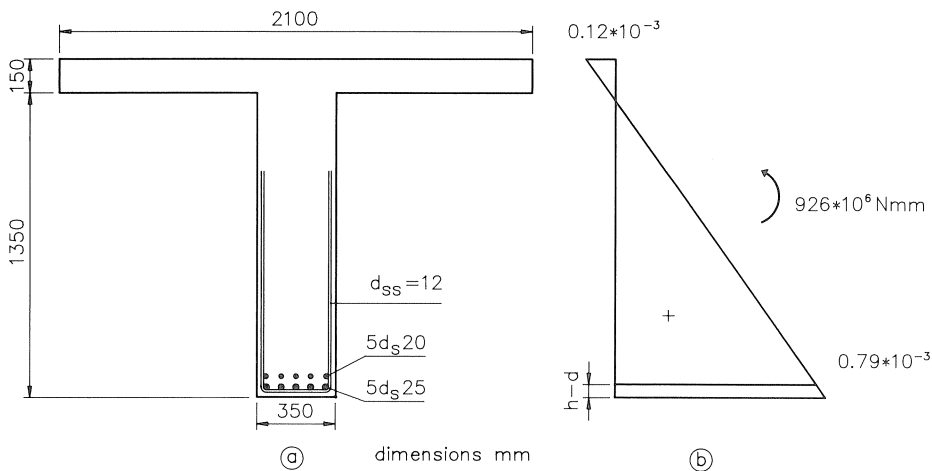

Fig. 8.4.   Cross-section of deep reinforced T-beam (a) and the strains in the cracked stage (b) [Leonhardt, 1976a].

forcement is placed in two layers, consisting of $5 * d_s$ 25 mm and $5 * d_s$ 20 mm respectively. The clear spacing between both layers is 25 mm. The effective depth $d = h - 67 = 1433$ mm. In the serviceability limit state, the bending moment is $1320 * 10^6$ Nmm. The cracking moment $M_{cr} = 458 * 10^6$ Nmm. Crack widths are checked at 40% of the live load, viz. $M = 926 * 10^6$ Nmm. The allowable characteristic crack width is $w_k = 0.20$ mm. Since $M \simeq 2M_{cr}$, the mean strains are equal to about 75% of the strains in the cracked stage (see formula (7.9)). In the uncracked stage, the compression zone is 525 mm deep. Thus, the coefficient k_3 for the main reinforcement is:

$$k_3 = \frac{1 + \dfrac{h - h_x - 2(h - d)}{h - h_x}}{2} = 0.93$$

$(h = 1500$ mm, $h_x = 525$ mm, $h - d = 67$ mm$)$

For the web reinforcement a somewhat lower value can be assumed. Therefore, $k_3 = 0.85$ is used in the web.

The bar spacing of the main reinforcement is $350/5 = 70$ mm. According to Fig. 8.1a $(2(h - d)/n_s = 100$ mm, $k_3 = 1.0$, $f_{ct} = 2.5$ MPa), it follows that the secondary crack spacing is 125 mm $(d_s = 20-25$ mm$)$.

In fact, since $k_3 = 0.93$ and $2(h - d)/n_s = 67$ mm should be used, the secondary crack spacing is (see formula (8.1)):

$$l_{sec} = 125 * (0.875 * 10^{-2} * 67 + 0.125) * 0.93 = 83 \text{ mm}$$

According to the Eurocode 1990, the mean crack spacing is:

$$l_m = 50 + 0.1 \frac{d_s}{\varrho_{eff}} = 83 \text{ mm}$$

According to Fig. 8.1b, the steel stress initiating secondary cracking $\sigma_{s,sec}$ is about 120 MPa.

The concrete quality $f_{cck} = 25$ MPa, i.e. $f_{ccm} \simeq 25 + 8 = 33$ MPa. According to Heilmann [1969] the mean concrete tensile strength is:

$$f_{ctm,0} = 0.24 * (33)^{0.67} = 2.5 \text{ MPa}$$

Thus, the tensile strength is in accordance with the one assumed in Fig. 8.1b.
Thus, $\sigma_{s,sec}$ is:

$$\sigma_{s,sec} = 120 * (0.875 * 10^{-2} * 67 + 0.125) * 0.93 * 1.0 = 79 \text{ MPa}$$

In the cracked stage, the steel strain is $0.79 * 10^{-3}$ (see Fig. 8.4b). Since $\varepsilon_{s,sec} \simeq 0.38 * 10^{-3}$, a fully developed crack pattern at the level of the main reinforcement can be assumed. The characteristic crack width is (see formula (8.10b)):

$$w_k = 1.20 * 83 * 0.79 * 10^{-3} = 0.08 \text{ mm}$$

With regard to the web reinforcement $d_s = 12$ mm is assumed. Thus, in this case $2(h - d)/n_s = 2(c + d_{ss} + \frac{1}{2}d_s) = 76$ mm. The bar spacing is assumed to be 125 mm. For

the web reinforcement this value must be halved in order to use the diagrams. From Figs. 8.1a-b it follows that $l_{sec} = 185$ mm and $\sigma_{s,sec} = 320$ MPa for $2(h - d)/n_s = 100$ mm. If $k_3 = 0.85$ is assumed for the web reinforcement, the secondary crack spacing and steel stress then become:

$$l_{sec} = 185 * (0.875 * 10^{-2} * 76 + 0.125) * 0.85 = 124 \text{ mm}$$
$$\sigma_{s,sec} = 320 * (0.875 * 10^{-2} * 76 + 0.125) * 0.85 * 1.0 = 215 \text{ MPa}$$

The mean strain in the case of a fully developed crack pattern is (see formula (8.9b)):

$$\varepsilon_{sm} = 0.9\varepsilon_{s,sec} = 0.9 * 215/2.1 * 10^5 = 0.92 * 10^{-3}$$

The mean strain at the level of the web reinforcement is less than this value (see Fig. 8.4b), In other words, the crack pattern is not fully developed. The characteristic crack width is (see formula (8.9a)):

$$w_k = 0.9l_{sec}\sigma_{s,sec} = 0.9 * 124 * 215/2.1 * 10^5 = 0.11 \text{ mm}$$

In the case where long-term or varying loading is applied, the crack width increases to (see formula (8.10a)):

$$w_k = 1.3l_{sec}\sigma_{s,sec} = 0.16 \text{ mm} < 0.20 \text{ mm}$$

Thus, a web reinforcement of d_s 12 mm ($s = 125$ mm) suffices to ensure a long-term characteristic crack width less than 0.20 mm. The part of the web where reinforcement must be applied is $h_w = 700$ mm (Fig. 8.3; $h - h_x \simeq 1300$ mm, $w_k = 0.20$ mm).

In his analyses, Leonhardt [1976a] found that the lower 250 mm of the web must be provided with d_s 12mm, $s = 70$ mm (see Fig. 8.5a). The remaining part contains d_s 10 mm ($s = 100$ mm) over 250 mm. The reinforcement according to the model presented is given in Fig. 8.5b.

The CEB [1981, 1985] design rules (see Table 3.3 and Fig. 8.3) lead to an amount of web reinforcement presented in Fig. 8.5c (concrete quality B25).

In most cases the crack pattern at the level of the main reinforcement will be not fully developed since $\sigma_{s,sec}$ is mostly rather high. Therefore, the Figs. 8.1a-b are combined so that the characteristic crack width can be determined directly. Furthermore, allowance is made for the fact that the bar spacing of the web reinforcement must be halved to use the Figs. 8.1a-b. Therefore, in Figs. 8.6a-b the actual bar spacing must be used.

Figs. 8.6a-b present the crack width when formula (8.10a) is used. In these figures it is assumed that $k_3 = 0.85$ and $f_{ct} = 2.5$ MPa. In other cases, the crack width is:

$$w_k = w_k^d \left(\frac{k_3}{0.85}\right)^2 \frac{f_{ct}}{2.5} \quad \text{[mm]} \tag{8.13}$$

Also in this formula the superscript "d" refers to the diagrams. If the parameter $2(h - d)/n_s$ differs from the 100 and 150 mm used in Figs. 8.6a-b, then the following formula can be used (see formulae (8.1–8.2) and (8.13)):

$$w_k = w_k^d \left(\frac{k_3}{0.85}\right)^2 \frac{f_{ct}}{2.5} \left(0.875 * 10^{-2} \frac{2(h - d)}{n_s} + 0.125\right)^2 \quad \text{[mm]} \tag{8.14}$$
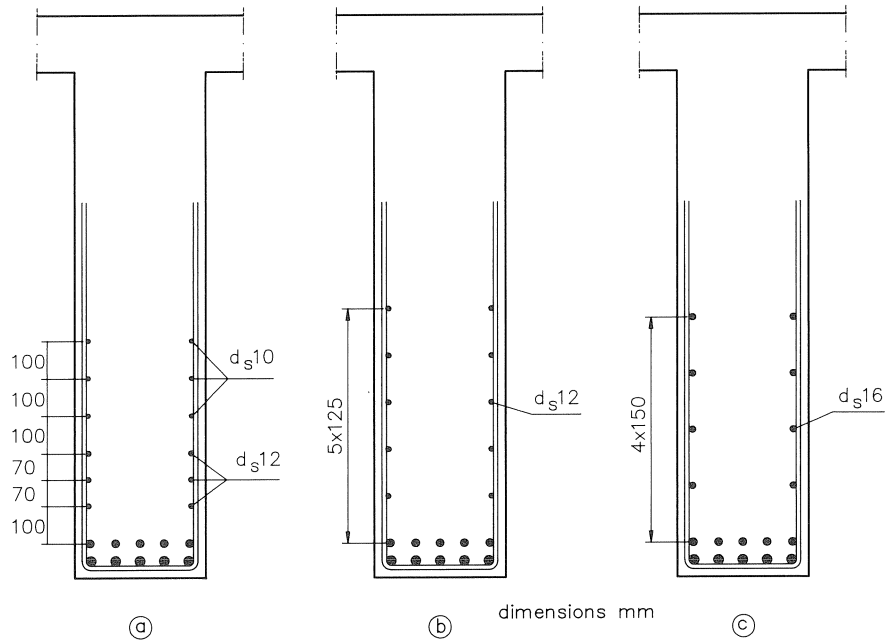
Fig. 8.5. Detailing of the web reinforcement according to Leonhardt [1976a] (a), the model presented (b) and the CEB [1981, 1985] (c).

In formula (8.14), the crack width from the diagram (w_k^d) refers to Fig. 8.6a $(2(h-d)/n_s = 100$ mm). Now, the web reinforcement of the beam will be detailed with Fig. 8.6a. The reinforcement must be detailed in such a way that $w_k^d = 0.20/(0.78)^2 = 0.33$ mm. From Fig. 8.6a it follows that the crack width requirement is satisfied
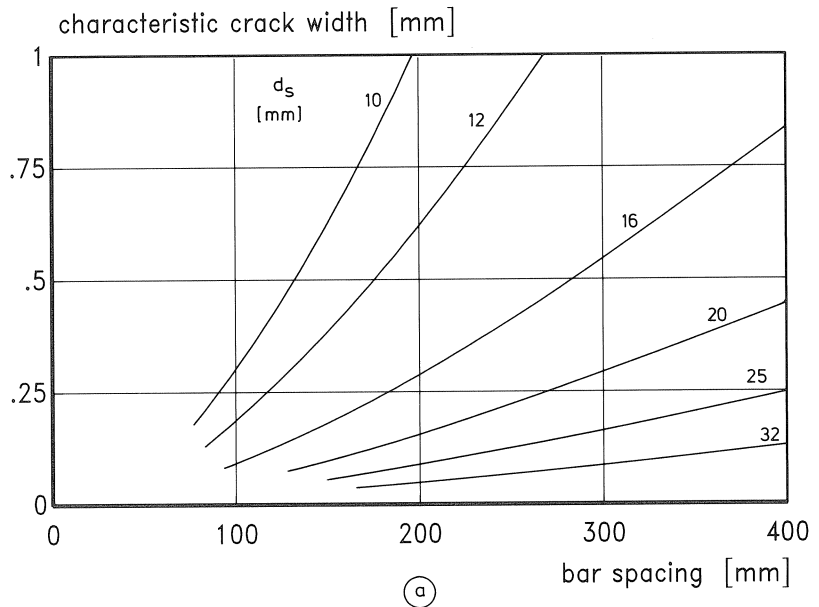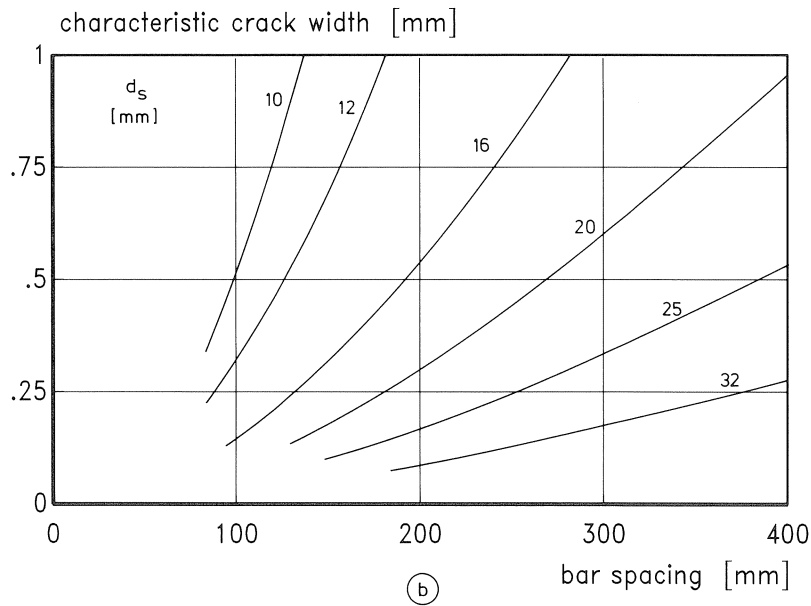
Fig. 8.6. The characteristic long-term web crack width in an not fully developed crack pattern for $2(h-d)/n_s = 100$ (a) and 150 mm (b) respectively ($k_3 = 0.85$, $f_{ct} = 2.5$ MPa).

for $d_s = 10$ mm, $s = 100$ mm; $d_s = 12$ mm, $s = 125$ mm or $d_s = 16$ mm, $s = 225$ mm. However, it must be checked whether the assumption that the crack pattern is not fully developed still holds. Thus it is required that the actual mean steel strain is less than about $0.9\varepsilon_{s,sec}$. This can be verified with Fig. 8.1b.

8.3.3 Tensile member

Helmus [1989] discussed the detailing of the reinforcement in a 2 m thick concrete foundation, see Fig. 8.7. Due to shrinkage, the structure is loaded in pure tension since it is assumed that the deformation is prevented along the whole length. The concrete tensile strength at the instant of cracking is $f_{ct} = 2$ MPa.

Fig. 8.7. Concrete foundation; Side-view (a) and cross-section with the reinforcement (b) [Helmus, 1989].

97

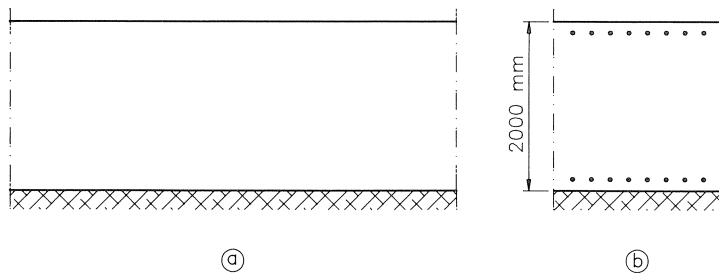According to the German code DIN 1045, the characteristic crack width must be less than 0.4 mm [Helmus, 1989]. With his model (see chapter 3), Helmus demonstrated that bars with a 25 mm diameter, spaced at 100 mm, are sufficient for the control of crack width. This reinforcement must be placed at both sides of the member, thus $A_s = 9820$ mm^2/m. Helmus performed calculations in the stage of a not fully developed crack pattern since the strain due to shrinkage was assumed to be $230 * 10^{-6}$.

Taking account of long-term loading, the new model presented in chapter 3 gives the following formula for the characteristic crack width in a not fully developed crack pattern (see formula (8.10a)):

$$w_k = 1.3 l_{sec} \varepsilon_{s,sec}$$

If the reinforcement according to Helmus is used, Figs. 8.1a-b give $l_{sec} = 150$ mm and $\sigma_{s,sec} = 120$ MPa. Since $f_{ct} = 2$ MPa and $2(h - d)/n_s = 150$ mm, these values must be adjusted, see formula (8.1) and (8.2):

$$l_{sec} = 150 * (0.875 * 10^{-2} * 150 + 0.125) = 216 \text{ mm}$$

$$\sigma_{s,sec} = 120 * (0.875 * 10^{-2} * 150 + 0.125) * \frac{2}{2.5} = 138 \text{ MPa}$$

The characteristic crack width is:

$$w_k = 1.3 * 216 * \frac{138}{2.1 * 10^5} = 0.18 \text{ mm} < 0.40 \text{ mm}$$

Thus, the amount of reinforcement can be further reduced if the new model is used. If the bar spacing is increased to 150 mm, the crack width requirement is still satisfied: $l_{sec} = 215 * 1.44 = 310$ mm and $\sigma_{s,sec} = 170 * 1.44 * 0.8 = 196$ MPa gives:

$$w_k = 1.3 * 310 * \frac{196}{2.1 * 10^5} = 0.38 \text{ mm} < 0.40 \text{ mm}$$

Compared to Helmus, the amount of reinforcement is reduced from 9820 to 6540 mm^2/m.

These calculations will be compared to the concept of the new CEB-FIP Model Code 1990. The code requires a minimum reinforcement ratio so that $\sigma_{s,cr} < f_{sy}$ where the total cross-section of the concrete is considered. The amount of reinforcement per m[1] becomes:

$$A_{s,min} = A_c \frac{f_{ct}}{f_{sy}} = 2000 * 1000 \frac{2}{500} = 8000 \text{ mm}^2$$

For the reinforcement the same amount as calculated with the new model is used, viz. $d_s = 25$ mm ($s = 150$ mm) at both side-faces ($A_s = 6540$ mm^2/m).

The transfer length is:

$$l_t = 25 + \frac{\sigma_{s,cr}}{\tau_b} \frac{d_s}{4} \quad [\text{mm}] \tag{8.15}$$

In this calculation the long-term bond stress $\tau_b = 1.4 f_{ct}$ must be used.

The crack width in a not fully developed crack pattern can be calculated by assuming that:

$$\varepsilon_{sm} = 0.6 \frac{\sigma_s}{E_s} \quad [-] \tag{8.16a}$$

with:

$$\sigma_s = \frac{f_{ct}}{\varrho_{eff}}(1 + n\varrho_{eff}) \quad \text{(tensile member)} \quad [\text{MPa}] \tag{8.16b}$$

Just as in the case of the Eurocode II, the reinforcement ratio in formula (8.16b) is calculated by reference to an "effective concrete area" at each side-face of the member:

$$\varrho_{eff} = \frac{A_s}{A_{c,eff}} = \frac{A_s}{2.5b(h-d)} = \frac{6540/2}{2.5*1000*75} = 0.017$$

$$\sigma_s = \frac{2}{0.017}(1 + 7*0.017) = 132 \text{ MPa}$$

$$l_t = 25 + \frac{132}{2.8}\frac{25}{4} = 319 \text{ mm}$$

$$w_k = 2l_t\varepsilon_{sm} = 2*319*0.6\frac{132}{2.1*10^5} = 0.24 \text{ mm}$$

In section 3.2.2 (see Table 3.1) it is demonstrated that the codes underestimate the crack spacing by about 20%, whereas the stress in the reinforcement is underestimated by 35%. If these findings are taken into account, the crack width becomes:

$$w_k = 1.2 * 1.35 * 0.24 = 0.39 \text{ mm}$$

This value is in correspondence with the crack width calculated with the new model presented in chapter 3.

This example clearly demonstrates that the codes present too optimistic values for the crack width in the case where the reinforcement is located at the side-faces of thick concrete tensile members. However, if corrections are introduced in accordance with the findings of section 3.2.2, good correspondence is obtained between the new model and the code.

In the case of thick members subjected to an imposed deformation, the crack pattern will mostly not be fully developed. Figs. 8.8a-b present the characteristic long-term crack width in a not fully developed crack pattern. In both figures $k_3 = 1$ and $f_{ct} = 2.5$ MPa is assumed. The following formula can be used to calculate the crack width in case where other parameters must be used:

$$w_k = w_k^d \left(\frac{k_3}{1.0}\right)^2 \frac{f_{ct}}{2.5} \left(0.875 * 10^{-2} \frac{2(h-d)}{n_s} + 0.125\right)^2 \quad [\text{mm}] \tag{8.14}$$

The crack width w_k^d refers to Fig. 8.8a. If this formula is used in this example, the reinforcement must be detailed provided that $(2(h - d)/n_s = 150$ mm):

$$0.4 = w_k^d * 1 * 0.8 * 1.44^2 \rightarrow w_k^d = 0.24 \text{ mm}$$

From Fig. 8.8a it can then be directly deduced that the following amounts of reinforcement satisfy the crack width requirement:

$$d_s = 16 \text{ mm}, \ s = 75 \text{ mm}$$
$$d_s = 20 \text{ mm}, \ s = 100 \text{ mm}$$
$$d_s = 25 \text{ mm}, \ s = 150 \text{ mm}$$
$$d_s = 32 \text{ mm}, \ s = 250 \text{ mm}$$

It should, however, be checked whether the crack pattern is not fully developed. It is emphasized that the foundation is assumed to be loaded only by an imposed deformation $\Delta\varepsilon$. In the case where a load N_F is also acting, the same procedure can be followed [Braam, 1990b]. One only has to calculate the actual steel stress by adding the imposed load and the load caused by the imposed deformation. The latter load depends on the axial stiffness of the structure. The stiffness can be deduced from the force-elongation curve. In this curve a point must be found where the total load N is in correspondence with the stiffness:

$$N = N_F + (EA)_x \Delta\varepsilon \quad \text{[N]} \tag{8.17}$$

The strength of the model presented is the possibility it offers for detailing the reinforcement independent of the thickness of the member, provided that the rebars are concentrated at the side-faces. In the codes however, the reinforcement must not only be detailed with regard to the control of crack widths, but also in such a way that the cracking force of the entire member can be carried by this reinforcement without the occurrence of yielding.

According to most of the research carried out in this field [e.g. Puche, 1988; Henning and Rostásy, 1990], the cracking force of thick tensile members can be reduced by a certain factor (e.g. 20–50%), but still depends on the total specimen depth. However, the model introduced in chapter 3 demonstrates that crack widths are controlled provided that $\sigma_{s,sec} < f_{sy}$. Thus, only an "effective concrete area" around the reinforcement has to be considered when calculating the minimum amount of reinforcement. The size of this area is independent of the total depth of the tensile member.
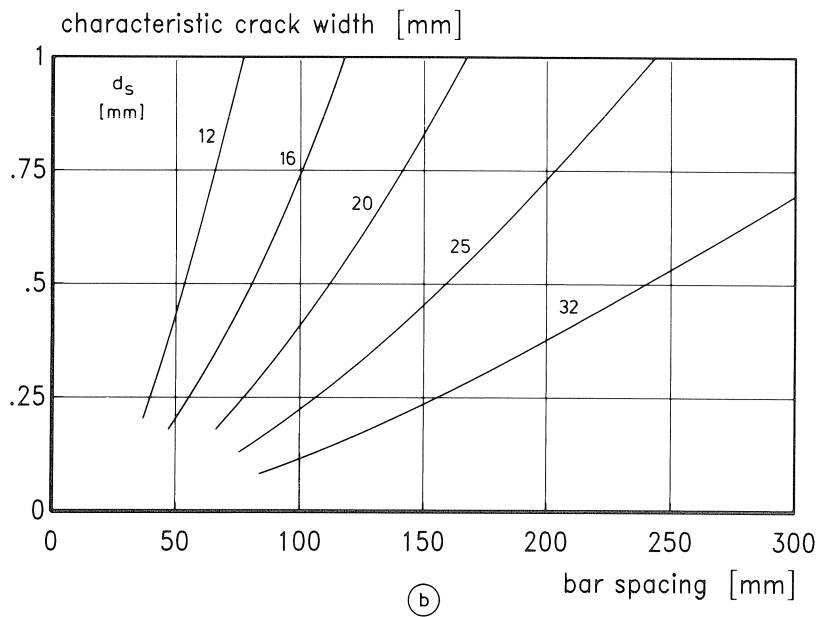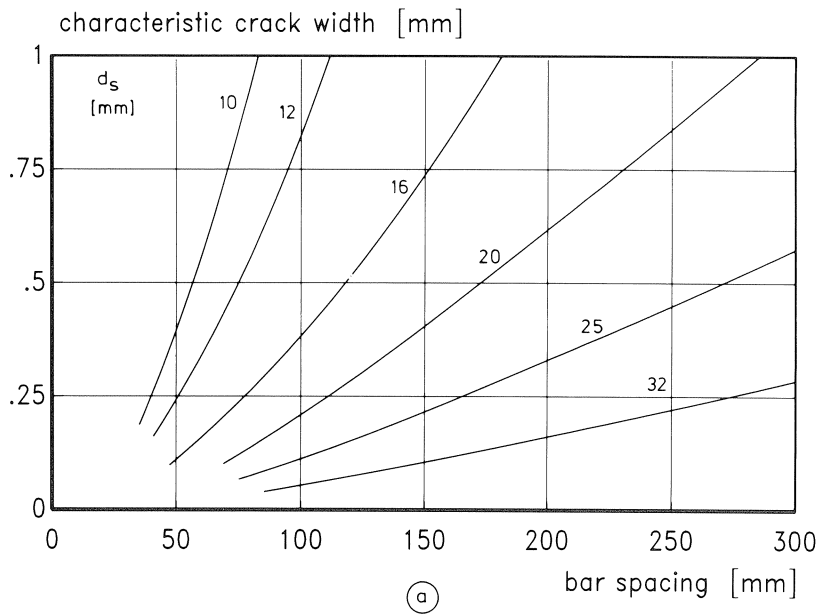
Fig. 8.8. The characteristic long-term crack width in a not fully developed crack pattern for $2(h-d)/n_s = 100$ (a) and 150 mm (b) respectively ($k_3 = 1.0$, $f_{ct} = 2.5$ MPa).

9 Notations

a, b	factors for the bond stress-slip relation	[–]
b	width	[mm]
b_{eff}	width of the "effective concrete area"	[mm]
c	concrete cover	[mm]
d	effective height	[mm]
d_s	bar diameter	[mm]
d_{ss}	stirrup diameter	[mm]
f_{cck}	characteristic cube compressive strength	[MPa]
f_{ccm}	mean cube compressive strength	[MPa]
f_{cspl}	cube tensile splitting strength	[MPa]
f_{ct}	concrete tensile strength	[MPa]
$f_{ctm,0}$	mean short-term concrete tensile strength	[MPa]
f_R	specific rib area	[–]
f_{sy}	steel yield stress	[MPa]
h	total height	[mm]
h_{cr}	initial crack height	[mm]
h_{eff}	height of the "effective concrete area"	[mm]
h_0	initial crack height	[mm]
h_t	distance from the compression zone to the main reinforcement	[mm]
l_0	"bond-free" length	[mm]
l_m	mean crack spacing	[mm]
l_{min}	minimum crack spacing	[mm]
l_{max}	maximum crack spacing	[mm]
l_{sec}	secondary crack spacing	[mm]
l_t	transfer length	[mm]
s	bar spacing	[mm]
u_s	circumference of reinforcing steel	[mm]
w_{cr}	crack width in a not fully developed crack pattern	[mm]
w_k	characteristic crack width	[mm]
w_m	mean crack width	[mm]
w_{max}	maximum crack width	[mm]
A_c	concrete cross-section	[mm²]
$A_{c,eff}$	effective concrete area	[mm²]
A_s	steel cross-section	[mm²]
A_{sw}	cross-section of the web reinforcement	[mm²]
G_f	fracture energy	[N/mm]
M_{cr}	cracking moment	[Nmm]
N_c	force in the compression zone	[N]
N_τ	bond force	[N]
δ	slip	[mm]
ε_m	mean surface strain	[–]
ε_s	steel strain in a crack	[–]

$\Delta\varepsilon_s$	tension stiffening	[–]
ε_{sm}	mean steel strain	[–]
ε_{sy}	steel yield strain	[–]
$\varkappa_m$	mean curvature	$[mm^{-1}]$
τ_b	bond stress	[MPa]
τ_m	mean bond stress along the transfer length	[MPa]
σ_{cm}	mean concrete stress	[MPa]
σ_{s0}	steel stress prior to cracking	[MPa]
σ_s	steel stress in a crack	[MPa]
$\sigma_{s,cr}$	steel stress after cracking	[MPa]
$\sigma_{s,sec}$	steel stress initiating secondary cracking	[MPa]
ϱ_d	reinforcement ratio	[–]
ϱ_{eff}	reinforcement ratio of the effective concrete cross-section	[–]

10 References

BEEBY, A. W., An investigation of cracking on the side faces of beams, Cement and Concrete Association, Technical Report 42.466, 1971, 11 pp.

BEEBY, A. W., A study of cracking in reinforced concrete members subjected to pure tension, Cement and Concrete Association, Technical Report 42.468, 1972, 25 pp.

BEEBY, A. W., Concrete in the oceans; Cracking and corrosion, Cement and Concrete Association, Technical Report No. 1, 1978, 77 pp.

BJUGGREN, U., Discussion of "Bond and anchorage", ACI-journal, Vol. 45, No. 4, 1948, pp. 552-1/552-10.

BLAAUWENDRAAD, J., G. M. A. KUSTERS, P. NAUTA and J. G. ROTS, Smeared crack approach and fracture localization in concrete, Heron, Vol. 30, No. 1, 1985, 48 pp.

BORGES, J.F. and J. A. LIMA, Crack and deformation similitude in reinforced concrete, RILEM, Bulletin No. 7, 1960, pp. 79-90.

BORST, R. DE, G. M. A. KUSTERS, P. NAUTA and F. DE WITTE, DIANA, a three-dimensional, nonlinear finite element package on a micro-computer, Conference on "Engineering software for microcomputers", Venice, 1984, pp. 435–446.

BRAAM, C. R. and M. S. LANGHOUT, Calculation of crack width in thick-walled concrete structures (in Dutch), PT/Civiele Techniek, Vol. 43, No. 3, 1988, pp. 51–57.

BRAAM, C. R., Bond between concrete and reinforcing steel; State-of-the-art 1989; Delft University of Technology, Stevin Laboratory, Report 25.5-89-17, 1989, 122 pp.

BRAAM, C.R., The cracking behaviour of reinforced concrete structures, Delft University of Technology, Progress in Concrete Research, Vol. 1, 1990a, pp. 1–17.

BRAAM, C. R., Reinforcement in thick-walled concrete structures (in Dutch), PT/Civiele Techniek, Vol. 45, Nos. 3/4, 1990b.

BRAAM, C. R., Deep reinforced concrete beams; Experimental results, Delft University of Technology, Stevin Laboratory, Report 25-5.90.5, 1990c, 203 pp.

BREEN, J. E. and G. C. FRANTZ, Control of cracking on the side faces of large reinforced concrete beams, University of Texas, Report 198-1F, 1978, 242 pp.

BREEN, J. E. and G. C. FRANTZ, Cracking on the side faces of large reinforced concrete beams, ACI-journal, Vol. 77, No. 5, 1980a, pp. 307–313.

BREEN, J. E. and G. C. FRANTZ, Design proposal for side face crack control reinforcement for large reinforced concrete beams, Concrete International, Vol. 2, No. 10, 1980b, pp. 29–34.

BRUGGELING, A. S. G., Structural concrete, Science into practice, Heron, Vol. 32, No. 2, 1987, 67 pp.

CEB, Bulletin d'information No. 12, 1959, 60 pp.

CEB, Bulletin d'information No. 61, 1967, 250 pp.

CEB, Bulletin d'information No. 72, 1970, 91 pp.

CEB-FIP, Model Code for Concrete Structures, Bulletin d'information No. 124/125, 1978, 348 pp.

CEB, Manual on "Cracking and deformations", Bulletin d'information No. 143, 1981, pp. 2.1-2.80.

CEB, Manual on "Cracking and deformations", Bulletin d'information No. 158, 1985, pp. 2.1-2.66.

CORNELISSEN, H. A. W., D. A. HORDIJK, and H. W. REINHARDT, Tensile tests and failure analysis of concrete, ASCE, Structural Division, Vol. 112, No. 11, 1986, pp. 2462–2477.

CUR, Cracking due to shrinkage and temperature variation in walls (in Dutch), CUR, Report No. 85, 1978, 102 pp.

DRAGOSAVIC, M., H. GROENEVELD, P. VAN DER HAAR and TH. MONNIER, Bond between concrete and steel (in Dutch), TNO-IBBC, Report BI-81-48, 1981, 66 pp. + appendices.

ELIGEHAUSEN, R., R. MALLÉE and G. REHM, Rissverhalten von Stahlbetonkörpern bei Zug-beanspruchung, Univ. Stuttgart, Untersuchungsbericht Nr. 76/4, Teil 1 & 2, 1976, 33 pp. + appendices.

Eurocode No. 2, Common unified rules for concrete structures, Second consolidated draft, 1988.

FEHLING, E. and G. KÖNIG, Zur Rissbreitenbeschränkung im Stahlbetonbau, Beton- und Stahl-betonbau, Vol. 83, Nos. 6/7, 1988, pp. 161–167, 199–204.

FELLMAN, W. and C. MENN, Zugversuche an Stahlbetonscheiben, ETH Zürich, Bericht Nr. 7604-1, 1981, 40 pp.

GERGELY, P. and L. A. LUTZ, Maximum crack width in reinforced concrete flexural members, ACI, SP-20, 1968, pp. 87–117.

GOTO, Y., Cracks formed in concrete around deformed tension bars, ACI-journal, Vol. 68, No. 4, 1971, pp. 244–251.

GROOT, D. DE, The cracking behaviour of deep reinforced concrete beams (in Dutch), Graduate thesis, Delft University of Technology, 1990, 123 pp.

HARTL, G., Die Arbeitslinie eingebetteter Stähle bei Erst- und Kurzzeitbelastung, Dissertation, University of Innsbruck, 1977, 159 pp.

HARTWICH, K. and F. S. ROSTÁSY, Rissbreitenbeschränkung im Stahlbetonbau durch Faserarmie-rung, T.U. Braunschweig, Forschungsbericht, 1984, 34 pp. + appendices.

HARTWICH, K., Zum Riss- und Verformungsverhälten von Stahlfaserverstärkten Stahlbeton-stäben unter Längszug, T.U. Braunschweig, Heft 72, 1986, 202 pp. + appendices.

HEILMANN, H. G., Beziehungen zwischen Zug- und Druckfestigkeit des Betons, Beton, Vol. 19, No. 2, 1969, pp. 68–70.

HELMUS, M., Mindestbewehrung Zwangsbeanspruchter dicker Stahlbetonbauteile, Dissertation, T.H. Darmstadt, 1989, 208 pp.

HENNING, W., Zwangrissbildung und Bewehrung von Stahlbetonwänden auf steifen Unter-bauten, T.U. Braunschweig, Heft 79, 1987, 226 pp.

HENNING, W. and F. S. ROSTÁSY, Zwang und Rissbildung in Wänden und Fundamenten, Deut-scher Ausschuss für Stahlbeton, Heft 407, 1990, 145 pp.

HILLERBORG, A., M. MODÉER and P.-E. PETERSSON, Analysis of crack formation and crack growth in concrete by means of fracture mechanics and finite elements, Cement and Concrete Research, Vol. 6, No. 6, 1976, pp. 773–782.

HORDIJK, D. A. and H. A. W. REINHARDT, Macro-structural aspects in a uniaxial tensile test on concrete, Int. Symp. on "Brittle matrix composites", Cedzyna, 1988.

HORDIJK, D. A., Deformation-controlled uniaxial tensile tests on concrete; A survey of the literature up to 1981, Delft University of Technology, Stevin Laboratory, Report 25.5-89-15, 1989, 118 pp.

KOCH, R., Verformungsverhalten von Stahlbetonstäben unter Biegung und Längszug im Zustand II auch bei Mitwirkung des Betons zwischen den Rissen, Dissertation, Univ. Stuttgart, 1976, 177 pp.

KRIPS, M., Rissbreitenbeschränkung im Stahlbeton und Spannbeton, TH Darmstadt, Heft 33, 1985, 155 pp.

KRUITHOF, T. H., The cracking behaviour of reinforced concrete tensile members (in Dutch), Graduate thesis, Delft University of Technology, 1990, 100 pp. + appendices.

LANGHOUT, M. S., Thick concrete structures; Crack width control and minimum reinforcement (in Dutch), Graduate thesis, Delft University of Technology, 1988, 90 pp. + appendices.

LEONHARDT, F., Grundlagen zum Bewehren im Stahlbetonbau, Vorlesungen über Massivbau, Teil 3, 1974, 244 pp.

LEONHARDT, F., Nachweis der Gebrauchsfähigkeit, Vorlesungen über Massivbau, Teil 4, 1976a, 194 pp.

LEONHARDT, F., Rissebeschränkung, Beton- und Stahlbetonbau, Vol. 71, No. 1, 1976b, pp. 14–20.

LEONHARDT, F., Zur Behandlung von Rissen in den deutschen Vorschriften, Beton- und Stahlbetonbau, Vol. 80, Nos. 7/8, 1985, pp. 179–184, 209–215.

MARTIN, H. and G. REHM, Zur Frage der Rissbegrenzung im Stahlbetonbau, Beton- und Stahlbetonbau, Vol. 63, No. 8, 1968, pp. 175–182.

MARTIN, H., P. SCHIESSL and M. SCHWARZKOPF, Berechnungsverfahren für Rissbreiten aus Lastbeanspruchung, Strassenbau und Strassenverkehrstechnik, Heft 309, 1980, pp. 33–66.

MIER, J. G. M. VAN, Mode I fracture of concrete: Discontinuous crack growth and crack interface grain bridging, Delft University of Technology, Stevin Laboratory, Report 25.5-90-7, 1990, 14 pp.

NEN 3880, Voorschriften Beton VB 1974/1984, NNI, Delft, 1984, 523 pp.

NOAKOWSKI, P., Die Bewehrung von Stahlbetonbauteilen bei Zwangsbeanspruchung infolge Temperatur, Deutscher Ausschuss für Stahlbeton, Heft 296, 1978, 144 pp.

NOAKOWSKI, P., Verbundorientierte, kontinuierliche Theorie zur Ermittlung der Rissbreite, Beton- und Stahlbetonbau, Vol. 80, Nos. 7/8, 1985, pp. 185–190, 215–221.

PUCHE, M., Rissbreitenbeschränkung und Mindestbewehrung bei Eigenspannungen und Zwang, Deutscher Ausschuss für Stahlbeton, Heft 396, 1988, 133 pp.

RAO, P. S., Die Grundlagen zur Berechnung der bei statisch unbestimmten Stahlbetonkonstruktionen im plastischen Bereich auftretenden Umlagerungen der Schnittkräfte, Deutscher Ausschuss für Stahlbeton, Heft 177, 1966, 47 pp.

REHM, G., Über die Grundlagen des Verbundes zwischen Stahl und Beton, Deutscher Ausschuss für Stahlbeton, Heft 138, 1961, 59 pp.

REHM, G. and H. RÜSCH, Versuche mit Betonformstähle, Deutscher Ausschuss für Stahlbeton, Heft 140, 1963a, 182 pp.

REHM, G. and H. RÜSCH, H., Versuche mit Betonformstähle, Deutscher Ausschuss für Stahlbeton, Heft 160, 1963b, 82 pp.

REHM, G. and H. RÜSCH, Versuche mit Betonformstähle, Deutscher Ausschuss für Stahlbeton, Heft 165, 1964, 52 pp.

ROTS, J. G., Computational modeling of concrete fracture, Dissertation, Delft University of Technology, 1988, 132 pp.

RÜSCH, H., Relation between crack formation and adhesion, taking into account highly stressed reinforcement bars, Proc. 5th congres IABSE, Lisbon-Porto, 1956, pp. 791-813.

SCHEIDLER, D., Experimentelle und analytische Untersuchungen zur wirklichkeitsnahen Bestimmung der Bruchschnittgrössen unbewehrter Betonbauteile unter Zugbeanspruchung, Deutscher Ausschuss für Stahlbeton, Heft 379, 1987, 94 pp.

SCHIESSL, P. and E. WÖLFEL, Konstruktionsregeln zur Beschränkung der Rissbreite, Beton- und Stahlbetonbau, Vol. 81, No. 1, 1986, pp. 8-15.

SCHIESSL, P., Grundlagen der Neuregelung zur Beschränkung der Rissbreite, Deutscher Ausschuss für Stahlbeton, Heft 400, 1989, pp. 157-175.

SMIT, E. J. M., The cracking behaviour of reinforced concrete beams (in Dutch), Graduate thesis, Delft University of Technology, 1989, 116 pp.

SORETZ, S. and J. COLONNA-CECCALDI, Grosse Stahlbetonbalken mit Hauptbewehrung aus 2 dicken Stäben, Betonstahl in Entwicklung, Heft 46, 1971, 30 pp.

VEEN, C. VAN DER, Bond stress-slip relationship at very low temperatures; Part 1 – Experimental results, Delft University of Technology, Stevin Laboratory, Report 25-87-43, 1987, 70 pp.

VEEN, C. VAN DER, Bond stress-slip relationship at very low temperatures; Part 2 – Appendices, Delft University of Technology, Stevin Laboratory, Report 25-88-2, 1988, 69 pp.

VEEN, C. VAN DER, Cryogenic bond stress-slip relationship, Dissertation, Delft University of Technology, 1990, 110 pp.

VOS, E., Influence of loading rate and radial pressure on bond in reinforced concrete, Dissertation, Delft University of Technology, 1983, 235 pp.

Curriculum vitae

3 juli 1961	Geboren te Vlissingen
1979	Atheneum diploma R.S.G. Scheldemond te Vlissingen
1985	Diploma T.U. Delft, Faculteit der Civiele Techniek (vakgroep Mechanica en Constructies)
sept. 1985–nov. 1987	Werkzaam bij de Sectie Betonconstructies van de Faculteit der Civiele Techniek, T.U. Delft
dec. 1987–heden	Werkzaam aan de T.U. Delft, Fac. der Civiele Techniek, als onderzoeker voor de Stichting voor de Technische Wetenschappen